

博士論文（要約）

Liposome MANSIONs:
quantitative and statistical analysis of the dynamics of
cell-sized liposomes under steady flow environment

（リポソーム MANSIONs：定常流れ場における
細胞サイズのリポソームの動態の定量・統計解析）

杉山 博紀

Table of Contents

1. General introduction and Purpose of the Thesis	3
1.1. Background of constructive biology	3
1.2. Liposomes as a scaffold for constructive biology	5
1.3. Liposomes as a chemical cell model	6
1.4. Blueprint to be aimed and bottlenecks	8
1.5. Overview of the contents of the paper	11
2. Machine assisted platform for direct observation of cell-sized liposomes based on the microfluidic device	13
2.1. Introduction	13
2.2. Materials and method	16
2.3. Design of the experimental system	21
2.3.1. Design of the arraying device	21
2.3.2. Design of the mixing device	28
2.3.3. Design and schema of the automated observation platform	29
2.4. Demonstration of the performance	34
2.4.1. Arraying device	34
2.4.2. Mixing device	39
2.5. Automated observation of liposomes upon an osmotic stress	42
2.6. Significance of the achievement	50
2.7. Conclusion	52
3. Microfluidic exploration of cell-sized liposomes prepared by the water-in-oil emulsion transfer method	53
3.1. Introduction	53
3.2. Materials and method	55
3.3. Surface modification of PDMS and microfluidic trap of cell-sized liposomes prepared by the WOET method	60
3.4. Distribution of encapsulated microbeads in liposomes prepared by the WOET method	65
3.5. Water permeability of liposomes prepared by the WOET method	68
3.6. Significance of the achievement	71
3.7. Conclusion	72

4. Hydrodynamic accumulation of small molecules and ions into cell-sized liposomes against a concentration gradient	74
4.1. Introduction	74
4.2. Materials and method	77
4.3. Accumulation of uranine into a liposome	82
4.4. Effect of external flow and physical contact on uranine accumulation in liposomes	98
4.5. Permeation and accumulation of fluorescein-tagged ATP	106
4.6. Significance and future perspectives of the current findings	109
4.7. Conclusion	110
5. Flow-induced disparity in disturbance between the inner/outer leaflets of charged liposomes enabled rapid accumulation of molecules against a concentration gradient	111
5.1. Introduction	111
5.2. Materials and Method <i>(This section is currently omitted because it includes unpublished data).</i>	113
5.3. <i>This section is currently omitted because it includes unpublished data.</i>	113
5.4. Scrutiny of candidates of the physicochemical key factors <i>(A part of this section is currently omitted because it includes unpublished data)</i>	113
5.5. <i>This section is currently omitted because it includes unpublished data.</i>	120
5.6. <i>This section is currently omitted because it includes unpublished data.</i>	120
5.7. Conclusion <i>(A part of this section is currently omitted because it mentions to unpublished data)</i>	120
6. General Conclusion <i>(A part of this section is currently omitted because it mentions to unpublished data)</i>	121
References	127
Acknowledgement	140

1. General introduction and Purpose of the Thesis

1.1. Background of constructive biology

The invention of the microscope led to the establishment of contemporary biology. The most primitive form of biology was the taxonomy based on the observation of morphological features of living things. In the 15th century, Hooke observed the surface of a cork with a hand-made microscope and found small reticulated structures on the surface¹. He termed the small structure as “cell.” In the 1830s, Schwan and Schleiden independently proposed the cell theory: cells are the basic structural/organizational unit of all organisms², which underlies the contemporary understanding of living things. The origin of the cell theory is found in the discovery that there exists some small structure which is characteristic to the living things, and the discovery was brought by the invention of the microscope.

Reductionism had thus been the basic methodology of biology. Biologists decomposed complicated living things into the constituents of the cell. One of the most succeeded examples of the reductive approach was the characterization of the double-helix structure of deoxyribonucleic acid (DNA)³. Formulation of the central dogma⁴, decipherment of the genetic code⁵, and arbitrary editing of genetic information^{6, 7} arose from the discovery. The characterization of DNA is also regarded as a landmark of the beginning of molecular biology. One of the unique orientations of molecular biology was an expectation that a careful and exhaustive exploration of molecules will reveal the essence of life. Namely, molecular biology can be distinguished from the previous type of biology by the underlying idea to seek the universal logic and mechanism of biological phenomena.

Around the beginning of the 21st century, other strategies began to be explored. For

example, in 1999, while being inspired by the development of computer science, Hartwell and his colleagues pointed out that many of the functions of cells were not necessarily reducible to individual molecules. Instead, they emphasized the importance of considering cells as a set of modular systems⁸. Systems biology⁹, which was also proposed in the early 2000s, also emphasized focusing on the features of the cellular dynamics. Their suggestions accelerated the interdisciplinary studies with mathematics¹⁰,¹¹. As one of the characteristic techniques in these research trends was to edit or modify the living cells, these approaches were classified as synthetic biology. As the methodology included the engineering of the cells, synthetic biology has also developed into the applied perspectives such as producing therapeutic proteins, cancer detection, and so on^{12, 13}.

Another symbolic proposition related to synthetic biology was brought from supramolecular chemistry. In 2001, Szostak and his colleagues published a paper titled “Synthesizing life.”¹⁴ They proposed constructing a chemical model of living cells from scratch to resemble the essence of living cells. The typical methodology was to combine artificially synthesized molecules or/and a part of bio-functional components such as DNA, RNA, proteins, lipids, and so on, aiming to mimic the essence of life¹⁵⁻¹⁷. Through the struggles to model complex cellular systems in a simple molecular aggregate, chemical logics behind the complexity would be unveiled¹⁸. The thesis is oriented to this supramolecular chemistry-based synthetic approach. The author believes that the approach, which explicitly involves chemical synthesis, is more appropriate to be classified as “synthetic” biology, but to distinguish it from the approach modifying current cells, hereafter we adopt the term “constructive biology,” referring to the previous literature¹⁹.

1.2.Liposomes as a scaffold for constructive biology

The spreading of electron microscopes played an indispensable role in the development of constructive biology. In 1964, Bangham and Horne found closed lamellar structures resembling cellular membrane in a dispersion of phospholipids by a transmittance electron microscope²⁰. The cellular membrane consists of lipids and various proteins, and other small molecules like sterols. The observation provided the first experimental evidence that the cellular membrane is a closed lipid bilayer and that phospholipids alone can form a lipid bilayer. Weissman termed this reconstructed closed lamellar bilayer of phospholipid as “liposome.”²¹ Since the cellular membrane defines areas of the cell as compartments, liposomes are considered to be the most simplified form of cells in the view of the structure of the compartment.

A liposome is a kind of molecular self-assembly. The driving force to form a liposome is attributed to the hydrophobic interaction of phospholipids. Phospholipids have hydrophobic moiety and hydrophilic moiety in a single molecular structure. Thus, under the coexistence of water, hydrophobic parts assembled each other to remove constitution water, and instead, hydrophilic parts are exposed to the water. There are various possible forms of self-assemblies such as spherical micelles, rod-like micelles, bilayers, inversed micelles, or so on²². Amphiphiles of a specific packing parameter form bilayer when dispersed into water. Closed lamellar structures emerge when the bilayers have a finite curvature. Thus, the constituents of the closed bilayer are not limited to phospholipid^{23, 24}. Closed bilayers composed of general amphiphiles of specific packing parameters are called vesicles. Vesicles larger than 1 μm , termed as giant vesicles, are of particular interest as a scaffold for constructing a cell-like system owing to their structural commonality to living cells²⁵. For example, oleic acid can form giant vesicles. Since fatty

acids are plausible even at the early stage of the earth, they are expected as promising candidates of the primitive style of the cell-like system at the origin of life, protocell²⁶.

One of the characteristic features of constructive biology is the simplicity of the system to be investigated. For example, the dynamic instability of microtubules, which had been doubted from the viewpoint of chemical equilibrium, was experimentally visualized for the first time in liposomes under darkfield microscopy²⁷. The simplicity excluded artifacts, which is useful to extract the pure character of the system. The simplicity is also useful for separating complicated interactions in living cells into individual elements. Hotani and his colleagues compared the deformation of liposomes and cells without cytoskeletons under osmotic stress^{28, 29}. As a result, they found that liposomes can have red-blood cell-like shapes without cytoskeletons, and in contrast, the deformation paths of cells without cytoskeletons resembled those of liposomes. Namely, the reports divided the factors stipulating the deformation of cells into the nature of the membrane itself and contribution from cytoskeletons. Besides, deformation of liposomes containing water-soluble polymers or colloidal particles preferred membrane fusion and budding-like dynamics^{30, 31}. By the artificial modeling of molecular crowding, these reports tackled the question of whether specific molecular constituents are essential or not. It is also regarded as an example of separating the entangled factors into isolated elements owing to the simplicity of the system.

1.3.Liposomes as a chemical cell model

One of the current research trends of constructive biology is somewhat familiar with engineering. The current living things have significant complexities. The constructive approach aims to explore the prospective connection between complexity and simplicity,

starting from simplicity. Simplicity can be rephrased as “well-defined.” Researchers struggle to reconstruct various cellular dynamics by specific sets of (bio-functional) constituents, which are explicitly and thoroughly listed in advance. The reconstructed systems are regarded as chemical models of contemporary living cells.

One of the critical dawn is protein synthesis in liposomes. Noireaux and Libchaber pioneeringly encapsulated the extract of *E. Coli.* into liposomes and achieved the production of alpha-hemolysin. Strikingly, the produced alpha-hemolysin inside the liposome were spontaneously embedded into the membrane and worked as a pore-forming membrane protein³². The further achievement in the *in situ* production and activation of proteins was, for example, the reconstruction of pheromone sensing, which needed the co-expression of two membrane proteins³³. Recently, liposomes that synthesize proteins inside the liposome using chemical energy produced in the very liposomes was established³⁴. Functionalization of liposomes combined with the enclosed proteins was thus a straightforward development of the field. For example, liposomes of motility driven by the encapsulated microtubules³⁵, liposomes worked as a logic gate using genetic circuits enclosed in the liposomes³⁶, liposomes divided by the reconstituted bacterial proteins, FtsZ³⁷, were reported. Coupling with the oscillatory wave of Min proteins³⁸ with FtsZ cytoskeletal patterns was also explored³⁹. Another direction related to the reconstruction of the protein synthesis is investigating the minimum set of enzymes for the transcription and translation in liposomes⁴⁰. This is complementary to the top-down approach, where the minimum set of the genome is examined with the modified living cells⁴¹.

On the other hand, the self-replicating ability of the cells also attracted the interest of constructive approach⁴² not only as a step toward evolvable chemical cell models² but

also as a unique property of micrometer-sized chemical reactor⁴³. For example, Luisi's group pioneeringly reported the auto-poietic growth and division of the vesicles using a chemical conversion^{44, 45}. As for the investigation of the auto-poietic chemical system, pseudo-autocatalytic phospholipid production followed by the growth and division of liposome was achieved^{46, 47}. Another significant achievement related to the self-replicating compartment was the coupling of the replication of the compartment and the inner constituents⁴⁸⁻⁵⁰: the amplification and redistribution of the encapsulated DNA molecules were achieved during the growth and division of the compartment.

1.4.Blueprint to be aimed and bottlenecks

The promising direction of the liposome investigation is sustainability. As we overviewed in the last section, reconstruction and mimic of various cellular dynamics have been (and will be) extensively explored. However, these were all limited to one or at most several generations. There is a qualitative gap between the reconstructed artificial cells in the short relaxation process and the living cells whose chemical processes persist throughout their lifetimes and over generations. Learning from synthetic biology, where the stochasticity of individual processes in the living cell is one of the central issues^{51, 52}, the importance is also remarkable for constructive biology, to integrate individual stochastic processes into a single coherent system.

Toward this end, the methodology to evaluate the long-term behaviors of chemical cell models should be improved. There is a technical but general conflict between the throughput of the measurement and the obtained information detail. For example, traditional spectroscopic and electrochemical approaches provide robust methodologies to grasp the averaged information, but the dynamics of one liposome cannot be obtained.

On the contrary, microscopy is advantageous for the detailed observation of one liposome, but massive demand was imposed on the experimenters to accumulate data compatible with the statistical analysis. The deficiency is brought from the Brownian motion of the liposomes floating as colloidal dispersion. Namely, the parallel tracking of multiple liposomes at a moderate time resolution is hindered since the contiguous manual tracking of a specific liposomes is required for the individual data acquisition. The Brownian motion brings another difficulty in the supply of substrates to the liposomes of interest: since most substrates are supplied as a solution, liposomes flowed away along to the supply process. The process also accompanies the dilution of the system. These technical deficiencies result in the deterioration of the throughput. Although there are reports using microinjectors to supply substrates while observing the liposome of interest in a bulk condition^{53, 54}, deep proficiency in the technique is required.

As we will discuss in detail in the later chapter, microfluidic technology could provide a solution. For example, the immobilization of the liposomes through the biotin-avidin linker on the glass surface in the microchannel is one of the simplest microfluidic devices to enable the massive assay of liposomes^{55, 56}. As the chemical immobilization requires additional membrane components, microfluidic devices arraying liposomes physically at the micrometer-sized trapping structure have also been proposed⁵⁷⁻⁵⁹. The microfluidic arraying of liposomes enabled the simultaneous observation of the liposomes using a microscope. The parallel measurement is striking because, as we discussed, the low throughput has hindered the statistical handling of the obtained detailed information of the dynamics. Microfluidic immobilization also solved the technical difficulty of substrates feeding since an arbitrary exchange of the external environment was easily realized. Thus, the combination of microfluidic technology and microscopy could be a

promising methodology for investigating the long-term behaviors of liposome-based chemical cell models.

While microfluidic technology has made remarkable progress, the peculiarity of the steady flow environment as a measurement environment has been relatively overlooked. In other words, inevitable effects to the liposomes under a microfluidic environment, such as shear stress, have been regarded as an artifact to be carefully addressed^{58, 60}. It is reliable because the development of microfluidic devices was oriented to establishing the methodology of upward compatibility to the traditional bulk assays. Aside from the ingenuities reducing or compensating the effect of flow, some characteristic behaviors of liposomes under a flow environment were reported, which are never observed under the bulk condition, such as morphological change⁶¹, shear-induced convection inside the liposome⁶², and domain formation at the liposomal membrane⁶³. However, in the previous research whose primary focus was the quantification and elucidation of the physical effect of the flow to the liposomes, less was discussed for the potential contribution and advantage of the flow environment to the construction and further development of the chemical cell model. For example, the steady flow environment can find its own significance in terms of the continuous supply of substrates to the liposomes of interest, which would be critical to the investigation of sustainability as we overviewed at the beginning of this section.

As will be discussed and demonstrated in the later chapter, the thesis presumably provides the proof for the promise of investigation of liposomes under a steady flow environment. We show a methodology for measuring liposomes with throughput, accuracy, and reproducibility based on direct observation by microscopy. The technical development leads us to clarify a new class of transportation of substrates across the

liposomal membrane, which would be a promising step toward the investigation of sustainability.

1.5. Overview of the contents of the paper

Chapter 1 first summarized and discussed the fundamental concept of constructive biology that the thesis stands for. Then, we reviewed the expected impacts that liposome-based cell model would bring and state-of-the-art establishments. Consideration of the next promising step of the liposome investigation led us to the microfluidic technology, which could solve the arising technical bottlenecks. Finally, the importance of exploring the unveiled dynamics of liposomes under a steady flow environment was discussed.

In chapter 2, an automated experimental platform for the direct observation of cell-sized liposomes is presented. As the platform is based on microfluidic devices, the development can be a promising tool to investigate liposomes under a steady flow environment. First, the design and primary verification of the devices are explained. Then, we describe the osmotic response of liposomes to verify and demonstrate the performance of the platform.

In chapter 3, a development of surface modification of microfluidic device is proposed, which expands the scope of microfluidic exploration of liposomes. Due to the undesired interaction with the surface of the microfluidic device, liposomes prepared by a specific method cannot be applied to the microfluidic exploration. As the preparation method can afford high encapsulation yield even for macromolecules and is frequently used to reconstruct the cellular dynamics inside liposomes, the incompatibility deteriorates the potential of the microfluidic device. We show that surface modification enables the microfluidic exploration of the liposomes prepared by the method.

In chapter 4, a novel class of transportation of substrates across the lipid membrane (termed as hydrodynamic accumulation) is described. We show that when liposomes trapped in the microfluidic device are exposed to a solution of some specific molecules, the molecules can be efficiently accumulated into the trapped liposomes against a concentration gradient. In other words, the concentration of the inner solutes become higher than that of the outer solutes without any explicit (known) concentrating mechanics such as pump proteins. We discuss the significance of the discovery not only as a straightforward methodology to supply molecules inside liposomes but also in the view of the origin of life research.

In chapter 5, perturbations occurring in the liposomal membrane under a steady flow environment is discussed using the mechanistic consideration of the hydrodynamic accumulation as the subject. We show an unexpected heterogeneity occurs in the liposomal membrane under a steady flow environment. We also demonstrate that the kinetics of the permeation becomes less significant to the molecular weight for some solutes. Taking together these observed results, we discuss the disturbance of the membrane exposed to a steady flow environment.

In chapter 6, the significance of the current findings and achievements are summarized. We also discuss the possible future works that the results reported in the thesis can stimulate.

2. Machine assisted platform for direct observation of cell-sized liposomes based on the microfluidic device

2.1. Introduction

The dynamics of liposome often accompanies variety²⁸. The uncertainty of the external condition may cause the diversity, or the variety can be derived from the variety of initial state. Although methodologies to prepare uniform liposomes have been developed⁶⁴⁻⁶⁷, the complete control over the initial conditions is unmanageable. Rather, it is difficult to directly prove that the very liposomes observed and compared are uniform under microscopic observation. Instead, according to the area differential elasticity model (ADE model), the most succeeded and accepted theoretical model on the shape of vesicles, the microscopic distribution of lipids between the inner and outer leaflet can differ even though the macroscopic shape looked similar⁶⁸. The heterogeneity often makes the analysis complicated. Thus, even with some ideal preparation methods, statistical assessment is indispensable. One technical problem lies in the parallel tracking of multiple cell-sized liposomes at a moderate spatial magnification because of the Brownian motion⁴³. In other words, accumulating data worthy of statistical analysis should involve a labor-intensive protocol. Conversely, high-throughput measurements such as flow cytometry, which have excellent statistical properties, are not suitable for the detailed tracking of the individual liposomes⁶⁹.

Besides, the degree of freedom and the accuracy regulating the external condition of liposomes under microscopic observation should be improved. Namely, since liposomes are floating as a colloidal dispersion, the liposomes dynamically flow away when some chemical stimuli are applied by mixing to another aqueous solution. A micro manipulator

is technically feasible to impose some chemical stimuli like osmotic stress while observing a specific liposome if throughput is not a concern^{53, 70}. However, accuracy could still be a problem: how can we regulate external concentration precisely with reproducibility. It depends on the skill of the experimenter, and it is not desirable for the adequate progress of science. Moreover, once a certain chemical stimulus is imposed, it is difficult to remove the effect of the stimulus even when one wants to add another stimulus. Preparing liposomes with biotin-modified lipid and immobilizing them via streptavidin on the biotin-modified glass slide can be a solution⁷¹. The method enables the precise exchange of the outer solution for a specific liposome of interest repeatedly, precisely, and completely. However, the state in which the liposomes are chemically anchored to the glass slide can be another factor of an artifact or is not suitable for some specific research interests, such as the study of deformation.

The development of microfluidic technology can provide another solution⁷². In cell biology, to meet the requirement of single-cell analysis and manipulation, the use of microfluidic devices has been explored⁷³⁻⁷⁵. The microfluidic device has recently been developed for multi-cellular systems. For example, Skelley and her colleagues enabled selective pairing of two different cells while arraying thousands of cells⁷⁶. Inspired by these trends, struggles to observe liposomes by arraying them under a microfluidic condition started^{57, 77, 78}. The wide distribution of the size of the liposomes in a dispersion compared to that of cells reduces the actual throughput if we intend to control the effect of diameters. Kazayama and his colleagues integrated size-sorting mechanics^{79, 80} and arraying structure in one microfluidic device enabling the parallel measurement of hundreds of liposomes with uniform diameters in one field of view⁵⁹. In these microfluidic devices, liposomes are trapped in the microstructures under a steady external

flow. Adding to the expectation of the positive effect of a steady flow environment, as discussed in chapter 1, the continuity of the substrate feeding and its flexibility should also be emphasized. Namely, by changing the kind of solution introduced into the device, the external condition can be switched repeatedly, precisely, and completely, as same as the immobilizing strategy. These technical advantages are promising for the investigation of sustainability in the reconstituted liposomes.

However, considering the trial to achieve sustainable dynamics combining multi-component chemical reactions, exhaustive searching for the optimal experimental parameters would be required. For example, what stimuli should be imposed on the liposomes, in what order, and at what intensity? The optimal solution could be changed depending on the state of the liposomes. No wonder, finding the optimal condition requires time-consuming trials and Herculean efforts of the experimenters, and tired human tends to be error prone⁸¹. Besides, the more complex the protocol, the more human errors tend to increase. Since the reproducibility of the protocol is the core of all scientific activity, the problem should be addressed.

This chapter provides an automated experimental platform for the direct observation of cell-sized liposomes based on the microfluidic device (termed as “MANSIONs”). MANSIONs consists of two microfluidic devices (termed mixing device and arraying device) connected to the syringe pumps through electric valves. The devices are placed on the microscopy stage. The peripherals of microfluidic experiments (microscope, stage, shutter unit, syringe pumps, and valves) are regulated through an in-house-developed program linking to the image analysis program. Thus, MANSIONs enables interactive controls of the external condition with feedbacks of the taken microscope images. First, the designs of the used microfluidic devices and plumbing are described. Next, the

performance of each microfluidic device and the whole system is demonstrated.

2.2. Materials and method

Chemicals

1-Palmitoyl-2-oleoyl-*sn*-glycero-3-phosphocholine (POPC) and 1-palmitoyl-2-oleoyl-*sn*-glycero-3-phospho-(1'-rac-glycerol) (sodium salt) (POPG) were purchased from NOF Corporation (Tokyo, Japan). Cholesterol was provided by Avanti Polar Lipids. Texas Red® 1,2-dihexadecanoyl-*sn*-glycero-3-phosphoethanolamine (triethylammonium salt) (Texas Red DHPE) was supplied by Thermo Fisher Scientific, Inc. (Waltham, MA, USA). Fructose, uranine, sodium hydroxide, methanol, and chloroform were purchased from FUJIFILM Wako Pure Chemical Corporation (Osaka, Japan). Fluorescent microbeads (Fluoresbrite® YG Microspheres, Calibration Grade 1.00 µm) were provided by Polysciences, Inc. (Warrington, PA, USA). All materials were used without further purification.

Fabrication of microfluidic device

The microfluidic devices used in this study were designed with commercially available software (Tenner Inc., L-Edit). The device design was transferred to a photomask using a mask-less lithography system (Nano System Solutions, D-Light DLS-50). Ultraviolet light was irradiated to SU8-3010 or SU8-3100 (MicroChem Co.) plated on a silicon wafer through the photomask to obtain a master mold. The height of the master mold was measured by a contact-type surface profiler (ULVAC, Dektak 6M). Polydimethylsiloxane (PDMS)-based resin (Dow Corning, SilPot 184) was poured onto the master mold with a curing agent (Silpot 184 CAT) and then heated on a heat plate

(75 °C) for more than 2 h. The cured PDMS block was separated from the master mold, and only the necessary parts were cut out. The obtained PDMS channels were perforated and then bonded quickly with glass slides (Matsunami Glass Industries, 0.25–0.35 mm in thickness) after O₂ plasma treatment (SAMCO, FA-1). Two-step plasma treatment was adopted: 25 W, 20 cc/min, 2 min for glass slide only, and then 25 W, 20 cc/min, 5 sec for glass slide and the PDMS channel (SAMCO, FA-1). The microfluidic device was then heated on the heat plate (75 °C) for more than 1 h.

General procedure to prepare the liposome dispersion

Stock solutions of POPC (40 mM in chloroform; 50 µL), POPG (4.44 mM in chloroform; 50 µL), cholesterol (4.44 mM in chloroform; 50 µL), Texas Red DHPE (14.5 µM in chloroform; 83 µL), and fructose (40 mM in methanol; 50 µL) were mixed in a glass vial. The organic solvents were removed with a rotary evaporator (EYELA, N1110V) and then dried under reduced pressure at 40 °C for 1 h to prepare a dry lipid film. The film was gently agitated with 2 mL of Milli-Q water in a thermostatic incubator (WAKENYAKU, MODEL 2290) under 40 °C for 1 h. Then, the liposome dispersion was placed into the thermostatic incubator under 26 °C for more than 10 h. The liposome dispersion used for the microfluidic experiments was diluted three-fold by 1 mM fructose solution and incubated at 26 °C for more than 1 h, and then the diluted dispersion was filtered by a nylon mesh filter (Merck Millipore Ltd., NY2002500) with a pore size of 20 µm four times to avoid the clogging in the microchannel, the height of which is approximately 16 µm. The filtrated liposome dispersion was placed in the thermostatic incubator under 26 °C for more than 3 h.

General procedure for the initial setup of the microfluidic devices

For the arraying device, a 1 mM fructose solution was introduced into the device from the outlet at $3000\ \mu\text{L h}^{-1}$ through the tube for the outer solution. When the solution reached the inlets and a droplet was formed in the vicinity of the inlets, the tube was re-connected to the inlet for the outer solution, and a guide tube was connected to the outlet for the drain. Subsequently, a tube for the liposome dispersion was connected to the device with flowing liposome dispersion to prevent trapping air in the device. The tube of the liposome dispersion was dammed back by changing the valve position to impose inner pressure to remove the small bubbles inside the device (see also chapter 2.3.3.). After the aqueous solution filled the device, the flow rate of the outer solution was set to $1000\ \mu\text{L h}^{-1}$, and the tube of the liposome dispersion was connected to the arraying device by valve manipulation as described above. The flow rate was slowed down to $300\ \mu\text{L h}^{-1}$ (1 min), $100\ \mu\text{L h}^{-1}$ (1 min), and finally $40\ \mu\text{L h}^{-1}$. The typical flow rate of the liposome dispersion was $6.5\ \mu\text{L h}^{-1}$. The same procedure was applied to the mixing device.

Image acquisition

Microscope images were taken using an inverted microscope (Olympus, IX71) equipped with a cooled charge-coupled device camera (Olympus, DP72) through commercially available software (Molecular Devices, MetaMorph). The shutter unit (Ludl Electronic Products Ltd., Mac 6000) and the electric stage (Sigma koki) were also controlled through MetaMorph. We wrote an ad-hoc regulating code of MetaMorph, called a journal. For the epi-fluorescence microscopy image, a dual-band excitation filter (excitation: 490–505 nm, 560–580 nm; emission: 515–545 nm, 600–650 nm) was typically used.

Observation of flow in an occupied nest

The green fluorescent microbeads dispersion (1 μL) was diluted to 5 mL by 1 mM fructose solution to afford a microbeads dispersion. The liposome dispersion was prepared, and the arraying device was set as explained above. After a moderate number of liposomes were trapped in the nests, the valve position was changed to shut off the flow of the liposome dispersion. After 5 min, the valve position was changed again to exchange the outer solution from a 1 mM fructose solution to the microbeads dispersion. The exposure time was 300 msec, and the flow rate was 40 $\mu\text{L h}^{-1}$. Because of the low density of microbeads and fast flow, we observed the stroboscopic images for the trace of microbeads instead of the streamline inside the occupied nest.

Observation of flow upon the abrupt stop of the flow

The green fluorescent microbeads dispersion (25 μL) was diluted to 5 mL by Milli-Q water. The dispersion was introduced into a microfluidic device, and a movie was captured with the optical exposure time of 300 msec.

Typical procedure for the image analysis

The areas of the trapping microstructure (termed nests) were detected through Hough transformation of the binarized bright-field image of the trapping region taken in advance. In the current arraying device, there were 28 nests in one field of view. When the fluorescence image was taken, the red channel of the image was separated and decomposed into 28 small binarized images based on the location of each nest. We adopted Otsu's method for binarization. If only one object with moderate size and

circularity was in the decomposed image, it was judged as a liposome. The binarized image was also used as a mask of the original image to measure the value of the liposomes. Size, centroid, and averaged intensity of each channel (blue, green, and red; abbreviated as BFI, GFI, and RFI, respectively) were recorded repeatedly. Time zero was determined as the time when the Python program was started.

Estimation of the water permeability

The diameter of each liposome was calculated from the value of their area. The decay of the diameter of the liposome under a hypertonic solution was described as follows ⁸²:

$$\frac{dR}{dt} = -P\alpha\Delta C$$

, where R is diameter, t is time, P is water permeability, α is the molar volume of water (18 mL mol^{-1}), and ΔC is the difference of the concentration. We calculated the water permeability by the linear regression of the time course of the diameter taken during 1900–2400 sec. Only liposomes having full data points during the time range were measured.

Mann-Whitney's U-test

Owing to the uncertainty of the noise distribution, we chose the non-parametric Mann-Whitney's U-test for the statistical analysis, in which the data sets ($k = 1, 2$) were ranked (r_{kn}) by their calculated concentration. The statistic index (U_k) was calculated based on the number of samples (N_k) and the sum of the rank for each data set ($R_k = \sum_{n=1}^{N_k} r_{kn}$). In our experiments, the number of samples was sufficient to calculate the p-value as the probability of Z_k distributed as a normal distribution:

$$U_k = N_1 N_2 + \frac{N_k(N_k + 1)}{2} - R_k$$

$$Z_k = \frac{\left| U_k - \frac{N_1 N_2}{2} \right|}{\sqrt{\frac{N_1 N_2 (N_1 + N_2 + 1)}{12}}}$$

2.3.Design of the experimental system

2.3.1. Design of the arraying device

The arraying device consists of two major regions. One is the size-sorting region, and the other is the trapping region (Figure 2. 1). Namely, the liposomes introduced into the arraying device are first sorted by their diameter, and then only liposomes with targeted diameter can enter the trapping region.

The size-sorting region was designed by referring to previous reports^{79, 80}. Here we summarized the essence of the principle and the design. Flow field bifurcates when flowing among the periodically arrayed micro-posts (Figure 2. 2). The height of the bifurcation (D_c) is determined by the row shift fraction (ε) and the gap between each micro-post (g):

$$D_c = g \left[1 + 2w + \frac{1}{2w} \right]$$

$$w^3 := \frac{1}{8} - \frac{\varepsilon}{4} \pm \sqrt{\frac{\varepsilon}{16} (\varepsilon - 1)}$$

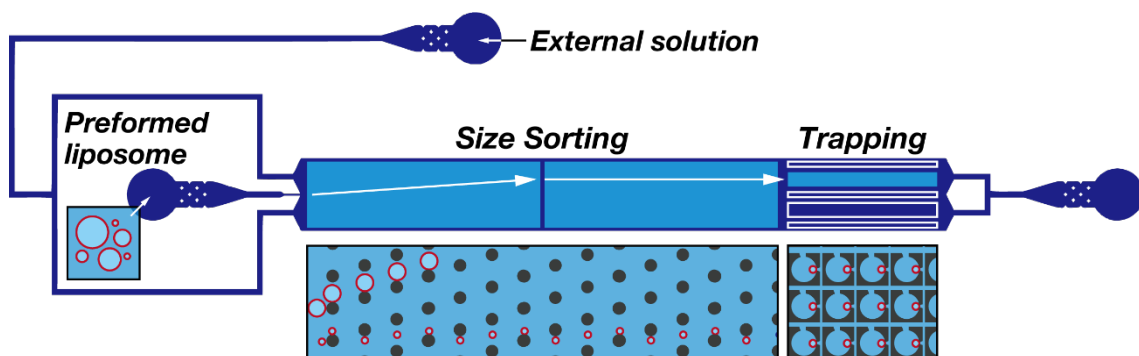


Figure 2. 1 Schematic illustration of the arraying device. The trajectory of the liposomes of the desired diameter was indicated in the white arrows. The white boxes at the rear part of the device represent the dummy traps to equalize the flow resistance. Schematic pictures of each part of the device were shown under the corresponding areas.

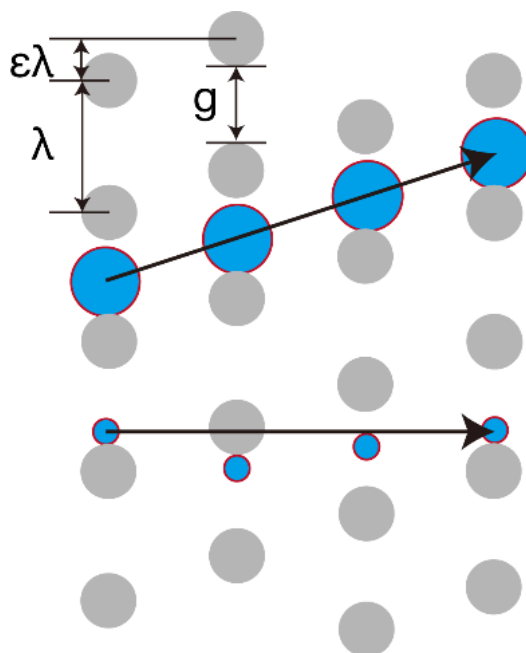


Figure 2. 2 A schematic illustration of the mechanism of the size-sorting. Black arrows represent the trajectory of the liposomes (red circles filled with blue) flowed in the micro posts (gray circles).

Small particles can swim straight among the micro-posts according to the flow of their center of mass positions (zig-zag mode). On the contrary, the center of mass of a particle with a diameter larger than D_c shifts to the upper side of the device because of the excluded volume when collides with the micro-post. As a result, large particles travel obliquely upward (bump mode). The principle is termed as deterministic lateral displacement (DLD)⁷⁹. By combining two DLD mechanics, only particles within a targeted diameter range can be guided to a specific height (see Figure 2. 1). For the device used in this chapter, the design parameters were $g = 40 \text{ } \mu\text{m}$, $\varepsilon_1 = 1/17$, and $\varepsilon_2 = 1/16$, respectively. The theoretical range of the targeted diameter was 11.8–12.2 μm .

On the other hand, the trapping region was newly designed to track the liposomes of interest stably even when the external flow field was stopped. Microfluidic devices which trap liposomes by the external flow field inevitably impose the continuous shear to the trapped liposomes. However, the shear is known to disturb the membrane and change the features of liposomes such as permeability^{58, 83, 84}. Simple stoppage of syringe pumps tends to cause transient backflows or other undesired and uncontrollable perturbations of the flow field, especially in a device with narrow channels. Thus, in the arraying device, circular microstructures (100 μm in diameter; termed as “nest”) were arrayed, which enable the occupational trap of only one liposome within a nest. The large space was adopted to slow down the flow inside, realizing a stable tracking even under transient backflows caused by the stoppage of the flow field.

The principle to accomplish the occupational trap is as follows. The flow at the entrance of the nest bifurcated into a trap path and a bypass path (Figure 2. 3-a). When the nest is empty, the fluid resistance of the two paths is equivalent, allowing the liposome to enter the nest. However, when a liposome is trapped in the nest, the balance of the fluid

resistances is broken because the trapped liposome increases the resistance of the trap path. Consequently, the amount of flow coming into the nest is reduced. In other words, the first trapped liposome reduces the bifurcation height at the entrance. Thus, the deterministic exclusion of the secondary liposomes is achieved since the center of mass is too large to enter the nest due to the size-sorting region at the rear part of the device: only liposomes within the targeted diameter range are introduced into the trapping region. Figure 2. 3-b summarized the principles described above.

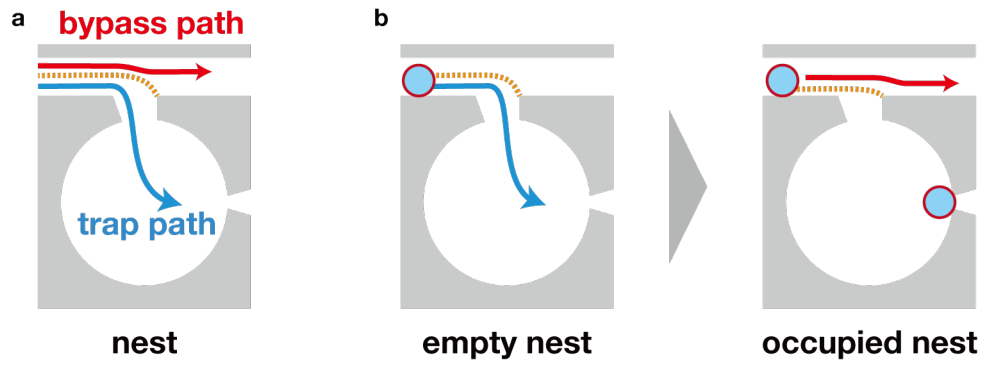


Figure 2. 3 Schematic illustrations of trapping structure. (a) Terminologies used in the paper, (b) Mechanism how to trap only one liposome in one nest. Orange dashed lines indicate the critical flowline of the bifurcation at each condition.

For the practical arrangement of the nests in one field of view, the most critical parameters are the shape of the entrance and exit of each nest and the horizontal (H) and vertical (V) lengths between the nests.

To keep the parameter space small, we first determined the parameters which do not require experimental trials. First, the diameter of the nest was fixed to 100 μm , which was large enough to slow down the flow in the nest. Second, the horizontal width of the exit is determined to 8 μm , considering the structural limitation on the aspect ratio (>0.5) and efficient alignment of nests in one observation field. Third, the width of the front side of the nest exit was determined to 3 μm because, according to the previous report, the gap size of the trapping structure is desirable to be 20–25% of the targeted diameter.

With these fixed design parameters, first, we optimized the shape of the exit of the nest. The flow in the trap path bifurcates again after going through the exit, and these bifurcated paths are not strictly symmetric, which made the accurate estimation of the total flow resistance of the trap path difficult. For simplicity, we assumed that the flow resistance of the trap path was determined only by the resistance of the exit of the nest. It seemed plausible because the width of the contacting part is much smaller than that of the other channels. We also assumed that a flow in the microfluidic channel was a Hagen-Poiseuille flow. To estimate the initial parameter for further experimental optimization, we relied on the following theoretical consideration about the proportion of the two flows bifurcated into two channels with different flow resistances⁸⁵.

Pressure drop (Δp) when a fluid with fluid viscosity of μ and volumetric flow rate of Q passes through a rectangular channel with a length of L , a cross-sectional area of A , and a perimeter of P was expressed as:

$$\Delta p = \frac{C(\alpha) \mu L Q P^2}{32 A^3}$$

, where $C(\alpha)$ is a constant determined by the aspect ratio (α). In our case, the channel was not a rectangle but a trapezoid. Thus, the expression of the pressure drop is arranged in an integral form:

$$\Delta p = \frac{\mu Q}{32} \int_0^L dl \frac{C(\alpha(l)) P(l)^2}{A(l)^3}$$

When the maximum width in the channel was smaller than the height of the channel, α is constant. Since P and A are linear functions of l , the integral can be analytically solved. For a flow bifurcated into path 1 and path 2 and then merged after that, pressure drops at each path should be balanced. Thus, the proportion of volumetric flow rate (Q_1/Q_2) is written as:

$$\frac{Q_1}{Q_2} = \frac{\int_0^{L_2} dl \frac{P_2(l)^2}{A_2(l)^3}}{\int_0^{L_1} dl \frac{P_1(l)^2}{A_1(l)^3}}$$

Based on these discussions and constraints, the promising width of the rear side of the trapezoid was estimated at around 11 μm . After the experimental optimization, we determined the value as 10 μm .

Next, H and V were experimentally optimized. The constraint was that the width should be large enough not to be clogged by the induced liposomes inside the channel. According to the previous report⁵⁹, because of the deformability of liposomes, the average diameter of size-sorted liposomes was slightly larger than that of the theoretical value (for example, 13.8 μm while the theoretical value was 11.8–12.2 μm). Integrating with consideration of the effective alignment of the nests in one field of view, H and V were experimentally determined as 14 μm and 16 μm , respectively.

Besides, for the shape of the entrance of the nest, a trapezoidal shape worked better

2.3.2. Design of the mixing device

Mixing devices are roughly classified into active and passive mixer⁸⁶. Active mixers apply external driving forces such as electrical force, magnetic force, pressure, or so on^{87, 88}. In contrast, passive mixers adopt microchannels enhancing the passive diffusion⁸⁹. Generally, active mixers are advantageous in throughput but require additional machines to regulate external forces. To keep the number of peripherals as small as possible, we adopted a passive mixer.

The fundamental strategy of passive mixers is chaotic advection^{90, 91}. When the Reynolds number (Re) is low, the flow is laminar flow with little turbulence⁹². As the expression of Re shows, the Re is typically low in microfluidic devices:

$$Re = \rho VL/\nu$$

, where ρ is the density, V is the average flow velocity, L is the hydraulic diameter, and ν is the viscosity. Thus, to mix two solutions efficiently in the microfluidic device, perturbations of flow are necessary. Numerous previous reports adopted non-planer 3D channels to enable a large magnitude of mixing by chaotic advection, but technical complexity was the problem⁸⁹. On the other hand, one of the most straightforward implementations of a passive mixer is meandering. Dean vortices and separation vortices, which are generated in a curved microchannel, enables efficient mixing⁹³. Similarly, periodic barriers also enhance mixing efficiency⁹⁴.

As the required throughput for our system was at most several minutes, we prioritized the simplicity of the design, which could bring the reproducibility in the fabrication process. Thus, we designed the mixing device according to the previous literature adopting periodic barriers⁹⁵. The design parameters were shown in Figure 2. 5. The length and width of the channel were experimentally optimized.

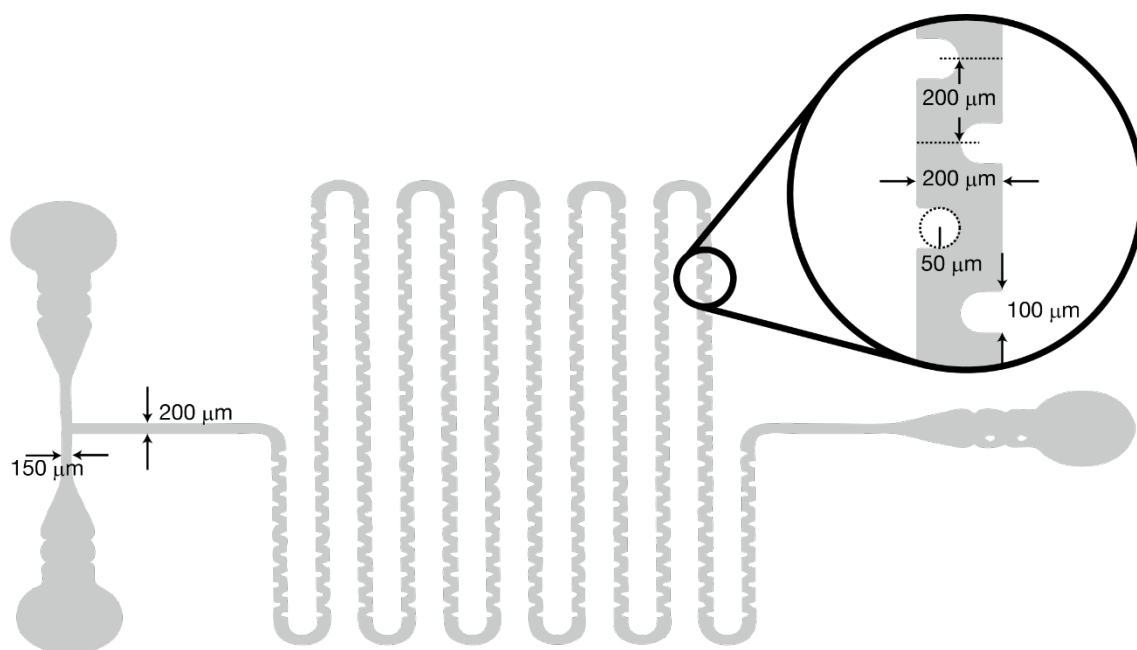


Figure 2. 5 Graphical summary of the design of the mixing device.

2.3.3. Design and schema of the automated observation platform

Overview of the system.

Schematic illustration and the picture of the whole setup was shown in Figure 2. 6. The arraying device and the mixing device were connected to the syringe pumps through electrical valves. The valves regulated which pumps (or tubes) were connected to the devices and which were disconnected. Syringe pumps determined the flow rate. These valves and pumps were regulated via a computer. Peripherals of the microscope, such as electric stage, light source, shutter unit, and camera, were controlled through commercially available software (Molecular Devices, MetaMorph). An in-house-developed script called “journal” ran on MetaMorph, which determined when and where to take pictures. The overall behavior of the system was regulated via the Python scripts. The scripts performed image analysis for taken images. When certain criteria were achieved during measurement, the Python programs output grayscale images as a

regulation code for the microscope. Namely, the journal code running on the MetaMorph searched the folder at fixed intervals (per 0.5 sec) and read the grayscale images. The size of the images and their averaged gray value were recognized as the conditional expressions for the journal code. Besides, the pumps and the valves were directly regulated from the Python scripts via the serial communication. Note that because the valves were equipped with TTL regulation, the control of the valves was used a digital I/O terminal (Contec Co. Ltd., DIO-0808LY-USB). We named this integrated experimental platform for MANSIONs as an abbreviation of Machine-Assisted, Numerous, Simultaneous, and Interactive Observation of Non-equilibrium self-assembly.

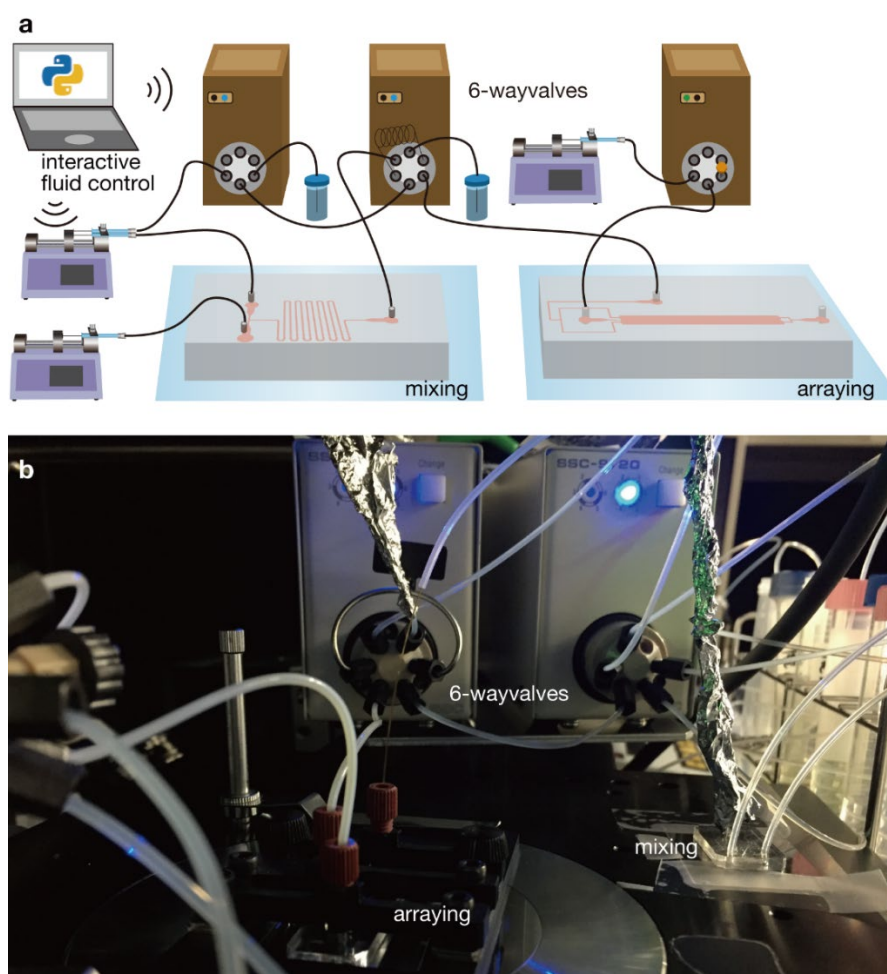


Figure 2. 6 The schematic illustration (a) and the picture (b) of the whole setup.

Summary of the plumbing and its design principle.

The geometrical connection of microfluidic devices, pumps, and valves was shown in Figure 2. 7-a. The valve used in MANSIONs is a two-way valve with six ports. Namely, there are three sets of connected channels, which can be connected in two different ways. Figure 2. 7-b described how each valve worked. Valve A switches the introduction of the liposome dispersion: the liposome dispersion flows in when the valve is in position 1 (top) and is dammed up when the valve is in position 2 (bottom). Valve B switches the insertion of the sample loop: when the valve position is changed from 1 to 2, the path to the microfluidic device goes through the sample loop. Since the content of the sample loop is arbitral, the external solution of the captured liposome can be freely changed. Valve C switches the flow of the external solution: the microfluidic device is connected to the syringe pump when the valve is in position 1 but to the atmosphere when the valve is in position 2. The inner pressure was immediately released to the atmospheric pressure, and thus the external flow stops suddenly. For the stable operation of MANSIONs, the air bubbles in the tubes should be carefully removed. In other words, the ports at the neighbor of the main tubes described above should not be open to air directly. Otherwise, some air bubbles possibly invade into the main channels directly connecting to the device during the valve exchanging collapsing the measurements repeated after that. The drain tubes were inserted in the falcon tubes or disposable syringes to prohibit the drying, which is critical to keep the whole plumbing filled with an aqueous solution even during the repeated valve manipulation.

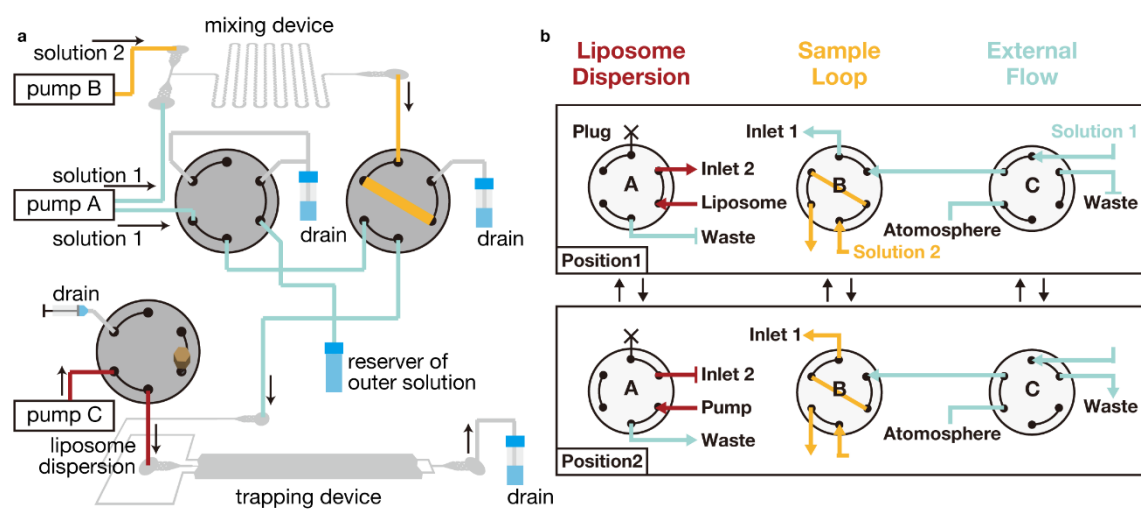


Figure 2. 7 The experimental setup of MANSIONs. Conceptual illustration of (a) plumbing and (b) roles of each valve.

Other ingenuities to improve the punctuality of the measurements.

We chose a fused silica tube ($\phi = 0.20$ mm) sleeved by an ethylene tetrafluoroethylene tube ($\phi = 0.33$ mm) for tubes directly connected to the device because the diameter of the fused silica tube is barely affected by a temperature shift and is homogeneous even for a narrow diameter (Figure 2. 8-a). When a fused silica tube narrower than 0.20 mm was used, the fluid resistance became too high to smoothly relax the pressure, resulting in backflows or unintended flow profiles when the state of the valves and pumps was changed. However, when a wider tube was used, the dead volume became too large to exchange the outer solutions quickly. As another important point of the setup of the system, the arraying device was housed by custom-made resin housing (Senshu Scientific Co., Ltd.) to have a better connection between the device and tubes (Figure 2. 8-b). Housing structure consisted of two parts: the part to put the arraying device (base) and the part to fix the tubes (adjuster). The adjuster was fixed to the base to fit the ports and the inlet/outlet. The insertion of the screws ensured verticality of the tube connection, resulting in a better adherence of the tube to the device and consequently improved the controllability of the flow. The contribution of the housing was apparent when the external flow was stopped for over 3 h after the trap of the liposomes.



Figure 2. 8 Pictures of the setup of tubes and the arraying device. (a) A typical setting of tubes connected to the arraying device. The fused silica capillary was sleeved by an ETFE tube. (b) Housing structure for the stabilize and reproducible connection.

2.4. Demonstration of the performance

2.4.1. Arraying device

First, the flow field was visualized in the vicinity of the nest by tracking fluorescent beads (Figure 2. 9). As the obtained streamline (green) showed, the flow bifurcated at the entrance. About half of the bifurcated flow in the trap path merged to the bypass path. Note that the latter half of the flow in the trap path merged with the bypass path at the next row. The bifurcation height was roughly estimated as 5–6 μm . Since the DLD adopted in the arraying device was designed to select 11.8–12.2 μm in theory, the current design was applicable to the further tests.

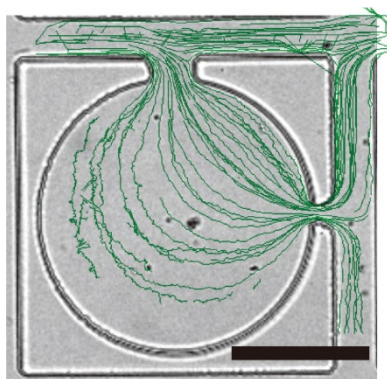


Figure 2. 9 Streamlines of microbeads flowing in the vicinity of the nest. Digitally generated streamlines (green) are depicted in the gray-scaled bright-field image of the nest. Scale bar: 50 μm .

Second, we tested if the mechanism described in 2.3.1 works as expected. The time courses of the number of nests that correctly trapped one liposome (trap number) and that trapped more than two liposomes (error number) were measured (Figure 2. 10). For the flow rate of the liposome dispersion, two conditions of 5.0 and 6.5 $\mu\text{L h}^{-1}$ were tried. The flow rate of the outer solution was fixed to 40 $\mu\text{L h}^{-1}$. After 200 min of the observation, trapped liposomes were flushed at 3000 $\mu\text{L h}^{-1}$. Note that the experiment was conducted six times (represented in different colors) for each condition automatically. The following

were common tendencies: the trap number rapidly increased in both flow rates of the liposome dispersion, while the error number increased only stochastically and slowly. Besides, the average diameter was consistent with the theoretical expectation (theory: 11.8–12.2 μm , measured: 11.7 μm (5.0 $\mu\text{L h}^{-1}$) and 12.7 μm (6.5 $\mu\text{L h}^{-1}$)), and the coefficient of variation (CV) was moderately narrow (CV<10%). Thus, the results well demonstrated the mechanism explained above.

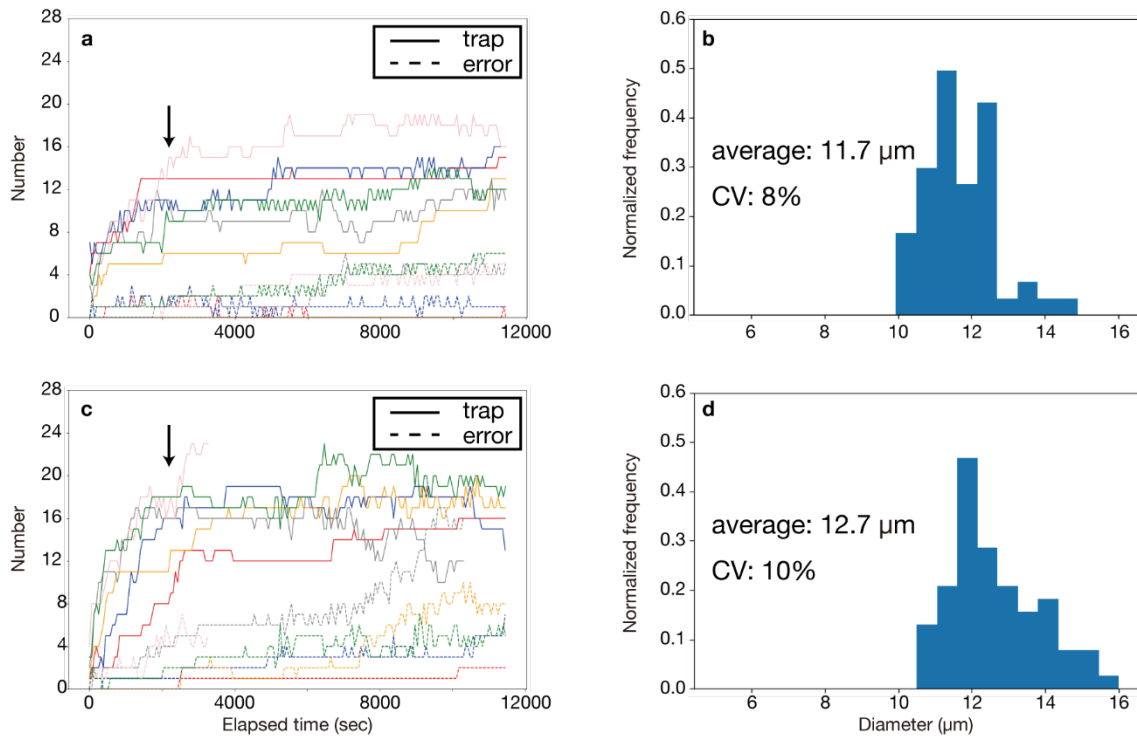


Figure 2. 10 Verification of trapping mechanism. Time courses of the trap number (solid line) and error number (dashed line) and corresponding histograms at each time point, which was indicated as black arrows. The flow rate of the liposome dispersion was 5.0 $\mu\text{L h}^{-1}$ for (a) and (b), and 6.5 $\mu\text{L h}^{-1}$ for (c) and (d). Plotted lines with the same color were generated from the same experiment.

A representative fluorescence image was shown in Figure 2. 11. One typical cause of trapping an unintended secondary liposome in an occupied nest is liposomes with a larger diameter than the targeted value. These liposomes could stochastically slip into the trapping region because of their deformability or interaction with other liposomes in the size-sorting region. When the bypass path was clogged to some extent by these large liposomes, the fluidic resistance of the bypass path increased. As a result, the flow resistances of the trap path and the bypass path could be balanced even for the occupied nest. The number of liposomes introduced into the trapping region per unit time corresponded to the flow rate of the liposome dispersion. In other words, liposomes with the untargeted diameter were more frequently introduced into the trapping region at a high flow rate. Thus, it was expected that the error number and the flow rate were positively correlated. This consideration was consistent with the results shown in Figure 2. 10 in the view of the time course and the average diameter. Namely, for $6.5 \mu\text{L h}^{-1}$ of the liposome dispersion, the trap number increased more quickly and then tended to be unchanged at a higher number (~ 16) than that of $5.0 \mu\text{L h}^{-1}$ (~ 10). Besides, the mean diameter of liposomes trapped at $6.5 \mu\text{L h}^{-1}$ was $12.7 \mu\text{m}$, which was larger than that of $5.0 \mu\text{L h}^{-1}$ ($11.7 \mu\text{m}$). Thus, for the accuracy of trapping, a more diluted liposome dispersion was desirable, but it resulted in low throughput of the experiments. In our case, the three-fold-diluted liposome dispersion was adopted as the best condition for compatibility with accuracy and throughput. The other cause for the increase of error number is that the trapped liposome was too small to dam up the flow into the trap path, or the secondary liposome was small enough to invade the occupied nest. These small liposomes are generated by rupturing the outer membrane of multilamellar liposomes with the target diameter during size sorting or after being trapped. This kind of error was

difficult to prevent by the current device design. Besides, once the nest was occupied by more than two liposomes, it rarely returned to a nest trapping only one liposome afterward. Thus, the error number tended to increase monotonically. Therefore, it was practically efficient to introduce liposomes at a high flow rate ($6.5 \mu\text{L h}^{-1}$) and stop the introduction after a moderate number of liposomes are trapped (typically 10–14).

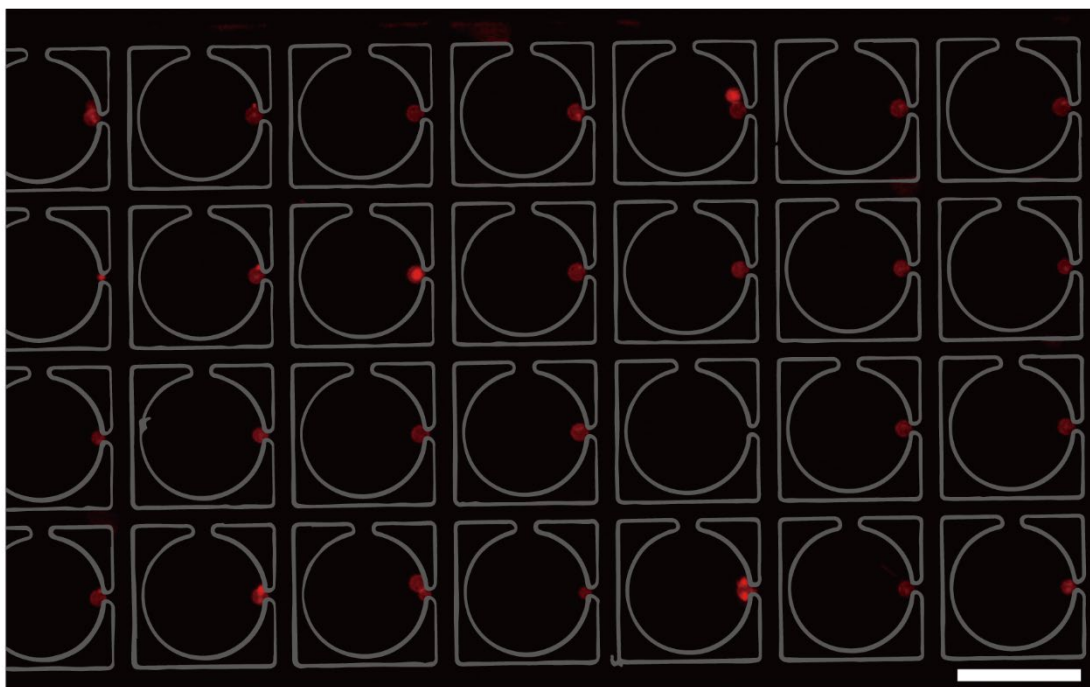


Figure 2. 11 Representative fluorescence microscopy image of the trapped liposomes in one field of view. Large circular structures to trap the liposome are overwritten in gray lines. Scale bar: 100 μm .

Finally, we confirmed that the small molecules could be rapidly supplied even in the occupied nest. We measured the green fluorescence intensity of the background (GFI_{BG}; measured for a small rectangular area at the center of each nest) for both occupied and empty nests during the exchange to the 15 μM uranine/1 mM fructose solution (Figure 2. 12). After a moderate number of liposomes were trapped in the nests, valve A was switched to shut off the flow of the liposome dispersion. After 5 min, valve B was

switched to exchange the outer solution from a 1 mM fructose solution to a 15 μ M uranine/1 mM fructose solution. The process of substitution was recorded as an AVI movie (3 frames/sec). The GFI_{BG} was manually measured by the freely available software ImageJ (National Institutes of Health, USA) for more than 10 nests for both occupied and empty nests. The time course of the GFI was plotted from 250 sec after valve B was changed. As the average time required to achieve the half intensity of the value at 340 sec, no significant difference was confirmed between the kinetics of exchanging in the occupied and empty nests.

Taken these results together, we concluded that the arraying device performed as we designed and was applicable to further research as a part of the automated platform for the direct observation of cell-sized liposomes.

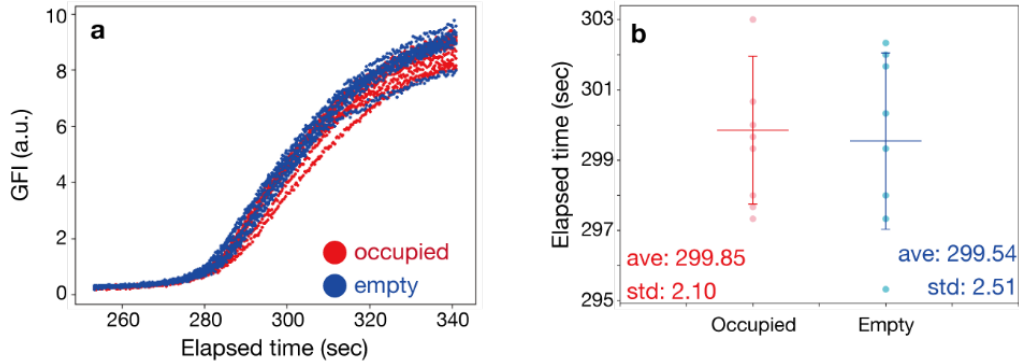


Figure 2. 12 Comparison of the exchange kinetics of uranine in occupied and empty nests. (a) Time course of GFI of each nest plotted from 250 sec after the beginning of the exchange. Red and blue dots denote the result of occupied and empty nests, respectively. (b) The time required to achieve half the intensity at the final data point (elapsed time = 340 sec). Pale colored dots (pink and cyan) denote all of the measured data, and intensely colored bars (red and blue, respectively) denote the averaged values (ave) with the standard deviations (std).

2.4.2. Mixing device

We introduced 200 μM uranine solution and Milli-Q water into the mixing device with different flow rates. Two solutions contacted at the T-junction were then mixed in the curved channels disturbed by the periodic obstacles. The mixing efficiency was quantified from the microscopic fluorescence image taken in the vicinity of the outlet (Figure 2. 13).

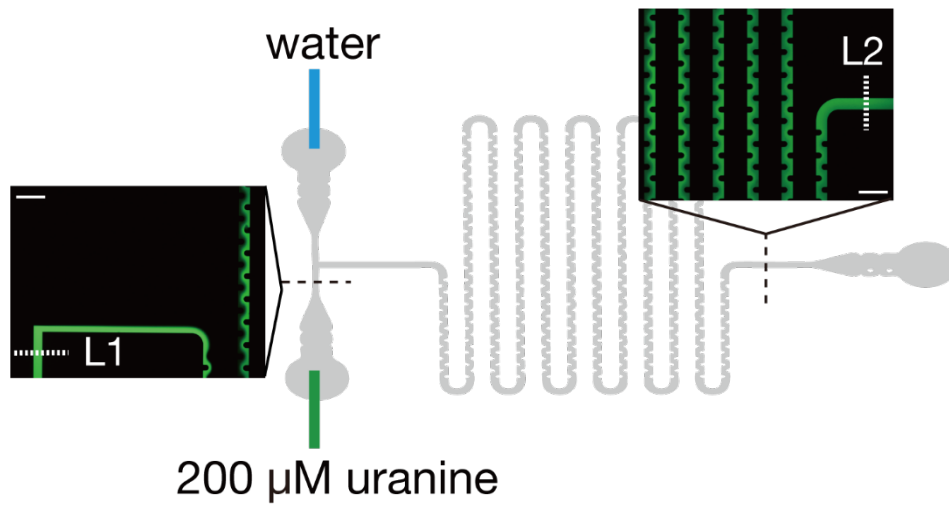


Figure 2. 13 Sketch of the experimental settings to evaluate the performance of the mixing device.

The representative fluorescence microscopy images at the point indicated in the black dashed lines are shown. White dashed lines indicated as L1 and L2 correspond to the regions used to evaluate the mixing efficiency. Scale bars: 500 μm .

To quantify the performance of the mixing, two indices (flatness (φ) and asymmetry (ε) index), were defined as follows:

$$\varphi(r, v_{tot}) = 1 - \int_0^h \frac{|k(l) - k_{ave}|}{|k_{ave}|} dl$$

$$\varepsilon(r, v_{tot}) = \frac{\left| \int_0^{h/2} k(l) dl - \int_{h/2}^h k(l) dl \right|}{|k_{ave}|}$$

, where r and v_{tot} are the programmed ratio and sum of the flow rate of the two solutions, respectively, and $k(l)$ is the relative GFI at the position l on the L2 normalized by the GFI of the unmixed fluorescent solution at L1. The subscript “ave” denotes the average of the relative intensity over the width of the channel. The asymmetry index is defined to distinguish a wavy line profile from an asymmetric line profile indicating poor mixing. In one measurement (represented as one red dot in Figure 2. 14), five consecutive images were used to calculate the average value. The experiments were repeated independently three times for each condition, and the average and standard deviation of the three cycles of experiments were plotted as a blue dot with its error bar in Figure 2. 14.

First, the ratio of the flow rate of the two solutions (r) was fixed at 0.1, which is the smallest ratio to avoid pulsating flow, and the total flow rate (v_{tot}) was tested in the range of 50–400 $\mu\text{L h}^{-1}$ for every 50 $\mu\text{L h}^{-1}$ (Figure 2. 14-a, c). As a result, the mixing efficiency got worse at a high flow rate, while at a low flow rate, the reproducibility got worse. Thus, v_{tot} was fixed at 200 $\mu\text{L h}^{-1}$. Second, the dynamic range of the mixer was investigated (Figure 2. 14-b, d). We found that at a low mixing ratio, the mixing efficiency strikingly got worse. Thus, the dynamic range was determined as 30–70%. We note that the average GFI was linear in the region we tested (Figure 2. 14-e). These experiments were conducted in an automated manner.

Taken these results together, we concluded that the mixing device performed as we designed and was applicable to further research as a part of the automatic platform for the direct observation of cell-sized liposomes.

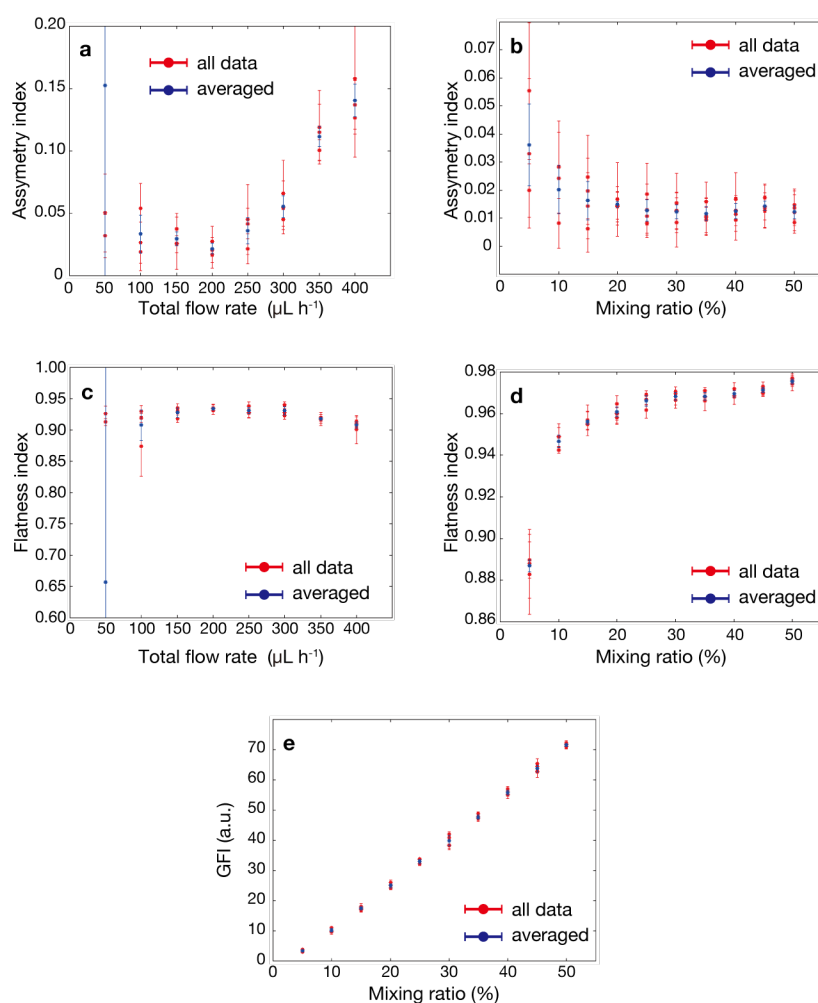


Figure 2. 14 Evaluation of the performance of the mixing device. Plots of (a, b) asymmetry index, (c, d) flatness index, and (e) average GFI. (a, c) are plotted to the total flow rate, and (b, d, e) are plotted to the mixing ratio. Red, blue, and black dots denote the average value of five images taken every minute, the average of three red dots, and data measured for the manually mixed solution, respectively. For (a) and (c), one red dot is outside of the plotted area at 50 $\mu\text{L h}^{-1}$ for graphical readability: asymmetric index = 0.38, and flatness index = 0.13.

2.5. Automated observation of liposomes upon an osmotic stress

In the last section, we individually verified the performance of the arraying device and mixing device, and they can be proceeded automatically to repeat the same protocol several times. In this section, we combined all the peripherals as one experimental platform, MANSIONs, and demonstrated its performance.

One of the typical strategies in microfluidic explorations was to trap liposomes and impose some chemical stimuli on them^{59, 71, 96}. Microfluidic devices can provide accurate control of the external condition, precise tracking of liposomes of interest, and high-throughput measurement. However, at least several pre-investigations to determine the kinds or strength of the stimuli imposed on the liposomes are required, which limit the total throughput of the experiment. Automation of the experiment, including the pre-investigation to determine the optimized condition, could improve the situation.

There is general reciprocity between the strength of the stimuli and the accuracy of the measurement. When the strength of the stimulus is too strong, some unintended side effects could be caused due to the inherent nature of drugs, while too weak stimulus only resulted in a boring result. Osmotic stress is also a simple side effect, which is recently pointed out as significant stress related to senescence in cell biology⁹⁷. Besides, in the view of liposome investigation with microfluidics, volume shrinkage of liposomes under the osmotic stress is technically non-negligible. Namely, when the volume of liposomes become small after the trap, the liposomes would slip out from the nest. Thus, the optimization of the strength of the chemical stimuli would be a good demonstration of MANSIONs. As the simplest demonstration, we measured the volume decay of liposomes under a hypertonic solution.

First, the concentration of the hypertonic solution was optimized. As described, if the

concentration is too high, the trapped liposomes would be lost (modeled side effect). Conversely, only a small change of the volume would be obtained when the concentration is too low, (modeled boring result). Here, the optimized concentration was determined as the highest concentration at which the number of trapped liposomes after 30 min of stimuli (N^*) was larger than the half number of the initial liposomes (N). We adopted the binary search method: If $X(t)$ mM of the hypertonic solution was judged as too high ($N^* < 0.5 N$), the intermediate value of $X(t)$ and maxima of the lower limit of the concentration (MaxL) was tested at the next step ($=X(t+1)$). After that, the minimum of the upper limit (MinU) was updated to $X(t)$. Conversely, if $X(t)$ mM of the hypertonic solution was applicable ($N^* > 0.5 N$), the intermediate value of $X(t)$ and MinU was tested at the next step ($=X(t+1)$). After that, MaxL was updated to $X(t)$. This cycle was repeated while $X(t+1)-X(t) > 0.05$. In this case, 1 mM fructose solution and 3 mM fructose solution were introduced into the mixing device (dynamic range of the concentration was 1.6–2.4 mM): $X(t=0) = 2.4$, MaxL = 1, MinU = None. As a result, after the five cycles, the optimized concentration was determined as 1.83 mM.

Then, the osmotic response of the trapped liposomes was measured under 1.83 mM of fructose solution. After the exchange of the external solution, the following dynamics was monitored by time-lapse imaging. The interval was 1 min. Besides, as discussed above, the external flow, a cause of shear stress, is one of the inherent artifacts in the microfluidic measurement. Using the abrupt stop mechanics of MANSIONS, we investigated the effect of the external flow on the water permeability across the liposomal membrane. Namely, for the static flow condition, the flow was suddenly stopped after the exchange process was finished. The timing to start time-lapse and stop the flow were determined from the experiment shown in Figure 2. 12. The diameter was estimated from

the cross-sectional area of each liposome, and the water permeability was calculated from the decay rate of the diameter (see 2.2). The overall flowchart was summarized in Figure 2. 15.

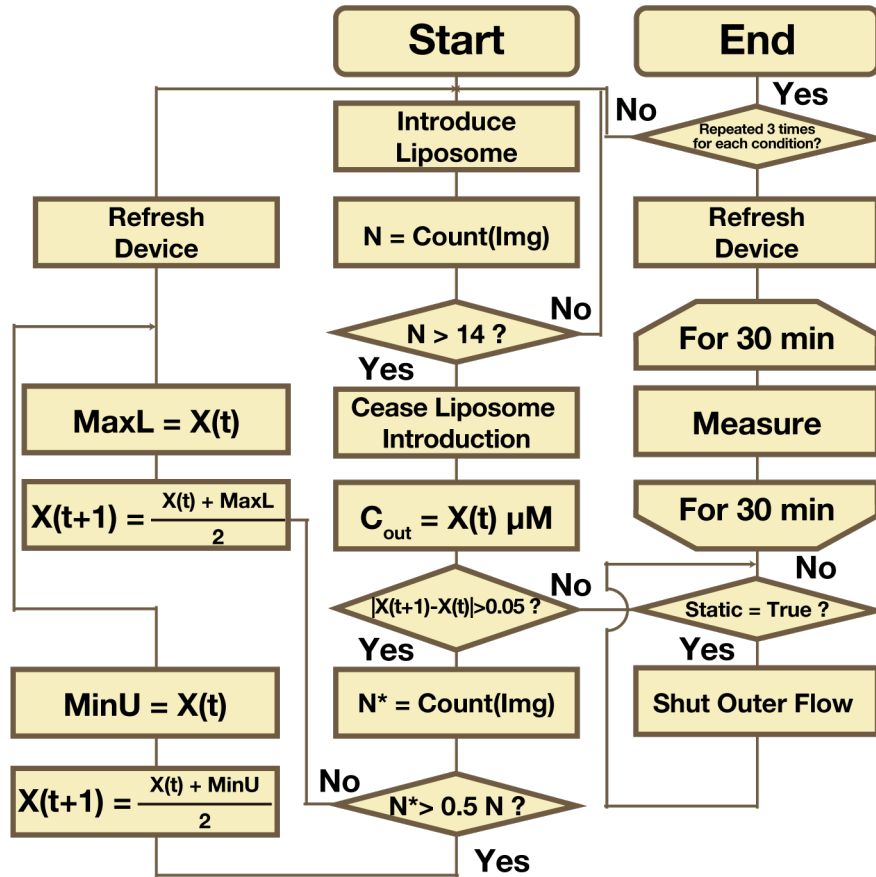


Figure 2. 15 Flowchart to measure the volume decay of liposomes under a hypertonic solution following the optimization of the concentration. Abbreviations used in the chart are as follows: Count(Img): Count the number of liposomes in the nests. X(t): Concentration of the hypertonic solution at t step (mM). C_{out}=X(t): Exchange the outer solution to X(t) mM. MaxL: maxima of the lower limit of the concentration. MinU: minimum of the upper limit of the concentration.

As a result, the time course of the volume decay was obtained (Figure 2. 16-a). In both cases, the diameter of the liposomes exposed to the hypertonic solution decayed to 94% of the initial value within 30 min. Averaged water permeabilities were $77.9 \pm 41.2 \mu\text{m s}^{-1}$ (n=25) for static condition, and $86.4 \pm 48.8 \mu\text{m s}^{-1}$ (n=26) for dynamic condition. The values were consistent with the previous reports⁵⁹. To statistically test if the external flow biased the kinetics, the distribution of water permeability of each liposome was compared (Figure 2. 16-b). Due to the uncertainty of the noise distribution, we adopted Mann-Whitney's U-test. These two distributions were not statistically distinguishable ($p = 0.47 > 0.05$). On the other hand, the trend in the correlation between initial diameter and permeability was slightly different (Figure 2. 16-c). The correlation coefficient was 0.02 in the static condition but was 0.37 in the dynamic condition. The results indicated that the larger liposomes tend to have higher water permeability although the effect of the external flow was not significant as an overall tendency. The insignificance of the shear stress in the overall trend was interpreted as a guaranty that the automated observation platform can be compatible with the conventional bulk experiments imposing some chemical stimuli on cell-sized liposomes.

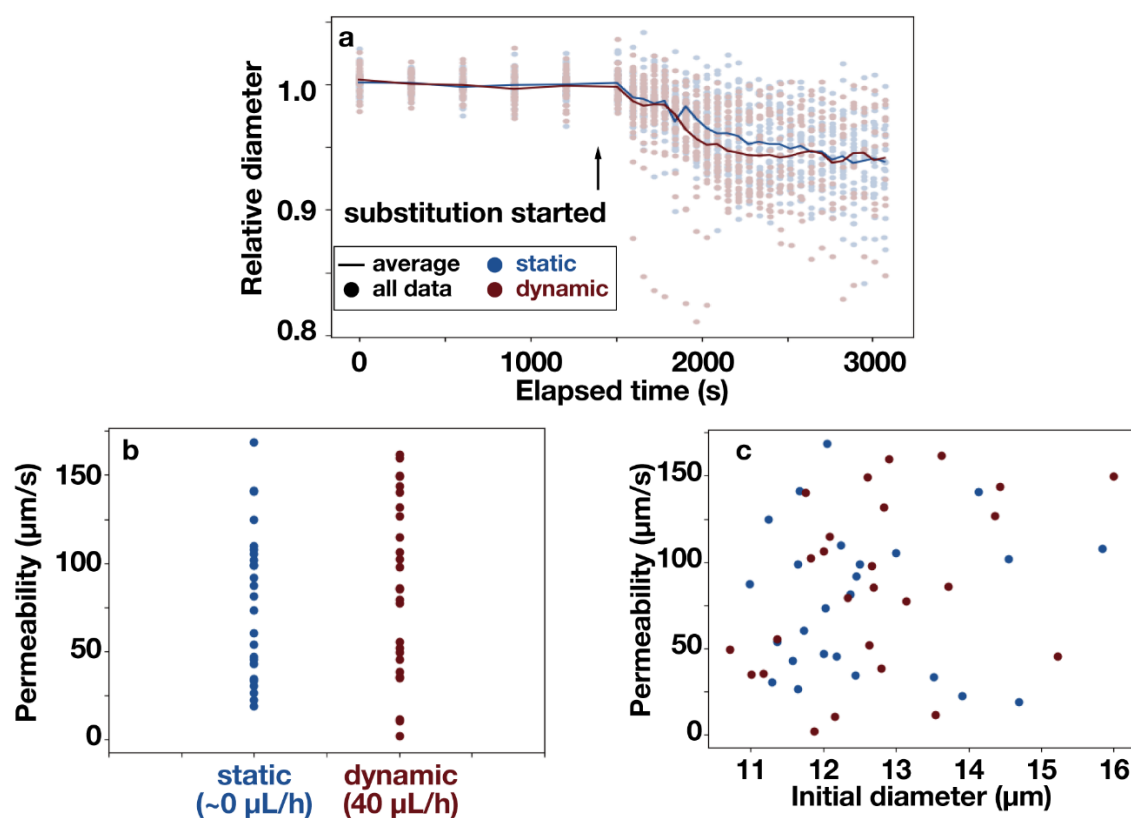


Figure 2. 16 Measurement of water permeability of the trapped liposomes. (a) Time course of the relative diameter exposed to the hypertonic fructose solution (normalized by their averaged values of the first five data point). Pale colored dots are the raw data, and the solid lines denote the averages. The black arrow indicates when substitution started. (b) Dot plot of the estimated water permeability of the liposomes. (c) Scatter diagram plotted for initial diameter and permeability. Blue color represents the data obtained under static flow condition, and red color represents the data obtained under the constant flow (40 $\mu\text{L/h}$).

The volumetric decay shown as the decrease of the diameter (94%) was less significant than the decrease expected from the theoretical consideration. To visualize the performance of the trapping structure under the osmotic stress, we plotted the diameter of liposomes at which the liposome escaped from the nest (D_{escape}) (Figure 2. 17-a). The distribution of D_{escape} under the dynamic condition was more polydisperse compared to that under the static condition: $11.2 \pm 1.6 \mu\text{m}$ (CV: 14 %) and $10.8 \pm 0.6 \mu\text{m}$ (CV: 5 %), respectively. It is reliable because the external flow imposes additional force during and even after the osmotic stress. Interestingly, for both conditions, most of D_{escape} was larger than the smallest diameter observed at the demonstration of the arraying device ($10.7 \mu\text{m}$; see Figure 2. 10). By multiplying the observed decrease of the diameter (94 %), we calculated the hypothetical cumulative histogram of the equilibrated diameters using the data shown in Figure 2. 10 (Figure 2. 17-b). As only 20 % of the liposomes were smaller than the smallest liposome at the original distribution, the result indicated that the osmotic stress imposes an additional effect to deteriorate the trapping efficiency other than the decrease of the diameter. One of the plausible candidates was the deformability caused by the excess membrane due to the volume reduction. A clear correlation was observed between D_{escape} and the initial diameter (Figure 2. 17-c). In addition, the histogram of the relative diameter (D_{escape} over the initial diameter) showed narrow distribution for both dynamic and static conditions: 0.92 ± 0.04 (CV: 5 %), and 0.92 ± 0.02 (CV: 3 %), respectively (Figure 2. 17-d). The results indicated that the reduced volume determined the timing when the liposomes escaped. On the other hand, interestingly, the correlation between the initial diameter and the relative diameter was significant for the dynamic condition, while the correlation was not clear for the static condition (correlation efficient: 0.50 and -0.20, respectively). The liposomes escaped

from the nest even after the equilibration of the diameter under the dynamic condition. The correlation could reflect the ease of loss of liposomes in a steady flow environment: larger liposomes escaped from the nest by the slight loss of their volume. Since the bending energy per unit area is smaller for the larger liposomes⁹⁸, the result was consistent with the energetic viewpoint.

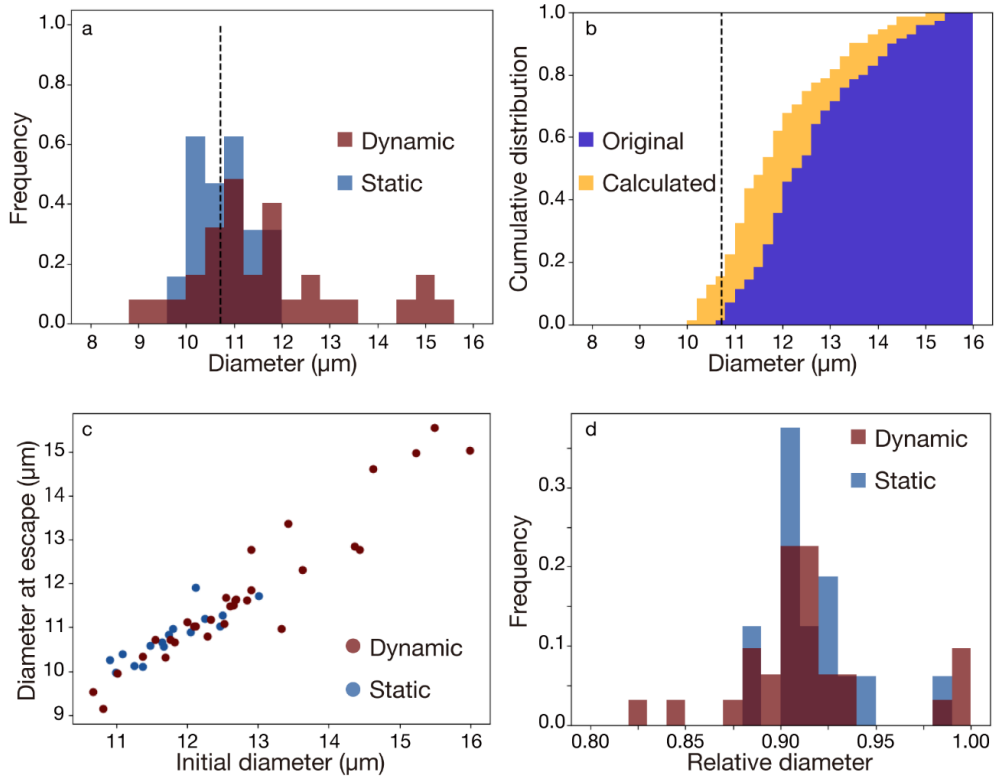


Figure 2. 17 Analysis of the volumetric decay based on the deformability. (a) Histogram of the diameter at which the liposome escaped from the nest (D_{escape}) plotted for dynamic (red) and static condition (blue). (b) Cumulative distribution of the trapped liposomes exposed to the hypertonic solution. Original diameters (blue) are modified to compensate for the volumetric decay (orange). The smallest diameter in the original distribution is emphasized by the black dashed line. (c) Relationship between D_{escape} and the initial diameter plotted for dynamic (red) and static condition (blue). (d) Histogram of the relative diameter (D_{escape} over the initial diameter) plotted for dynamic (red) and static condition (blue).

The consistency between the relative diameter of D_{escape} (92 %) and observed volumetric decay at the final data point (94 %) was also noteworthy. The time course of the diameter was saturated meaning the relaxation of the osmotic stress as shown in Figure 2. 16-a. However, if the osmotic shrinkage occurred in an isotropic manner, the diameter should be 82 % of the initial value theoretically. As for the reason why osmotic stress was balanced much swiftly than theoretical expectation, we postulated two candidates: the initial variety of the concentration of fructose inside the liposome and the leakage of fructose during the exchange process. Considering that the initial inner concentration to justify the 94 % decay was around 1.5 mM, which was 150 % of the targeted concentration, the latter possibility was much more plausible. Further investigations are needed to distinguish these two candidates strictly.

2.6. Significance of the achievement

The discussion provided to justify the unexpected insignificance of the volumetric decay presumably demonstrated the potential application of the system to assess the membrane tension under the steady flow environment based on the deformation assay. While several arraying devices have been developed thus far from various research groups^{57-59, 99}, the application of the devices for the elaborate research works was relatively limited despite their expected potential. One possible reason is that the external flow, which inevitably imposes the shear to the observed liposome, has raised another technical difficulty.

In this viewpoint, we considered that MANSIONs achieved two technical significances which enabled the microfluidic arraying system to be the fundamental tool in the research field using liposome (and giant vesicle). First, MANSIONs provided accuracy in one experiment, which is a common advantage of microfluidics, and at the same time, in the sequence of one research activity. Due to the Brownian motion, direct observation of one liposome demands labor-intensive and time-consuming protocol to the experimenters jailing them in front of their microscope. Tired human tends to make mistakes. Although mistakenly obtained data could sometimes open an unexplored research field, in most cases, these careless data just resulted in the additional supplemental examinations to prove that the experiments were mistakenly performed. In MANSIONs, the procedure is automatically recorded, and also, the procedure is easily repeatable just performing MANSIONs with the same protocol files. The traceability and reproducibility of the procedure would provide a cornerstone for the substantial progress of the research field. We also emphasize the throughput of the system. Notably, in this demonstration, the 10 microfluidic measurements were conducted. Each process included

the trapping of liposomes, exchange of the external solution, observation, washing of the device, and analysis. Since the optimization process require tense image analysis if the data was obtained manually, the overall process should take at least 3 or 4 days even using the microfluidic device. By MANSIONs where image analysis was parallely conducted with the measurement, all the procedure was finished within 12 h. These advantages were derived from the property as an automated measurement platform. MANSIONs was the first machine-assisted platform for the measurements of the cell-sized liposome based on the direct observation with a microscope.

Second, MANSIONs was even applicable to investigate the dynamics of liposomes under the static flow condition. In the previous research, the static condition was achieved by immobilizing liposomes to the glass slide via the biotin-avidin linkage or multi-layered microfluidic device to enable an ad-hoc valving system for each trap. However, the former strategy was not always applicable to the arbitrary purpose, and the latter strategy was challenging to be an alternative to the traditional methods since it required advanced know-how. Conversely, MANSIONs consisted only of planer microfluidic devices, which were easy to fabricate and manipulate. The following point is a technical advantage and not a note for a novelty, but the ease of fabrication and simplicity of the whole setup was advantageous for the reimplementation of MANSIONs by other laboratories which would contribute to the efficient development of the related research field. As for the novelty in the scientific outputs described in chapter 2, as shown in the demonstration, the effect of the external flow was not significant in the water permeability at the current experimental design. To the best of our knowledge, this was the first experimental confirmation using the dynamic array-type microfluidics. On the contrary, as described in the later chapter, the steady flow environment can affect the non-negligible effect on the trapped liposomes.

Thus, MANSIONs was useful for both research interests: a high throughput assay resembling the bulk condition and a unique measurement environment apart from the bulk condition. Considering these points together, we concluded that MANSIONs could extend the scope of the liposome investigation and accelerate further research.

2.7. Conclusion

This chapter described an automated experimental platform for the direct observation of cell-sized liposomes based on the microfluidic device, MANSIONs. As a demonstration, we measured the volumetric decay of the liposomes under hypertonic conditions. We estimated the water permeability of liposomes with/without the external flow and found that the effect of the flow was not significant, at least for the water permeability. MANSIONs provided easy access to exhaustive investigations with high reproducibility, adding to the general merits of microfluidic experiments of high throughput and precise control of the external condition.

3. Microfluidic exploration of cell-sized liposomes prepared by the water-in-oil emulsion transfer method

3.1.Introduction

As we discussed in chapter 1, one of the promising applications of liposomes is reconstituting the cellular mechanics inside the cell-like compartment. In 2004, pioneering work was reported by Noireaux and Libchaber³². They encapsulated the extracts of *E. Coli* into liposomes and demonstrated the production and activation of alpha-hemolysin, a pore-forming membrane protein. The report accelerated the various related research in the field. For example, Adamala and her colleagues encapsulated different kinds of genetic circuits to liposomes and achieved the modeling of cell-cell communication by liposomes³⁶. Kuruma and his colleagues created liposomes capable of energy production by themselves³⁴. Liposomes were also applicable to more practical research, such as a platform for the synthesis of therapeutic proteins inside the tumor¹⁰⁰, ethanol production with enzymatic metabolism¹⁰¹, and the development of liposomes as carriers for targeted drug delivery¹⁰².

Among various preparation methods of liposomes^{20, 103-106}, the so-called water-in-oil (w/o) emulsion transfer method (WOET method) is useful for the research to reconstruct cellular dynamics inside the liposomes^{107, 108}. The WOET method can encapsulate macromolecules and even micrometer-sized colloidal particles into liposomes at a high yield. In the WOET method, the w/o emulsion is put onto an aqueous phase, and lipid-coated emulsion droplets are transferred from the upper oil phase to the lower aqueous phase (Figure 3. 1). Liposomes are formed during the transferring process of the emulsion droplets because the lipid monolayer formed at the interface of the upper and lower phases

wraps the emulsion droplets. The inner water phase of the formed liposome is determined at preparing the w/o emulsion so that loss of encapsulated substances including macromolecules and water-dispersed colloidal particles to the outer aqueous phase is much less than other traditional preparation methods of liposomes. In the hydration method^{20, 106}, for example, the concentration of the inner substances is determined by the concentration of the swelling solution. In other words, much amount of substances is lost in the outer phase. Another merit of the WOET method is that the method can be performed without any sophisticated apparatus other than a benchtop centrifuge. Thus, the WOET method enables a wide range of investigation by various researchers of versatile backgrounds.

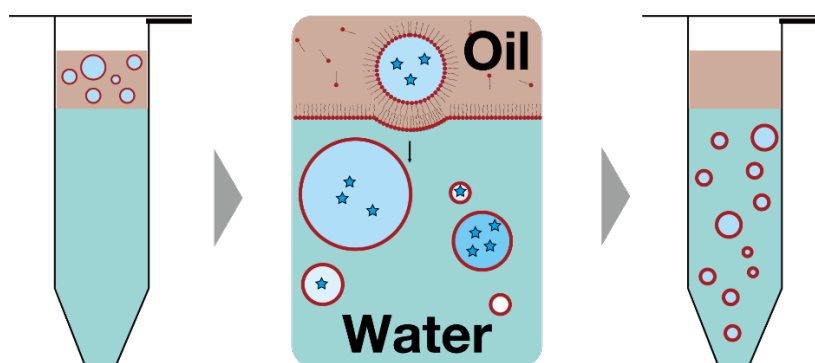


Figure 3. 1 Schematic illustration of the w/o emulsion transfer method. Water droplets in the emulsion are wrapped by the lipid layer at the oil/water interface during the centrifugation to afford liposomes.

Conversely, the WOET method is pointed out to afford some contamination of residual oils in the liposomal membrane^{109, 110}. It would be a critical deficiency in the case of the careful investigation of the folding of membrane proteins, for example. The contaminants raise another problem for investigating the liposomes prepared by the WOET method by PDMS-based microfluidic devices because of their hydrophobicity¹¹¹.

The hydrophobic property of PDMS causes the adhesion of hydrophobic molecules¹¹², and the liposomes prepared by the WOET method afforded strong adhesion of lipid aggregates as described later, perhaps because of the residual oils in the membrane. Hydrophilic surface modification effectively suppressed the part of such undesired adsorptions¹¹³⁻¹¹⁶. However, the wetting of liposomes to a hydrophilic surface is known to afford the membrane spreading^{117, 118}. Thus, it would be problematic for a long period of observation with the arrayed liposomes since the phospholipids include hydrophilic moiety in their molecular structure.

In this chapter, we show that the surface modification of the microfluidic device using the perfluoroalkyl group was useful to reduce the undesired adhesion of lipid aggregates and following observation by the microscope. Based on the microfluidic device described in chapter 2 (arraying device), we enabled a sequential size-sorting and trapping of the cell-sized liposomes prepared by the WOET method. As demonstrations, we used cell-sized liposomes encapsulating multiple polystyrene-made fluorescent microbeads (diameter = 1.0 μm), which are hardly encapsulated by other traditional preparation methods. Furthermore, to demonstrate that our system is applicable for tracking liposomes upon the external stimuli, we first compare the intrinsic variance in the distribution of encapsulation yield evaluated in the device and the bulk measurement. Second, we measure the water permeability of the liposomes prepared by the WOET method under precisely regulated perfusion of a hypertonic solution.

3.2. Materials and method

Chemicals

1-Palmitoyl-2-oleoyl-sn-glycero-3-phosphocholine (POPC) was purchased from

NOF Corporation (Tokyo, Japan). Cholesterol was provided by Avanti Polar Lipids. Texas Red® 1,2-dihexadecanoyl-sn-glycero-3-phosphoethanolamine (triethylammonium salt) (Texas Red DHPE) was supplied by Thermo Fisher Scientific, Inc. (Waltham, MA, USA). Glucose, sucrose, tris(hydroxymethyl)aminomethane (Tris), hydrochloric acid, methanol, chloroform, hexadecane, liquid paraffin, and pH standard solutions (phthalate pH standard solution, phosphate pH standard equimolal solution, and tetra-borate pH standard solution) were purchased from FUJIFILM Wako Pure Chemical Corporation (Osaka, Japan). Trimethoxy (1H, 1H, 2H, 2H, heptafluorodecyl) silane (PFS), and fluorescent microbeads (Fluoresbrite® YG Microspheres, Calibration Grade 1.00 μm) were provided by Tokyo Chemical Industry Corporation (Tokyo, Japan) and Polysciences, Inc. (Warrington, PA, USA), respectively. For PDMS fabrication, SILPOT 184 W/C was purchased from Dow Toray Co., Ltd was used. All materials were used without further purification.

Measurement of contact angle of PDMS block

PDMS block used for the measurement of the contact angle was fabricated as follows. The base of SILPOT 184 W/C and its curing agent were mixed in 10:1 in a weight ratio (Thinky, Inc., AR-100). The mixture was heated at 75 °C for more than 2 h. For the surface modification of the PDMS block, we further adopted the following procedures. We exposed the PDMS block to a single-step oxygen plasma treatment: 25 W, 20 cc/min 5 sec (SAMCO, FA-1). After heated at 75 °C for 30 min, the PDMS block was dipped into an approximately 10 wt% of PFS/methanol solution containing an aliquot of 6 M hydrochloric acid for 60 min. Then, the PDMS block was washed with an excess amount of methanol and dried under room temperature (approximately 25 °C). The fabricated

PDMS block was placed onto the horizontal table, and 10 μL of Milli-Q water or hexadecane was put on the PDMS block. The image of the droplet was taken by a commercially available contact angle meter (Excimer Inc., SImage Entry5). The measurement was conducted independently 5 times for each experimental condition.

Preparation of microbeads dispersion

Fluorescent microbeads dispersion (ca. 100 μL) was diluted by 600 μL of Milli-Q water. The beads dispersion was centrifuged (1900 g, 5 min, 25 $^{\circ}\text{C}$) by a high-speed microcentrifuge (HITACHI, Ltd., himac CT15RE). The resultant supernatant was removed. 600 μL of Milli-Q water was added, and the dispersion was vigorously vortexed. The procedures were repeated 5 times. After the fifth centrifugation, 350 mM glucose/150 mM sucrose/50 mM Tris-HCl buffer (measured pH: 8.05; inner phase solution) was added instead of Milli-Q water. The beads dispersion was stored under 4 $^{\circ}\text{C}$ (at most 3 days) and used after further dilutions (typically diluted 3-fold).

Preparation of cell-sized liposome dispersion

Stock solutions of POPC (40 mM in chloroform, 96 μL) and Texas Red DHPE (14.5 μM in chloroform, 160 μL) were mixed in liquid paraffin (1 mL). The oil dispersion was heated at 80 $^{\circ}\text{C}$ by the dry bath (Rocker Scientific Co., Ltd, Sahara 310) for 6 h. After cooling the oil dispersion, the beads dispersion (100 μL) was poured into the lipid/paraffin solution and vigorously vortexed for 20 sec. The resultant emulsion (200 μL) was gently put onto the 1 mL of 500 mM glucose/50 mM Tris-HCl buffer (measured pH: 8.06; outer phase solution) in a microtube. The microtube was centrifuged (18800 g, 30 min, 25 $^{\circ}\text{C}$), and the supernatant was removed. The residual (\sim 50 μL) was re-dispersed by a gentle

pipetting and put in a fresh microtube. 1 mL of the outer phase solution was added to the microtube and gently pipetted to disperse. The liposome dispersion was centrifuged again (18800 g, 30 min, 25 °C). Almost all the supernatant was carefully removed. Finally, to eliminate the density difference, 100 μ L of the inner phase solution was added to the precipitate and gently pipetted to re-disperse. The prepared liposome dispersion was used within 1d, although it remained stable at least 2 d after the preparation.

Surface modification of PDMS-based device

The PDMS device was designed and fabricated as described in chapter 2. The notable difference was as follows. To bond the glass slide and the PDMS channel, we adopted a two-step oxygen plasma treatment: 25 W, 20 cc/min, 2 min for glass slide only, and then 25 W, 20 cc/min, 5 sec for glass slide and the PDMS channel (SAMCO, FA-1). After the plasma treatment, the glass slide and PDMS channel were quickly contacted together and then heated on the hot plate at 75°C for 30 min. The microfluidic device was cooled for 5 min under room temperature (ca. 20 °C), and approximately 10 wt% of PFS/methanol solution mixed with an aliquot of 6 M hydrochloric acid was introduced into the device. After 60 min of incubation under room temperature (approximately 20 °C), the device was washed with the excess amount of methanol (> 5 mL) and then Milli-Q water (> 5 mL).

Trapping and observation of liposomes

The liposome dispersion and the outer solution were introduced into the arraying device by two syringe pumps (YMC, YSP-202, and Harvard Apparatus, Pump 11 Pico Plus Elite) for typically 30 min. Flow rates were set to 6.5 μ L h⁻¹ and 40 μ L h⁻¹,

respectively. Schematic description of the plumbing of the whole experimental system was described in Figure 2. 7. After a moderate number of liposomes (10 ~ 14) were trapped in the nests, the flow of the liposome dispersion was shut out by switching the valve A. For the osmotic stress experiments, the outer solution was exchanged by connecting the sample loop to the microfluidic device by switching valve B. Another pump (Harvard Apparatus, Pump 11 Pico Plus Elite) was used to fill the sample loop. For the abrupt stop of the flow of the outer solution, valve C was switched. The trapped liposomes were observed as described in 2.2. For counting green fluorescent microbeads in cell-sized liposomes stained by Texas Red DHPE, the image processing was performed as follows: once green and red fluorescence from those liposomes were captured in one snapshot or movie, the original snapshot or movie was decomposed into each color channel (blue, green, and red). Since we did not use blue fluorescence, we omitted the blue channel image and re-assembled red and green channel images assigning pseudo colors of red and cyan, respectively.

Counting of encapsulated beads inside liposomes

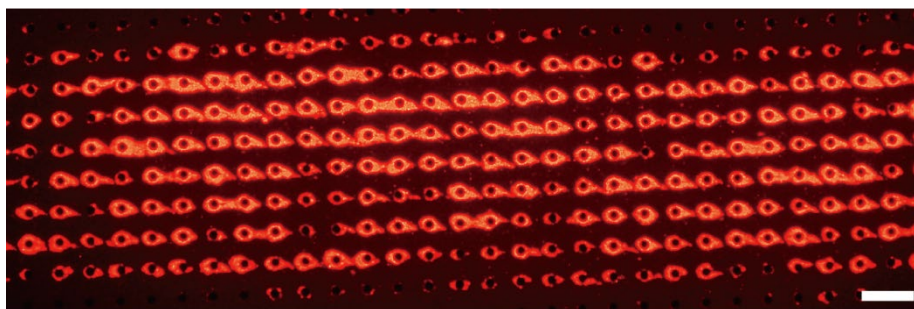
Microscopic observation was performed as explained above. Especially for the microfluidic measurements, the movie was captured after the flow of the liposome dispersion, and the external solution was shut off to visualize individual fluorescent microbeads. On the other hand, for the bulk measurement, we selected liposomes larger than approximately 5 μm to observe. During the capturing of the movie, the focal plane was carefully scanned by hand not to overlook the microbeads out of the focal plane. The captured movie was analyzed with ImageJ.

Estimation of the water permeability

Liposomes were arrayed in one observation field as described above. The initial outer solution (350 mM glucose/150 mM sucrose/50 mM Tris-HCl buffer (measured pH: 8.05)) was then substituted to a hypertonic solution (385 mM glucose/165 mM sucrose/55 mM Tris-HCl buffer (measured pH: 8.08)). After 5 min, fluorescence images were taken every 30 sec. Taken images were trimmed for each trapped liposome. The images were binarized, and the cross-sectional area was measured by ImageJ. The diameter of each liposome was calculated from the value of their area. The equation to estimate the water was described in 2.2. We calculated the water permeability by the linear regression of the time course of the diameter taken during 480–690 sec. Only liposomes having at least four data points were measured during the time range.

3.3. Surface modification of PDMS and microfluidic trap of cell-sized liposomes prepared by the WOET method

As shown in Figure 3. 2, a considerable amount of adhesion of lipid aggregates was observed in the size-sorting region when we used an unmodified device. Since the collision of particles and the micro-posts is the key to DLD mechanics, such adhesion collapsed the performance of the device.



Size sorting region

Figure 3. 2 Adhesion of lipid aggregates to the surface of the arraying device. A representative fluorescence microscopy image of the size-sorting region in the arraying device taken after 12 h of the introduction of the liposome dispersion prepared with the WOET method. Scale bar: 100 μm .

We considered modifying the surface of the device to hydrophobic and lipophobic. During the bonding process of the PDMS channel with the glass slide, the silanol group was generated on the surface through O_2 plasma treatment (Table 3. 1; run 1 and 2)¹¹¹. However, after 30 min of the bake (experimentally determined shortest bonding time, by which PDMS channel and glass slide were bonded without any leakage), the contact angles of both water and hexadecane got remarkably recovered (Table 3. 1; run 3), indicating that the reactive sites diminished. Thus, we chose the trifunctional silane coupling reagents expecting the polycondensation of PFS. We measured the contact angles for water and hexadecane according to the previous report¹¹⁹ with PDMS blocks baked 30 min after the plasma treatment followed by the surface modification. Compared to the unmodified but plasma-treated PDMS block (water: $96.1 \pm 1.6^\circ$, hexadecane: $42.3 \pm 1.5^\circ$, Table 3. 1; run 3), the modified PDMS block showed larger contact angles both for water and hexadecane (water: $107.7 \pm 6.1^\circ$, hexadecane: $71.4 \pm 2.2^\circ$, Table 3. 1; run 4). The contact angle of the modified PDMS block for water was comparable to the initial value ($107.7 \pm 6.1^\circ$ and $105.33 \pm 2.3^\circ$, respectively), and that for hexadecane was clearly

increased ($43.9 \pm 2.1^\circ$ and $71.4 \pm 2.2^\circ$, respectively). Since the plasma-treated PDMS block did not recover the initial contact angle for water even after 20 h without further modification ($83.2 \pm 9.1^\circ$), we deduced that the modification increased both hydrophobicity and lipophobicity of the surface of PDMS. Note that the contact angles were unchanged even after 20 h from the modification (Table 3. 1; run 5).

Table 3. 1 Contact angle of water and hexadecane on PDMS blocks before and after the modification (n=5 for each run).

Run	Condition	Contact angle / °	
		Water	Hexadecane
1	Untreated PDMS block	105.3 ± 2.3	43.9 ± 2.1
2	Just after plasma treatment	32.9 ± 3.7	32.2 ± 2.3
3	30 min after plasma treatment	96.1 ± 1.6	42.3 ± 1.5
4	30 min after PFS treatment	107.7 ± 6.1	71.4 ± 2.2
5	20 h after PFS treatment	103.8 ± 2.0	68.4 ± 3.7

We then examined the performance of the surface-modified device for the liposomes prepared by the WOET method. The adhesion of the lipid aggregates, which collapsed the size sorting mechanics based on the DLD method, was considerably reduced (Figure 3. 3-a, b). Moreover, the liposomes were trapped in the trapping region within 2 h (Figure 3. 3-c). The fluorocarbon surface was known to localize lipid film formation when the dropped liposome dispersion was evaporated on the surface¹²⁰. As the membrane spreading was primarily governed by the interaction between the surface and the

hydrophilic part of the lipid molecules, the report indicated the hydrophobicity of the fluorocarbon surface. The modification of the PDMS surface by the perfluoroalkyl group was previously adopted to hinder the wetting of lipid-containing water-insoluble organic solvent¹²¹. In other words, fluorides grafted on the surface decreased the affinity of the surface to the lipophilic molecules. Taken together these previous reports and obtained data, we deduced that the surface modification of the PDMS device improved the applicability of the device to the liposomes prepared by the WOET method by reducing the adhesion of lipophilic aggregates because of their lipophobicity and inhibiting the wetting of the liposome because of their hydrophobicity.

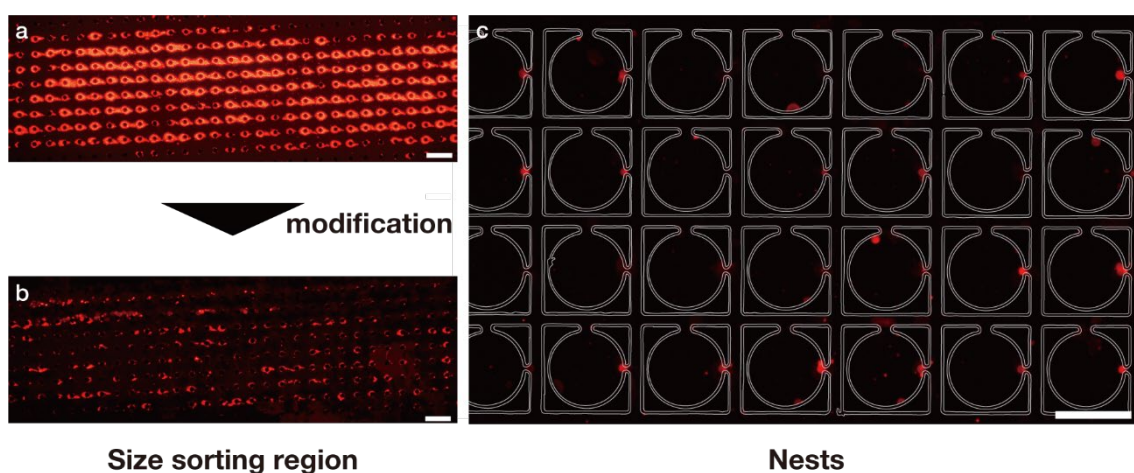


Figure 3. 3 Effect of the surface modification. (a, b) Fluorescence microscopy images of the start point of size sorting region (a) before and (b) after the modification, taken after 12 h of the introduction of the liposome dispersion prepared with the WOET method. (c) Fluorescence image of arrayed liposomes after 2 h of the introduction of the liposome dispersion. Contours of the nests were superimposed by the gray lines. Scale bars: 100 μm .

In Figure 3. 3-c, 57% of nests (16/28) were occupied, and only one liposome was trapped for 81 % of the occupied nests (13/16). Trapping efficiency (57%) was relatively

low compared to the performance described in chapter 2 (93% in Figure 2. 11), while the stability of the trapped liposomes was comparable. Note that in chapter 2 we used liposomes prepared by sugar-doped thin-film hydration method¹⁰⁶. We considered the low trapping efficiency would be assigned to the fraction of liposomes of the desired diameter in the liposome dispersion. On the other hand, although a slight amount of lipid aggregates was observed in the size-sorting region and trapping region, the one-to-one rate (81%) was equivalent to the former result in chapter 2 (88% in Figure 2. 11), suggesting that the trapping strategy worked well.

The averaged diameter of the trapped liposomes was 10.1 μm (coefficient of variation = 15%). Compared to the theoretical expectation on the average size calculated from the design of DLD (11.8–12.2 μm), the average diameter of the trapped liposomes was smaller. According to the previous report, due to the deformability, DLD tends to select slightly larger particles when applied to liposomes ($\sim 10\%$ larger than theoretical estimation)¹²². However, the obtained tendency in this research was the opposite. We considered the reason as follows. The trapping structure used in the device imposed an additional step of size selection at the entrance of the nest. Namely, the only liposomes whose diameter was smaller than the bifurcation height could enter the nest. It could be partly why the average diameter can be small. Note these small liposomes could be introduced into the trapping region when a liposome collides to micro-posts with the other adjacent liposomes and when an inner liposome was released by the rupture of the outer liposome during the size-sorting region. However, as discussed in the last chapter, the arraying device was capable of trapping liposomes larger than 12 μm . Thus, the primary reason that the diameter of the trapped liposomes was smaller than the theoretical range should be attributed to the original distribution of the liposomes in the prepared dispersion.

Note that the coefficient of variation of the diameter of trapped liposomes (15 %) was better than those obtained in the previous preparation protocols based on the WOET method^{123, 124}. Taking the results together, we deduced that the modification was sufficient to change the surface property of the PDMS and thus extended the applicability of the device to the liposomes prepared by the WOET method.

3.4. Distribution of encapsulated microbeads in liposomes prepared by the WOET method

One of the most striking advantages of the WOET method is to encapsulate even macromolecules and the colloidal particles of micrometer-scale at a high volume fraction in liposomes^{31, 125}. To prove that the device is appropriate for investigating liposomes prepared by the WOET method, we prepared liposomes with fluorescent polystyrene microbeads and observed them with the microfluidic device. As a result, streamlines of fluorescent microbeads were visualized, which indicated the bipolar convection inside the liposomes (Figure 3. 4-a). Since the stroboscopic lines shown in cyan corresponded to the trajectory of the microbeads during the exposure time, we could see the convection in the trapped liposome parallel to the cross-section of the liposome. The tendency was common to all the observed liposomes ($n = 80$ in total). When the flow was abruptly stopped after the trapping, the convection was suspended following the stoppage of the external flow (Figure 3. 4-b–d). Note that the contrast of monochromatic images was independently modified from the original composite images. Recently it was theoretically and experimentally reported that shear could generate bipolar convections inside liposomes under the fluidic condition⁶⁰ and hemispherical liposomes adhered to the solid surface^{62, 126}. Although the details of the fluidic property and state of liposomes were different, we consider that the convection observed in our system is analogous to the

previous reports. In any case, since the microbeads were hardly encapsulated inside the liposomes other than the WOET method, the applicability of the device to the liposomes prepared by the WOET method was presumably demonstrated.

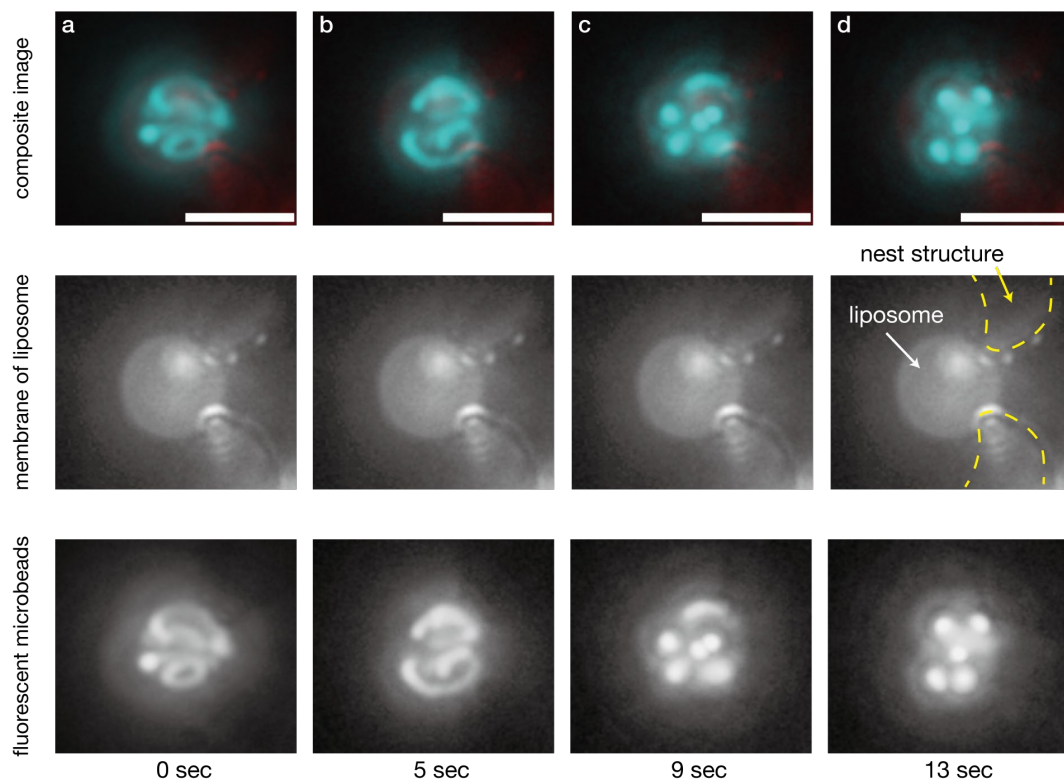


Figure 3. 4 Visualized shear-induced bipolar convection in the liposome. Composite fluorescence microscopy images are shown at the top. Red and cyan colors represent the lipid membrane (emission: 600–690 nm) and fluorescent microbeads (emission: 515–545 nm), respectively. The decomposed images are shown separately (middle: lipid membrane, bottom: fluorescent beads). Images are taken under (a) constant flow ($40 \mu\text{L h}^{-1}$) and (b–d) a static condition: (b) 5 sec, (c) 9 sec, and (d) 13 sec after the manipulation of the valve. Optical exposure time is 500 msec. Scale bars: 10 μm .

The liposomes captured and observed in one experiment are only a part of liposomes in the original liposome dispersion. Namely, the coefficient of variation of the diameters in the microfluidic device was smaller than that obtained in the bulk measurement (15%

in the device and 32% in the bulk measurement) (Figure 3. 5a). Therefore, it is essential to validate if the distribution of the trapped liposomes is not biased from the original dispersion other than the diameter. Since the encapsulation yield is the core competence of the WOET method¹²⁷, we counted the number of fluorescent microbeads encapsulated in the trapped liposomes after abruptly stopping the external flow and compared the result to that obtained in the batch observation. Note we used a far diluted microbeads dispersion compared to the previous reports^{31, 125} to count the number of microbeads inside correctly. To avoid the effect of the difference of the volume, we calculated the volume fraction of the encapsulated microbeads to the liposome. As shown in Figure 3. 5-b, the shape of the frequency plot of the volume fraction obtained from the microfluidic measurement (n=113) and that obtained from the batch measurement (n = 173) showed a similar tendency. On the contrary, when the 2-fold diluted microbeads dispersion was used for the inner aqueous phase of the liposome dispersion, frequency distribution slightly left-shifted (n = 64). The difference in the distribution was also seen as the average number of microbeads encapsulated in liposomes (1.5 for the 2-fold diluted dispersion and 2.1 for the original dispersion). Thus, the results provided one ground that the liposomes arrayed in the microfluidic device were not biased, at least in terms of the distribution of encapsulation yield.

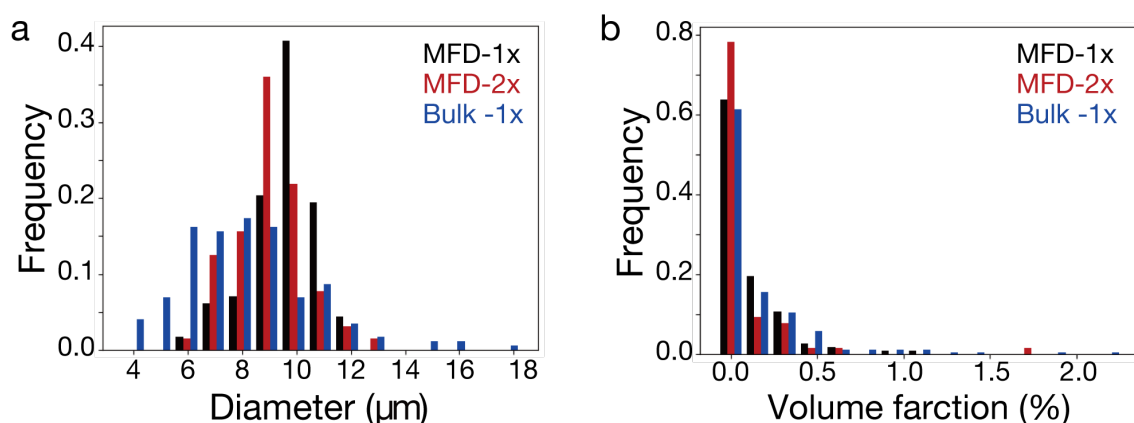


Figure 3. 5 Evaluation of the bias of microfluidic device in the encapsulation yield. (a–b)

Histograms of (a) the diameter of the liposomes and (b) the volume fraction of fluorescent beads in the liposomes. Liposomes prepared with the beads dispersion of the initial density (1x) or 2 times diluted (2x) condition were observed under the microfluidic device (MFD) or bulk specimen.

3.5. Water permeability of liposomes prepared by the WOET method

As stated above, one of the advantages of microfluidic observation is the sequential and simultaneous tracking of liposomes under a controlled outer environment. As a demonstration, we observed the liposomes exposed to a hypertonic solution under a microfluidic environment to evaluate the water permeability. Namely, after the trap of the liposomes, the external solution was exchanged for the hypertonic solution, and the following dynamics were monitored by microscopic observation. In Figure 3. 6-a, representative time-lapsed fluorescence images and their binarized images were shown. Diameters of each liposome calculated from the area of the cross-sectional image linearly decreased during 480–690 sec (Figure 3. 6-b, c). Thus, it was plausible that liposomes shrank as previously known¹²⁸, and further, the uniformity of the concentration of the external solution during the time range. The averaged water permeability of liposomes was calculated as $10.2 \pm 5.0 \mu\text{m/s}$ ($n=10$), and even in maxima, it was $18.1 \mu\text{m/s}$. The

calculated value was remarkably smaller than the previously reported value for the pure POPC membrane ($\sim 10^2$ $\mu\text{m/s}$)^{129, 130}. Instead, the value was comparable to that of the POPC membrane containing ca. 40% of cholesterol¹³⁰. According to the previous report¹²² and as shown in chapter 2, the measurement of water permeability in the device afforded comparable average water permeability to the other bulk measurements⁸² for liposomes prepared by the film-swelling method. Moreover, in our experimental system, continuous external flow was imposed, which is known to enhance the permeability across the membrane^{83, 84}, while the actual effect was proved to insignificant at least in the current condition. Therefore, the obtained low water permeability should not be attributed to the methodology using microfluidics. We suspect that the oil residue afforded the low water permeability, according to the previous report pointing out the contamination of the liquid paraffin during the emulsification process.¹¹⁰

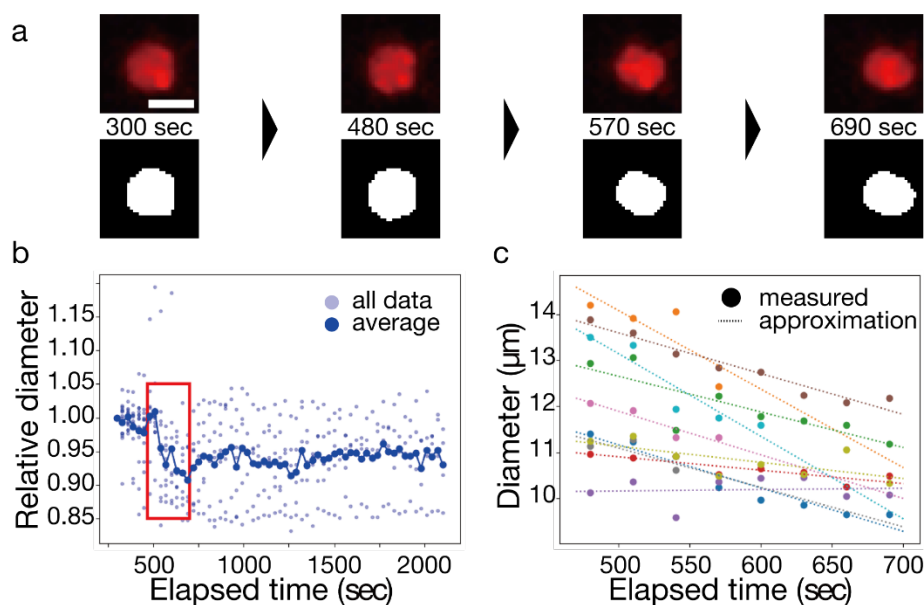


Figure 3. 6 Measurement of the water permeability. (a) Representative fluorescence images (top) and their binary images (bottom) of a liposome exposed to the hypertonic solution. Scale bar: 10 μm . (b) Time course of relative diameter normalized by the initial diameter of each liposome. The diameter is estimated from the binary image in (a). The average values are plotted in a dense blue, and raw data are plotted in a pale blue. (c) The time course of the diameter of liposomes plotted for 480–690 sec (indicated as the red rectangle in (b)) with their linear regression curves (broken lines). Each color represents the data of each liposome.

We should also note that the obtained variance of the water permeability was not negligible. Although the estimation strategy based on the cross-sectional image associated considerable intrinsic variance (up to 30% in the coefficient of variation (CV)),⁸² the obtained variance (CV ~50%) could suggest another factor of variation. We suspect the amount of residual oil was the cause. However, it is technically difficult to directly measure the amount of contaminated oil in the observed individual liposomes in the device. Further elucidation is desired. In any case, the molecular transportation across the

lipid membrane is of great interest in views of, for instance, future application of liposomes as a therapeutic evaluation platform of drugs^{55, 131}, mechanistic investigation of cell-penetrating peptides¹³², and synthetic approach toward cell model³⁴. Therefore, it should be remembered as a potential nature of the preparation protocol affecting the membrane property that even the maximum of the water permeability of the liposomes prepared by the WOET method was much smaller than that of the liposomes prepared by film swelling method^{129, 130}.

3.6. Significance of the achievement

As we demonstrated, the WOET method can afford liposomes encapsulating even micrometer-sized colloidal particles at a high yield. Since the WOET method can be performed only with a benchtop centrifuge, the method is easy to introduce for laboratories of various research backgrounds. Thus, the WOET method has the potential to develop a wide variety of liposome-based cell models. In this chapter, we achieved the simultaneous parallel measurement of size sorted liposomes prepared by the WOET method. The current achievement would facilitate the progress of various liposome research with various interests by combined with the automated observation system (MANSIONS). The high accuracy of the microfluidic measurement developed here would unveil overlooked properties and natures on previously performed experiments.

We also emphasized the following two results: that the external shear caused the bipolar convection and that the long-tailed distribution of the number of microbeads was found. As stated above, the WOET method can encapsulate bio-functional substances like cell-free transcription and translation reagents³⁴. The shear-driven convection could generate spontaneous stirring and thus increase the efficiency of the chemical reaction

inside. Besides, the long-tailed distribution meant that the WOET method stochastically afforded liposomes of the enormous encapsulation yield. Since the perfusion chamber presented here can provide highly reproducible and accurate measurement, such a rarely observable liposome would also be captured in the scope of investigations with a substantial discussion.

3.7. Conclusion

In this chapter, we showed that the modification of the surface of the device by the perfluoroalkyl group enabled the steady trapping and parallel observation of liposomes prepared by the water-in-oil emulsion transfer method. Simultaneous direct observation of the trapped liposomes prepared by the WOET method is advantageous for the easy and precise tracking of the time course of liposomes with a statistical data set, which demands time-consuming repetition of the batch measurements, and impossible for the flow cytometry. We demonstrated the potential of the device as a perfusion chamber by the following three measurements: visualization of the bipolar convection in the liposomes under a microfluidic environment, evaluation of the encapsulation yield, and long-time tracking of liposomes upon the osmotic stress. Significantly, the water permeability of the liposomes was much smaller than the previous reports. It should be noted as the potential artifact on the future development of liposome-based cell models using the WOET method. Nevertheless, it is significant merit of the WOET method that liposomes containing even large colloidal particles and hence bio-functional polymers without special apparatus were easily prepared. The combination of microfluidic experiments and the WOET method can encourage the further development of liposome-based supramolecular chemistry and constructive biology. In this viewpoint, the bipolar

convection can work as an efficient mixer for the inner reaction of the liposomes. Since the stoppage of the external flow ceased the convection, it should also be noted as a unique characteristic observed in a steady flow environment.

4. Hydrodynamic accumulation of small molecules and ions into cell-sized liposomes against a concentration gradient

4.1.Introduction

As discussed in chapter 1, liposomes are a promising scaffold to reconstruct the current form of living systems. The underlying prospect was to explore the hidden chemical logic behind the complexity of the current cellular dynamics. In other words, how the simple system can behave elaborately was the question. The research question was more emphasized when considering the earliest emergence of the life-like system at the early earth. For example, the difficulty lay even for maintaining the concentrated condition steadily to activate the chemical reaction inside. Thus, the investigation using liposomes was often related to the exploration of the origin of life. In this chapter, we discuss the point in more detail and show a novel finding which could provide an insight into the earliest emergence of functional liposome-based chemical systems.

The emergence of the early cell-like system compartmentalized by lipid bilayer membrane in the early earth has drawn much attention¹³³⁻¹³⁵. The compartment is indispensable in retaining molecules inside and evolving a metabolic system as implemented in contemporary living cells¹³⁶. Also, compartmentalization is the key to realize the resistance to a freeloader chemical replicator, representing another central issue regarding the continuous replication in the prebiotic era^{137, 138}.

How can such functional compartmentalized systems emerge spontaneously? Moderate concentration of substances is a prerequisite for the chemical functions, including replication cycles. As for the first generation of such a concentrated compartment, the super concentration effect could provide a promising clue, by which an

unexpectedly large number of macromolecules is spontaneously encapsulated during the liposome formation^{136, 139}. Such liposomes containing macromolecules inside retain their contents even upon the strong membrane perturbations¹⁴⁰. However, for the preformed compartment, the supply of the molecules to the inside could be the problem due to the very compartment. In other words, the compartment could hinder the maintenance, propagation, and development of metabolic systems. The backwash of the compartment on the supply of substances is especially emphasized for the phospholipid membrane, which is widely implemented in the current living cells, due to their low permeability^{134, 141}. Prebiotically plausible amphiphiles such as alkyl phosphate, alkyl sulfates, and fatty acids also formed membrane. The membrane consists of such simpler amphiphiles have larger permeability¹⁴². However, the low permeability of the phospholipid membrane must be overcome at the stage of the early cell-like system. Living cells implement a cooperative reaction network composed of various membrane proteins involving the consumption of chemical energy sources such as adenosine triphosphate (ATP)^{143, 144} to overcome this low permeability of the phospholipid membrane. Recently, there has been remarkable progress on the prebiotically plausible synthetic pathways of phospholipid¹⁴⁵⁻¹⁴⁹, but the physicochemical insights toward a generation of functional compartments composed of phospholipids are limited.

The supply to the pre-formed compartment is also the central issue in constructive biology aiming to reconstruct cell-like chemical systems. Since liposomes were widely utilized for their commonality to the composition of the compartment of the current cells, the low permeability of the phospholipid membrane is the matter to be handled. Thus far, the understanding and application of pore-forming mechanics at the membrane have been developed^{36, 150-152}. However, the strategy based on the passive diffusion of molecules and

ions confronts a limitation of their concentration gradient across the membrane. In other words, the concentration of the substances in the compartment must be smaller than or at most equivalent to the outer solution.

A simple mechanism to accumulate and concentrate molecules and ions from the external environment into the preformed compartment with the phospholipid bilayer membrane would be crucial to develop liposome-based model cells^{153, 154} in the context of exploration on the origin of life and constructive biology. Thus far, a possible molecular scenario for the origin of life was elucidated in views of molecular candidates in the early earth^{155, 156}, possible prebiotic synthesis of biomolecules¹⁴⁵⁻¹⁴⁹, and potential environments for the birth of the earliest life^{157, 158}. The bottom-up construction of model cells has been partly achieved by the synthetic chemical cell models mimicking essential features of contemporary cells^{32, 34, 65, 159, 160}. However, an abiotic mechanism to accumulate substances into the compartment composed of phospholipid bilayer membrane is still unveiled.

In this chapter, we demonstrate that small molecules and ions can be accumulated into preformed cell-sized liposomes against the concentration gradient repeatedly. The process does not require any membrane proteins but is driven only by physical contact to some surface under a steady flow environment.

4.2. Materials and method

Chemicals

1-Palmitoyl-2-oleoyl-*sn*-glycero-3-phosphocholine (POPC) and 1-palmitoyl-2-oleoyl-*sn*-glycero-3-phospho-(1'-rac-glycerol) (sodium salt) (POPG) were purchased from Avanti Polar Lipids (Alabaster, AL, USA) and NOF Corporation (Tokyo, Japan). Cholesterol was provided by Avanti Polar Lipids. Texas Red® 1,2-dihexadecanoyl-*sn*-glycero-3-phosphoethanolamine (triethylammonium salt) (Texas Red DHPE) was supplied by Thermo Fisher Scientific, Inc. (Waltham, MA, USA). Fructose, uranine, fluorescein, sodium hydroxide, hydrochloric acid, methanol, chloroform, and pH standard solutions (phthalate pH standard solution, phosphate pH standard equimolal solution, and tetraborate pH standard solution) were purchased from FUJIFILM Wako Pure Chemical Corporation (Osaka, Japan). A solution (1 mM) of fluorescein-12-adenosine triphosphate (FL-ATP) with 10 mM Tris-HCl, pH 7.6, 1 mM EDTA was purchased from PerkinElmer, Inc. (Waltham, MA, USA). All materials were used without further purification.

General procedure to prepare the liposome dispersion

Lipid films were prepared as described in 2.2. The film was gently agitated with 2 mL of Milli-Q water or 1 mM Tris-HCl buffer (pH 7.87) in a thermostatic incubator (WAKENYAKU, MODEL 2290) under 40 °C for 1 h. Then, the liposome dispersion was placed into the thermostatic incubator under 26 °C for more than 10 h. The liposome dispersion used for the microfluidic experiments was diluted three-fold by 1 mM fructose solution and incubated at 26 °C for more than 1 h, and then the diluted dispersion was filtered by a nylon mesh filter (Merck Millipore Ltd., NY2002500) with a pore size of 20 µm four times to avoid the clogging in the microchannel, the height of which is

approximately 16 μm . Filtrated liposome dispersion was placed in the thermostatic incubator under 26 °C for more than 3 h.

Image acquisition

Microscopic images were taken using an inverted microscope (Olympus, IX71) equipped with a cooled charge-coupled device camera (Olympus, DP72). For the epifluorescence microscopy (EFM) image, a dual-band excitation filter (excitation: 490–505 nm, 560–580 nm; emission: 515–545 nm, 600–650 nm) was typically used. The microscope also equipped an apparatus for the spinning-disk confocal fluorescence microscope (SDCM) observation: a confocal scanning unit (Yokogawa Electric, CSU22) and a scientific complementary metal-oxide-semiconductor camera (Andor, Zyla) under control of an image capture software (Andor, iQ3).

In most of the experiments in chapter 4, MANSIONs was used. For the methods related to the microfluidic experiment, including fabrication and setup, see chapter 2. The experiment using another microfluidic device or performed under different conditions, see later subsections.

Vortex and pipetting of the liposome dispersion with uranine solution

The liposome dispersion was prepared as explained above. The dispersion was diluted by 10-fold to afford a 15 μM uranine/1 mM fructose solution. The dispersion was then vortexed at 500 rounds per minute for 60 min or pipetted vigorously with a pipet for more than 5 min. The sample was placed onto a 25 μL specimen with two cover glass slips (thickness $\sim 280\ \mu\text{m}$) and observed with EFM and SDCM. Several images were taken for each condition, and the incorporation of uranine was evaluated by the line profile over the liposomes.

Nuclear magnetic resonance measurement of the liposome dispersion

The liposome dispersion was prepared as explained above. A part of the prepared liposome dispersion (approximately 500 μL) was placed in a microtube and rapidly frozen by liquid nitrogen. The tube was then placed in an insulated glass container and freeze-dried for more than 12 h. The dried lipid mixture was dissolved into deuterated methanol (methanol- d_4), and the ^1H NMR spectra were obtained by AVANCE 500 (Bruker). The freeze-drying of the liposome dispersion was conducted immediately after, and then at one and four days after the preparation of the liposome dispersion.

Investigation of the relationship between the fluorescence intensity of uranine and pH

A commercially available pH meter (HORIBA Advanced Techno, Co., Ltd., Model: D-51) equipped with an ISFET pH electrode (HORIBA Advanced Techno, Co., Ltd., Model: 0040-10D) was used for the pH measurement. The pH meter was calibrated by three points with standard solutions: phthalate pH standard solution (pH 4.01), phosphate pH standard solution (pH 6.98), and tetraborate pH standard solution (pH 9.18).

Specimens (~1 mL) were placed onto a glass slide and measured as a droplet on the solid surface according to the manufacturer manual. The same procedure was adopted throughout the measurement of pH values in the latter part. We prepared 14 types of aqueous solutions of different pH values from the standard pH solution with sodium hydroxide and hydrochloric acid (pH 4.41, 4.82, 5.13, 5.70, 6.03, 6.51, 6.86, 7.26, 7.67, 8.21, 8.82, 9.18, 9.75, and 11.22). Uranine solution was added to obtain a uranine concentration of 5 μM . The pH value of each sample was measured again and put onto a 25 μL specimen with two cover glass slips (thickness ~280 μm). Fluorescence images were taken with an exposure time of 25 msec. The images were cropped to analyze common regions of interest to remove contaminants, and the GFI was measured.

Microfluidic observation of liposomes with another arraying device of narrow trapping structure

The microfluidic device was designed according to the previous report¹²². The fabrication method was described in 2.2. The flow rate of the outer solution and the liposome dispersion was 40 $\mu\text{L h}^{-1}$ and 6.5 $\mu\text{L h}^{-1}$, respectively. After a moderate number of liposomes were trapped, the valve-A was changed to shut off the flow from the pump introducing the liposome dispersion (see Figure 2.7). The outer solution was substituted to the 5 μM uranine/1 mM fructose solution at a flow rate of 40 $\mu\text{L h}^{-1}$, and the fluorescence image was taken after 30 min of exposure to uranine. The image was manually analyzed by ImageJ for all of the liposomes in the image: the contour was manually fit with the red channel of the image, and GFI was measured for the region of interest.

Statistical analysis for uranine concentration inside trapped liposomes

After the programmed experimental procedure was finished, the recorded GFI_{lipo} was converted to a pseudo-concentration (C_{calced}) to avoid the influence from the deterioration of the mercury lamp over time using the following formula:

$$C_{calced} = GFI_{lipo} \times \frac{C}{GFI_{BG}}$$

, where C is the actual concentration of the uranine solution introduced into the device as the external solution, and GFI_{BG} denotes the GFI of the background. The distributions of the pseudo-concentration under each experimental condition were statistically compared by a two-sided test. We adopted Mann-Whitney's U-test (see 2.2).

Investigation of the relationship between the GFI of FL-ATP and pH

Nine types of aqueous solutions of different pH values were prepared from standard pH solutions with sodium hydroxide and hydrochloric acid (pH 4.01, 4.58, 5.08, 5.13, 5.59, 6.39, 6.88, 7.37, 8.18, and 9.17). The purchased solution of 1.0 mM FL-ATP with 10 mM Tris-HCl, pH 7.6, 1 mM EDTA was diluted to afford a 15 μ M FL-ATP/1 mM fructose solution for the microfluidic experiments. This solution was then mixed with each buffer solution to obtain a uranine concentration of 5 μ M with various pH values. The pH values of each sample were measured again and put onto a 25 μ L specimen with two cover glass slips (thickness \sim 280 μ m), and fluorescence images were taken with an exposure time of 300 msec. The images were cropped for the common region of interest to remove contaminants, and the GFI was measured.

4.3. Accumulation of uranine into a liposome

The liposome dispersion was introduced into the arraying device. The average diameter was 12.1 μm , and the coefficient of variation (CV) was 12%. When the trapped liposomes were exposed to a 15 μM uranine/1 mM fructose solution at a flow rate of 40 $\mu\text{L h}^{-1}$ for 15 min, approximately 80% of the liposomes showed green fluorescence, which was brighter than the background in an epi-fluorescence microscopy (EFM) image (Figure 4. 1).

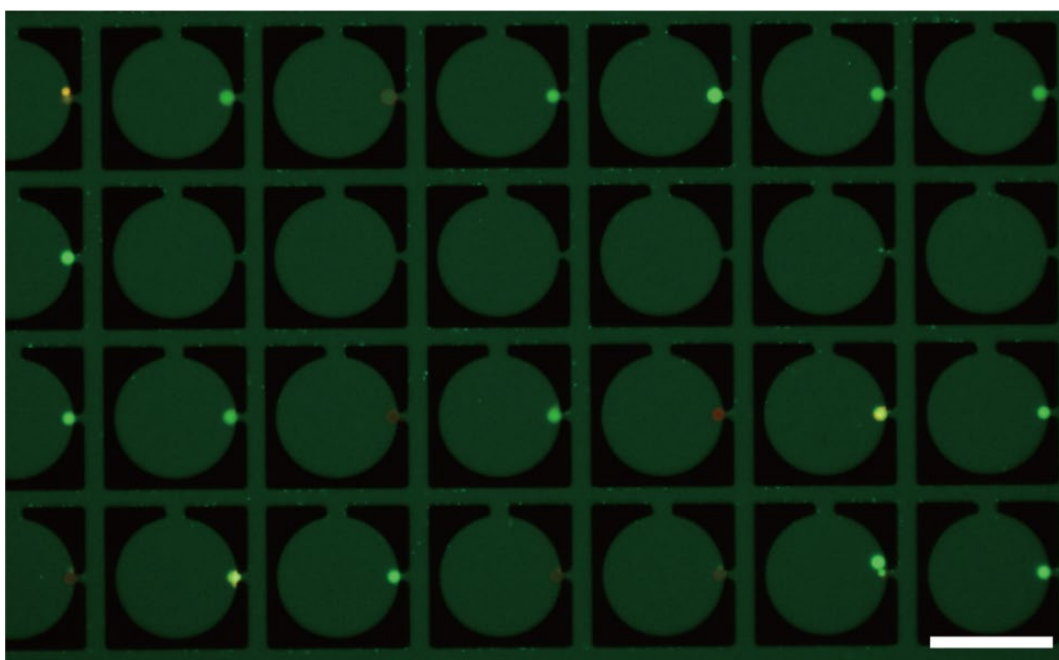


Figure 4. 1 Epi-fluorescence microscopy image of liposomes trapped and exposed to uranine solution. Red and green fluorescence denote membrane and uranine, respectively. Scale bar: 100 μm .

To test if the uranine existed inside the liposomes, we checked spin-disk confocal microscopy (SDCM) images. As a result, all the obtained line profiles showed a common tendency. Namely, the line profile of the membrane (red) had two peaks and was concave between the peaks, while that of uranine (cyan) was unimodal and convex (Figure 4. 2). The result strongly suggested that a considerable amount of uranine was retained inside the liposomes and not compiled on the surface of the liposomes. Interestingly, there was a liposome whose inner liposome-in-liposome showed relatively weaker fluorescence intensity (Figure 4. 2-e). Since trapped liposomes in the nests were exposed to considerable flow, we focused on the hydrodynamic conditions of the trapped liposomes.

In advance of the further detailed investigations with MANSIONs, we conducted two preliminary examinations to exclude simple artifacts. First, we prepared liposome dispersions using phospholipids and other chemicals purchased from different companies and confirmed that the dynamics were not caused by unintended contamination or materials of a specific lot number. Moreover, no degradation of phospholipid molecules used in the liposome dispersion was confirmed for 4 days (Figure 4. 3).

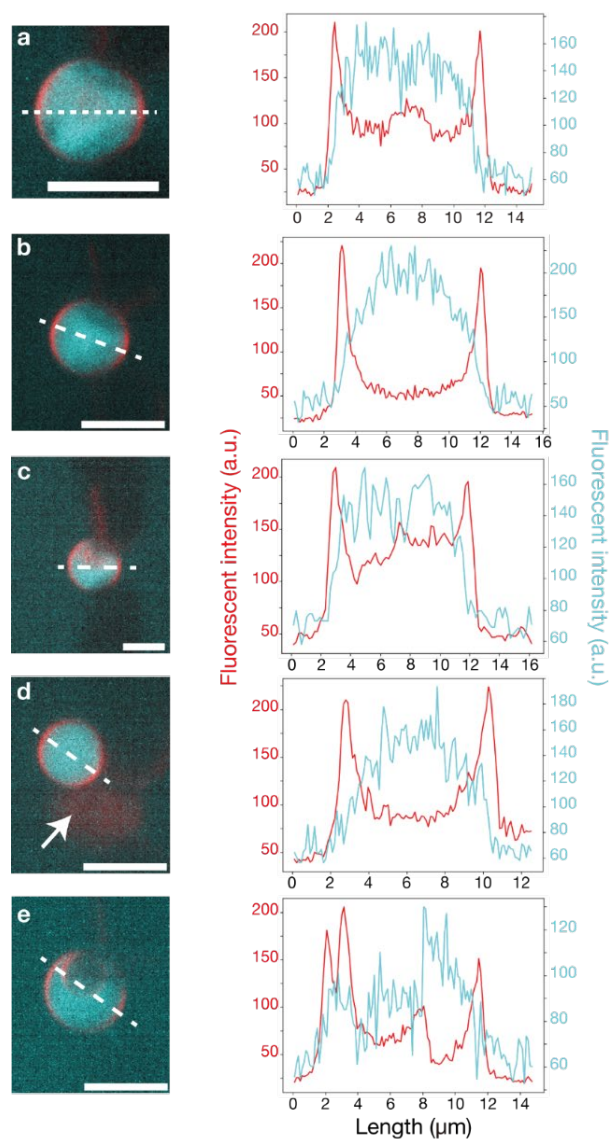


Figure 4.2 SDCM images of trapped liposomes exposed to uranine solution under a microfluidic environment. SDCM images in pseudo color (red, 561 nm excitation; cyan, 488 nm excitation) (left) and corresponding line profiles (right). (a–d) Liposomes exposed to a 15 μM uranine/1 mM fructose solution. (e) A liposome at approximately 5 min after starting the washout. The color of the line profiles reflects the color of the SDCM images. The white arrow in (d) is the first liposome (out of focus), and the line profiled liposome is the secondary liposome trapped in the nest (incorrect trapping). Scale bars: 10 μm .

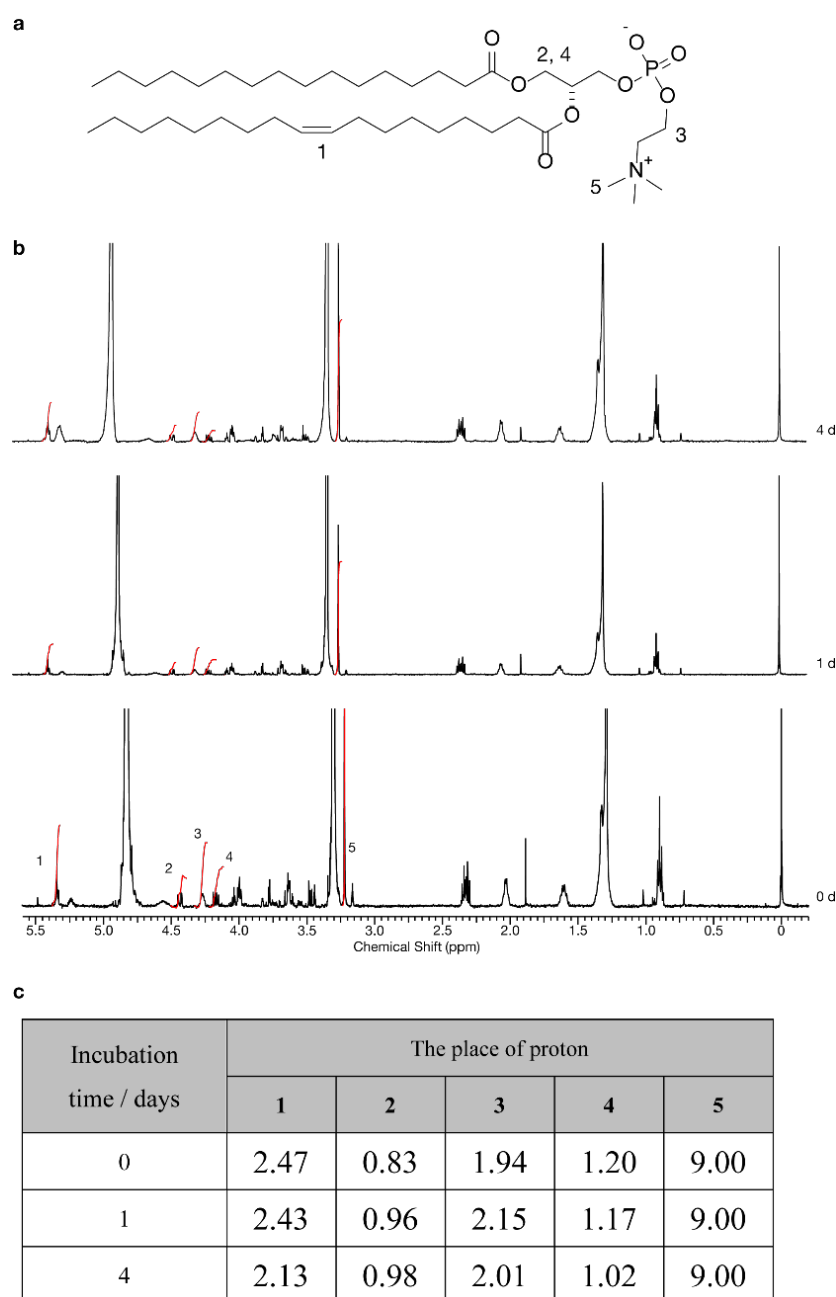


Figure 4. ^1H NMR spectra of the sample of the liposome dispersion (500 MHz, CD_3OD). (a) Molecular structure of POPC, the main component of the liposome used in the experiments. (b) ^1H NMR spectra of the liposome dispersion immediately after preparation (0 d) and after 1 and 4 days. Important protons to check the oxidation or hydrolysis of phospholipids are denoted by the numbers (1–5), which are common between (a) and (b). (c) Table of integration values described in (a) and (b).

Second, we tested if the flow field alone was enough for the accumulation suggested above. However, vortex and pipetting of the liposome dispersion with uranine did not afford such unpredicted accumulation of uranine into the preformed liposomes (Figure 4. 4). Therefore, we hypothesized that the dynamics were a non-trivial phenomenon that was never investigated.

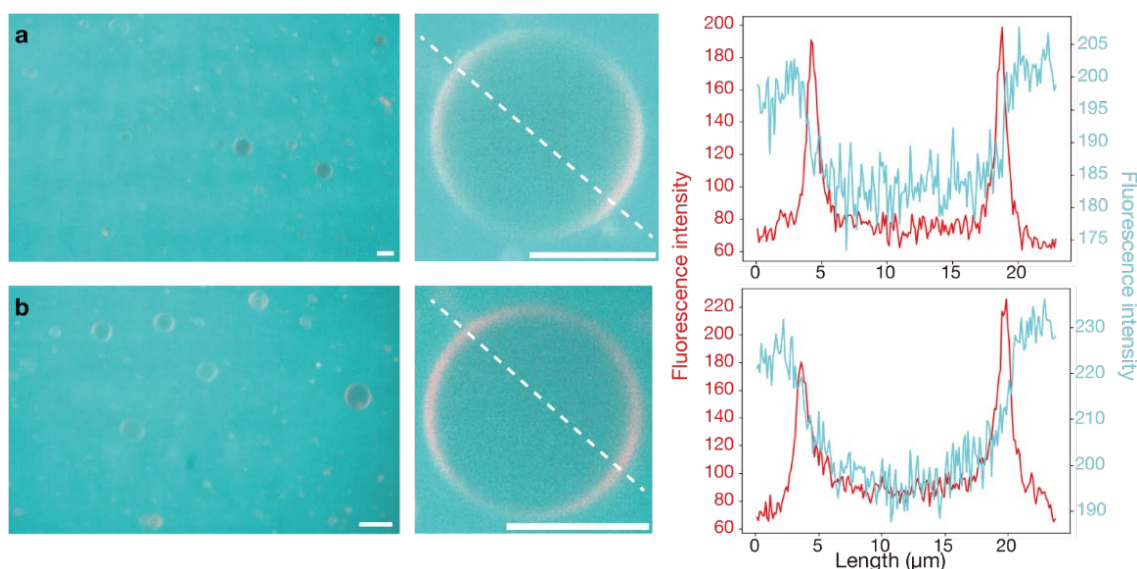


Figure 4. 4 Liposome dispersion imposed external flow in bulk solutions. (a–b) SDCM images of low magnification of liposomes (left) and high magnification (middle) of another liposome, and corresponding line profiles of the liposome (denoted as white dashed lines in the SDCM images in the middle) (right). The liposome dispersion was (a) vortexed at 500 rpm for 60 min and (b) vigorously pipetted (5 min). Images are shown in pseudo color (red, 561 nm excitation; cyan, 488 nm excitation). The colors of the line profiles reflect the colors of SDCM images. Note that high magnification and low magnification SDCM images were taken for the different positions of the samples to avoid the photobleaching of uranine. Scale bars: 10 μm .

To more directly verify this unique event of liposomes, we performed the following experiments with MANSIONs. First, we focused on the pH dependence of uranine: the fluorescence intensity of uranine was suppressed at low pH in the used aqueous solution of uranine (Figure 4. 5). By exchanging the outer solution to a low pH solution, which has the same concentration of uranine to the original solution, uranine encapsulated in the liposomes and compiled on the surface of the liposomes can be distinguished.

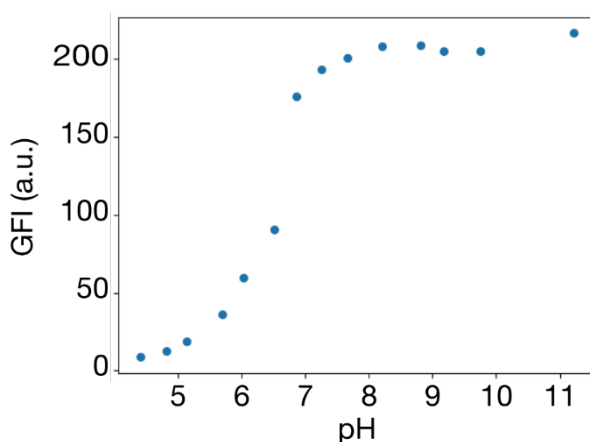


Figure 4. 5 Diagram of the dependency of GFI of the EFM image of uranine solution on pH. The concentration of uranine was fixed at 10 μ M, and the exposure time was 25 msec.

We thus changed the outer solution from a 5 μ M uranine/1 mM fructose solution (pH 6.42) to a 10 μ M HCl/5 μ M uranine/1 mM fructose solution (pH 4.68) after trapping the liposomes (Figure 4. 6). As a result, for approximately 30% of the trapped liposomes, the green fluorescence intensity (GFI) obtained from the EFM image was maintained at 80% or more of the initial value throughout the exchange of the outer solution ($n = 3$) (Figure 4. 6-a–d). Note that there were two more different types of the time course of GFI of liposomes (GFI_{lipo}): (i) GFI_{lipo} decayed in the first 5 min during the substitution to the low pH solution and did not recover during re-substitution to the initial solution ($n = 5$) (Figure

4. 6-e-h), and (ii) GFI_{lipo} decayed suddenly at a certain time point during the re-substitution process delayed from the first 5 min ($n = 3$) (Figure 4. 6-i-l). In every case, the GFI of the background (GFI_{BG}) instantaneously decreased during substitution to the low pH solution. Thus, the delay or total tolerance of fluorescence intensity of uranine against the exchange to the acidic external solution (Figure 4. 6-a-d, i-l) provided clear proof that uranine was encapsulated into the liposomes. On the other hand, it should be noted that for about half of the trapped liposomes, GFI_{lipo} decreased in the first five minutes. This type of dynamics suggested two possibilities: one is that uranine was encapsulated, but the liposomal membrane had high permeability of proton, and the other is that in these cases, uranine was piled up on the surface of the liposomes. Considering that all the SDCM images of the liposomes exposed to the uranine solution showed a common tendency for the line profiles of the membrane (bimodal and concave) and uranine (unimodal and convex), it was plausible to assume that the uranine was encapsulated in the same manner throughout these three types. However, the variance of the composition of liposomes, hence the permeability of proton¹⁶¹, could emerged the three different dynamics.

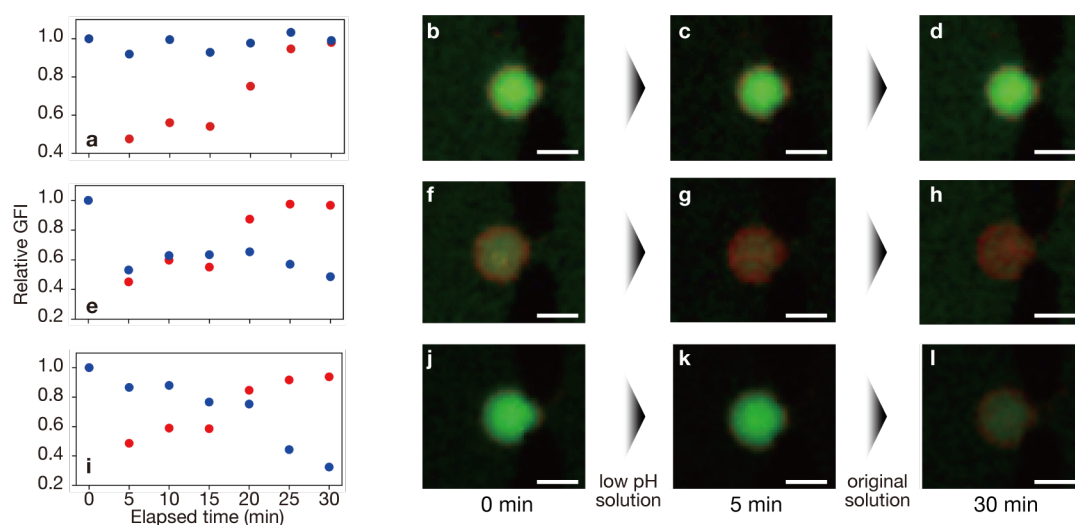


Figure 4. 6 Confirmation of the encapsulation of uranine inside the liposomes. (a–l) Three types of (a, e, i) time courses of GFI_{lipo} (blue) and GFI_{BG} (red) upon the exposure to low pH solution followed by the washout and (b–d, f–h, j–l) the representative EFM images. The contrast of EFM images was modified for visual readability. Scale bars: 10 μ m.

Second, we examined whether the hypothetical pH gradient between inside and outside of the liposomes could justify the obtained stronger intensities of liposomes. Since the fluorescence intensity of uranine is strongly suppressed under the low pH region, under a hypothetical pH gradient, the fluorescence intensity could be larger than the outside, even if the concentrations were equivalent between each other. First, we used a buffered uranine solution (pH 7.87) to prepare the liposome dispersion and the external uranine solution. Even in this case, most of GFI_{lipo} were larger than GFI_{BG} (Figure 4. 7). This result apparently shows the encapsulation and further accumulation of uranine inside of the liposomes. However, the pH buffered solution cannot be safe to exclude the hypothetical concentration gradient across the liposomal membrane. The buffer reagents potentially could influence the phenomena of the accumulation of uranine against the concentration gradient, or the distribution of these reagents themselves could be affected

under the hydrodynamic condition, where might be some unknown dynamics across the membrane.

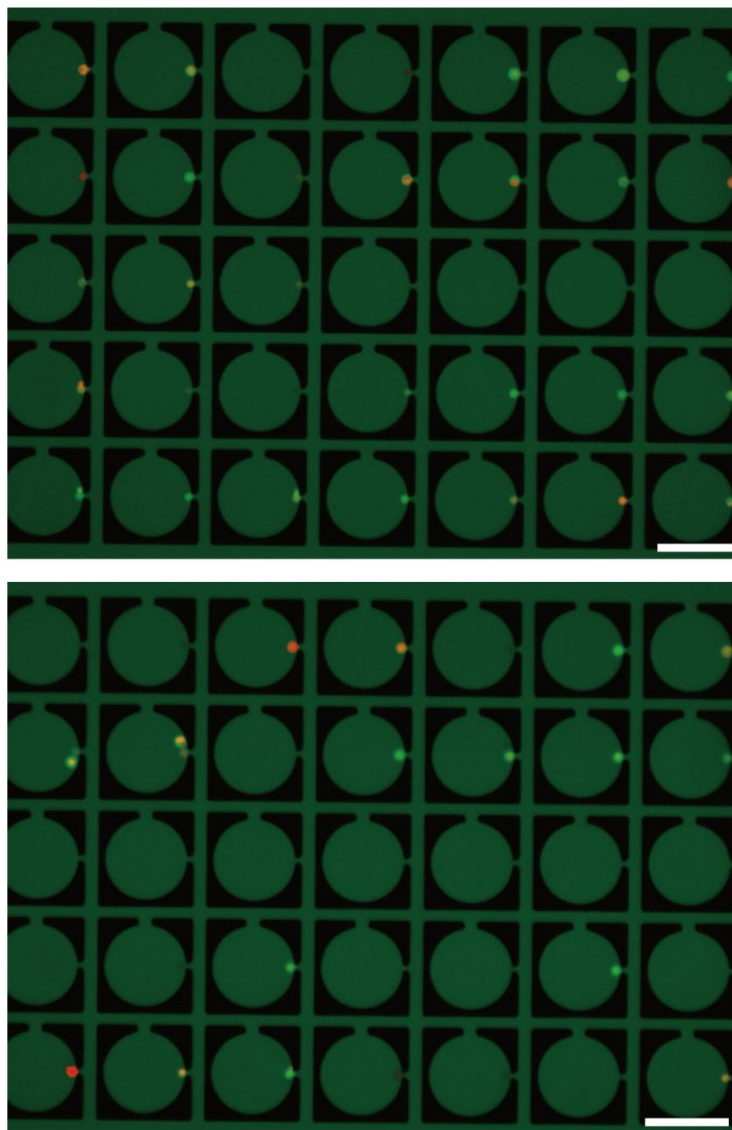


Figure 4. 7 Liposomes exposed to the buffered uranine solution. Two representative EFM images of the trapping region upon 30 min of exposure to the 5 μ M uranine/1 mM fructose/1 mM Tris-HCl solution (arranged to pH 7.87) taken at individual experimental trials. The liposome dispersion was prepared by the swelling of lipid thin film doped with fructose using the buffered solution (1 mM Tris-HCl solution (arranged to pH 7.87)). Scale bars: 100 μ m.

To carefully eliminate the possibility of overvaluation of the uranine concentration inside liposomes caused by the hypothetical concentration gradient between inside and outside of liposomes, we used a more diluted uranine solution (0.5 μ M uranine/1 mM fructose) as the outer solution, with the expectation of enhancing the ratio of GFI_{lipo} to GFI_{BG}. The pH values of the 0.5 μ M uranine/1 mM fructose solution and that of the liposome dispersion ranged from 5.79 to 6.18 and from 6.52 to 7.07 (based on five independent measurements per sample), respectively. Therefore, the overvaluation of uranine concentration inside should be less than a factor of 5.4 (the ratio of GFI at pH = 7.3 to that at pH = 5.7, see Figure 4. 5). GFI_{lipo} at each time point was subtracted by the initial GFI_{lipo} to avoid the effect of the fluorescence crosstalk of the two fluorescent molecules, uranine, and Texas Red DHPE. We repeated the experiments 3 times to confirm the reproducibility. As a result, after 1 h of the exposure, the average ratio of GFI_{lipo} to GFI_{BG} was 37.2 (Figure 4. 8-a). Interestingly, a gap in the ratio appeared between 17.8 and 6.2, and 90% of the liposomes showed a ratio larger than 17.8 (n=34 in total). GFI_{BG} (0.5 μ M uranine/1 mM fructose) was detected as the meaningful signal compared to that obtained from the 1 mM fructose solution: these two distributions were both fitted with Gaussian distribution, and the mean values were separated from each other by larger than the 3 times of standard deviation (Figure 4. 8-b, c). Thus, even if we assume the hypothetical pH gradient across the liposomal membrane at the maximum (factor of 5.4), still the additional factors of 3.3 and 6.9 are required to justify the ratio of 17.8 (minimal value) and 37.2 (average value). However, judging from the deviation of GFI_{BG} (Figure 4. 8-c), it was not plausible to justify even the additional factor of 3.3 by the variation of GFI_{BG} (< 0.05% for one measurement on one liposome). Note even at the highest ratio, the estimated concentration of uranine was smaller than the concentration

where self-quenching of uranine may occur (see Figure 2-14e that showed the linear relationship between the concentration and the fluorescence intensity under 100 μM). Taking these results into account, we reliably deduce that the concentration of uranine inside liposomes became higher than that of the outer solution.

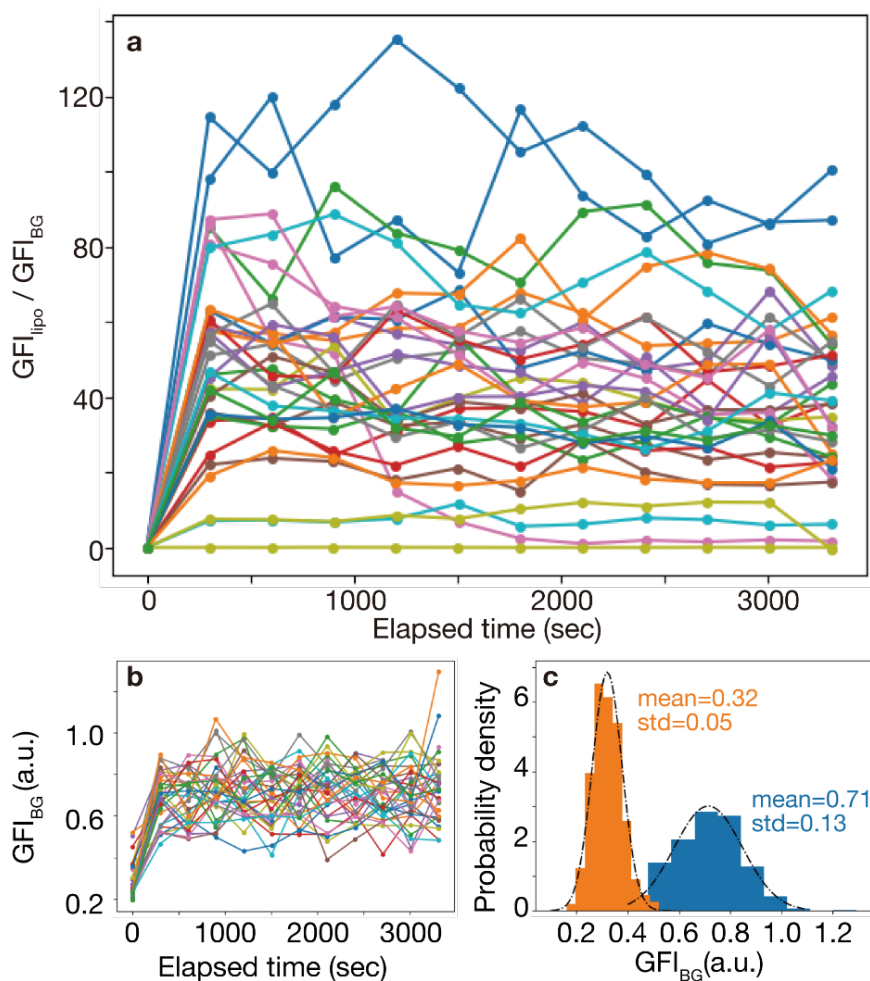


Figure 4. 8 Accumulation of uranine against a concentration gradient. (a) Time course of the ratios of GFI_{lipo} to GFI_{BG} exposed to a 0.5 μM uranine/1 mM fructose solution. (b) Time courses of GFI_{BG} measured for each liposome. (c) Comparison of histograms of GFI_{BG} for 0.5 μM uranine/1 mM fructose solution (blue) and 1 mM fructose solution (orange). Means (mean) and standard deviations (std) of each histogram are shown with the corresponding Gaussian distribution (black dashed lines).

Third, a numerical simulation was performed to estimate in which situation can this accumulation against the concentration gradient be justified. To simulate the accumulation of uranine in the trapped liposomes, we set several assumptions to simplify the situation to avoid overfitting in terms of phenomenological considerations. First, permeation dynamics are described by three kinetics of uranine: permeation from outside to inside (k_{in}) and from inside to outside (k_{out}), and photo-bleaching (k_{bleach}). Second, the fluorescence intensity inside the liposome is proportional to the amount of the intact uranine. Third, no photo-bleached uranine exists in the environment.

Uranine and POPG are negatively charged at the current experimental range of pH. Therefore, the Donnan potential can be involved along with the transport of the molecule. We included the repulsive interactions among the charged molecules confined in the membrane as a correction factor of k_{in} and k_{out} . We heuristically implemented this effect by an exponential function of the whole amount of inner and external charged substances. As explained above, the time course of the amount of uranine in the environment (I_{BG}) was initially the same as the time course of GFI_{BG} and was then interpolated by the simple arithmetic average of two consecutive intensities:

$$I_{BG}\left(\frac{t(n) + t(n + 1)}{2}\right) := \frac{I_{BG}(t(n)) + I_{BG}(t(n + 1))}{2}$$

The interpolation was repeated until the time interval $(t(n + 1) - t(n))$ became smaller than 0.01. Thus, the amount of intact uranine (I_{int}) and photo-bleached uranine ($I_{bleached}$) was sequentially calculated as follows:

$$I_{int}(t(n+1)) = I_{int}(t(n)) + I_{BG} \times k_{in} \exp(-\beta I_{tot}) - I_{int} \times k_{out} \exp(-\beta I_{tot})$$

$$I_{bleached}(t(n+1)) = I_{bleached}(t(n)) - I_{bleached} \times k_{out} \exp(-\beta I_{tot})$$

, where I_{tot} is the sum of uranine ($I_{tot} = I_{int} + I_{bleached} + I_{BG}$). Note that I_{int} and $I_{bleached}$ were further calculated at some time points corresponding to when the fluorescence image was taken:

$$I_{int}(t(n+1))^* = I_{int}(t(n+1)) \times (1 - k_{bleach})$$

$$I_{bleached}(t(n+1))^* = I_{bleached}(t(n+1)) + I_{int}(t(n+1)) \times k_{bleach}$$

First, the kinetics of photo-bleaching was estimated experimentally. A lipid film was swelled with 5 μ M uranine solution. The resultant liposome dispersion was diluted 10-fold by the 1 mM fructose solution and immediately put onto a 25 μ L specimen with two cover glass slips (thickness \sim 280 μ m). EFM images were taken every 7 sec with the same lens and irradiation conditions used in MANSIONS. The uranine-rich liposomes whose focal planes were unchanged for over 10 slices (\sim 70 sec) were manually analyzed with ImageJ: the contour was manually fit using the red channel of the image, and GFI was measured for the region of interest. As shown in Figure 4. 9, $k_{bleached}$ was set to 0.004.

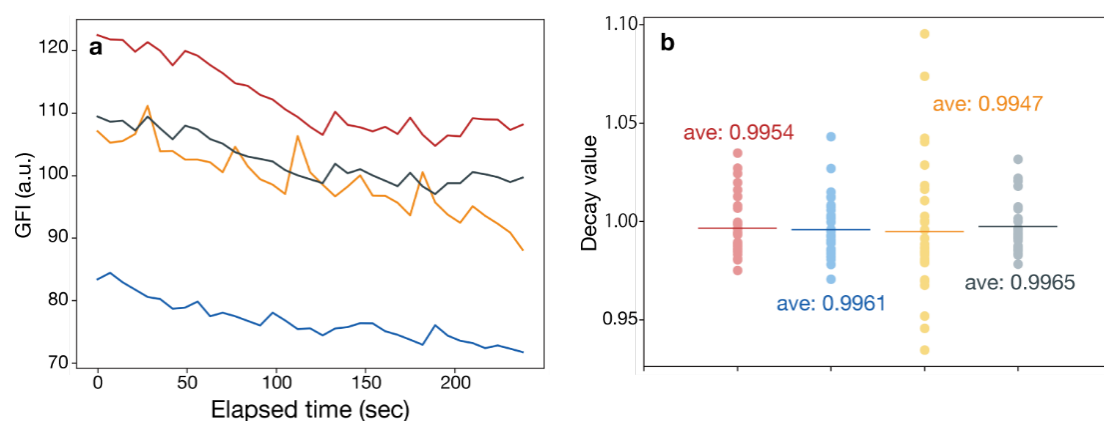


Figure 4. 9 Photo-bleaching kinetics of uranine solution included in liposomes. (a) Time course of GFI_{lipo} . (b) Dot plots of the decay rate of GFI_{lipo} calculated from each time course shown in (a). Decay rate is defined as the ratio of GFI_{lipo} at each time point to that of just before 7 sec. Pale colored dots represent all the measured data, and bars with intense colors denote their average. Colors of each bar are the same in (a) and (b).

Then, other kinetics parameters were fitted. A rapid increase followed by saturation with a gradual decrease in intensity was moderately reproduced when, for example, $k_{in} = 0.05$, $k_{out} = 0.004$, and $\beta = 0.2$ (Figure 4. 10). Notably, the fitted parameters reflecting the permeation of uranine from outside to inside and those from inside to outside the liposome were non-equivalent.

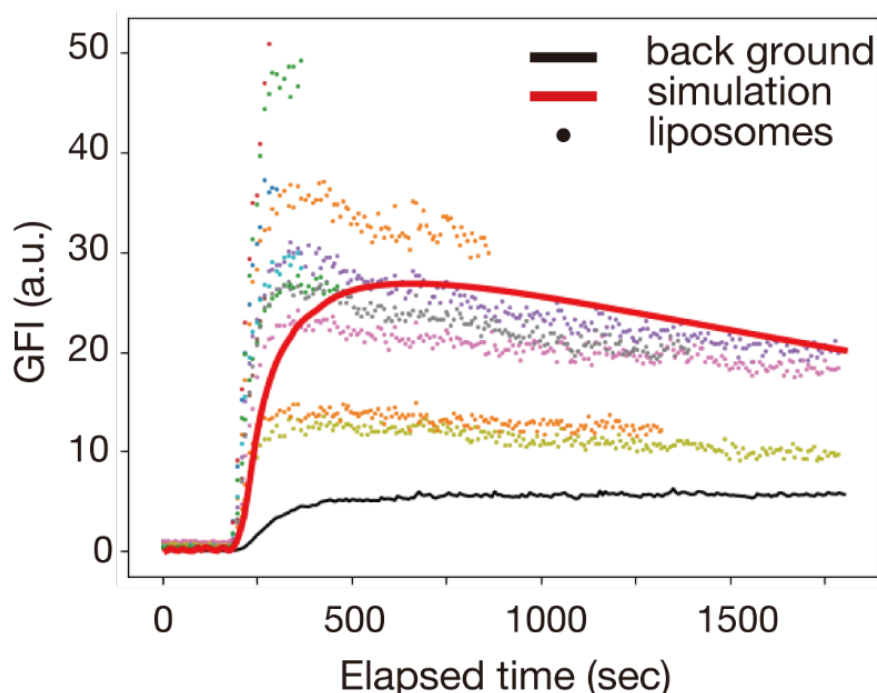


Figure 4. 10 Comparison of experimental result and numerical simulation. Diagram showing the result of the numerical simulation on the time course of GFI_{lipo} (red line) plotted with the experimental results (colored dots, liposomes; black line, background).

Fourth, the unequal kinetics of intake and release was experimentally visualized, which was suggested from the numerical simulation. During the measurement to show the repeatability of the unexpected increase of GFI_{lipo} , the outer solution of the trapped liposomes was sequentially exchanged to the uranine solution (5 μ M uranine/1 mM fructose) (exposure; 30 min) and then, re-substituted to the original solution (1 mM

fructose) (washout; 60 min) (Figure 4. 11-a). The measurement presumably evidenced the repeatability of the cycle of the accumulation and the release, while the peak-top value tended to decrease slightly over the cycles with reasons that were not clear currently. Besides, the measurement provided a clue of the kinetics when the data was plotted as the ratio of GFI_{lipo} to GFI_{BG} (Figure 4. 11-b). Namely, the peaked time-course was observed at the beginning of the exposure and washout repeatedly. The observed peaks at the beginning of the washout indicated the delay of the release compared to the re-substitution process which determined the upper limit of the transportation kinetics across the lipid membrane. Thus, to justify the peaks at the beginning of the exposure, the kinetic imbalance of the uranine transportation was required. Note that the GFI_{lipo} at each time point was subtracted by the initial GFI_{lipo} . Taking all the results into account, we deduced that uranine was accumulated in liposomes against a concentration gradient due to the non-equivalent kinetics of the intake and release of uranine.

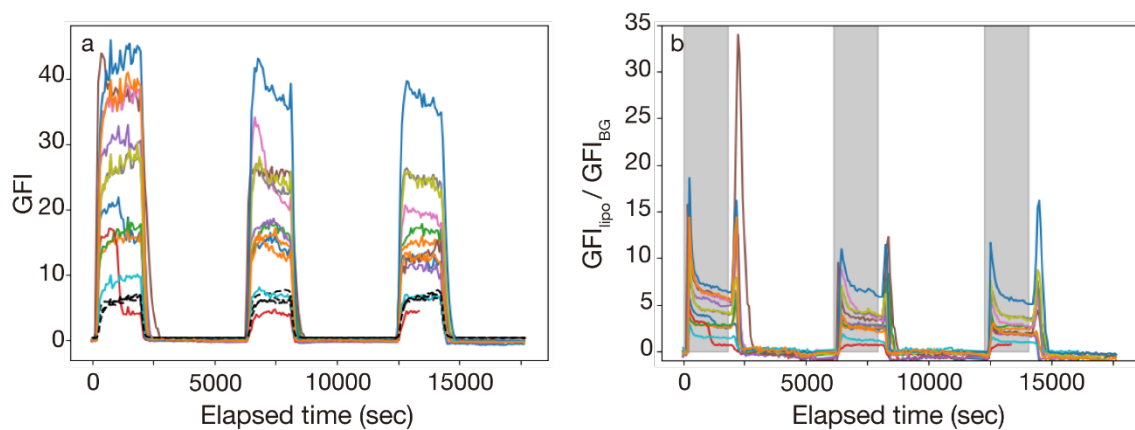


Figure 4. 11 Visualization of unequal kinetics of permeation across the membrane. (a, b) Time courses obtained during the repeated exposure-washout cycles: (a) GFI of each liposome (colored solid lines) and GFI of the background (black dashed lines), and (b) ratio of GFI_{lipo} to GFI_{BG} . The gray boxes in (b) denote the durations of the exposure (5 μ M uranine/1 mM fructose).

4.4. Effect of external flow and physical contact on uranine accumulation in liposomes

The accumulation described above is distinguished from the passive diffusion observed in a static condition. To clarify the phenomenological key factor, first, we used another trapping device, in which liposomes are trapped in narrow spaces¹²². As a result, we found that for approximately 75% of the liposomes (n=166), GFI_{lipo} was larger than GFI_{BG} during exposure to a 5 μ M uranine/1 mM fructose solution (Figure 4. 12). The result suggested that the shape of the trapping structure did not have a critical role in the accumulation. As for the statistical viewpoint of the distribution of GFI_{lipo} shown in the double logarithmic plot, a negative correlation between the GFI_{lipo} and its frequency was observed for the liposomes of high GFI_{lipo} (approximately larger than 40 where GFI_{BG} was 16), while the correlation was not clear for the liposomes of low GFI_{lipo} . Currently, it was difficult to recognize any clear information for the shape or characteristics of the distribution. However, the distribution indicated another issue to be discussed that the degree of accumulation was divergent for each liposome. We attributed the variety to the distribution of the liposomes. Thin hydration method, the adopted preparation method in this chapter, was known to afford inhomogeneous distribution of the composition of the liposomes¹⁶¹.

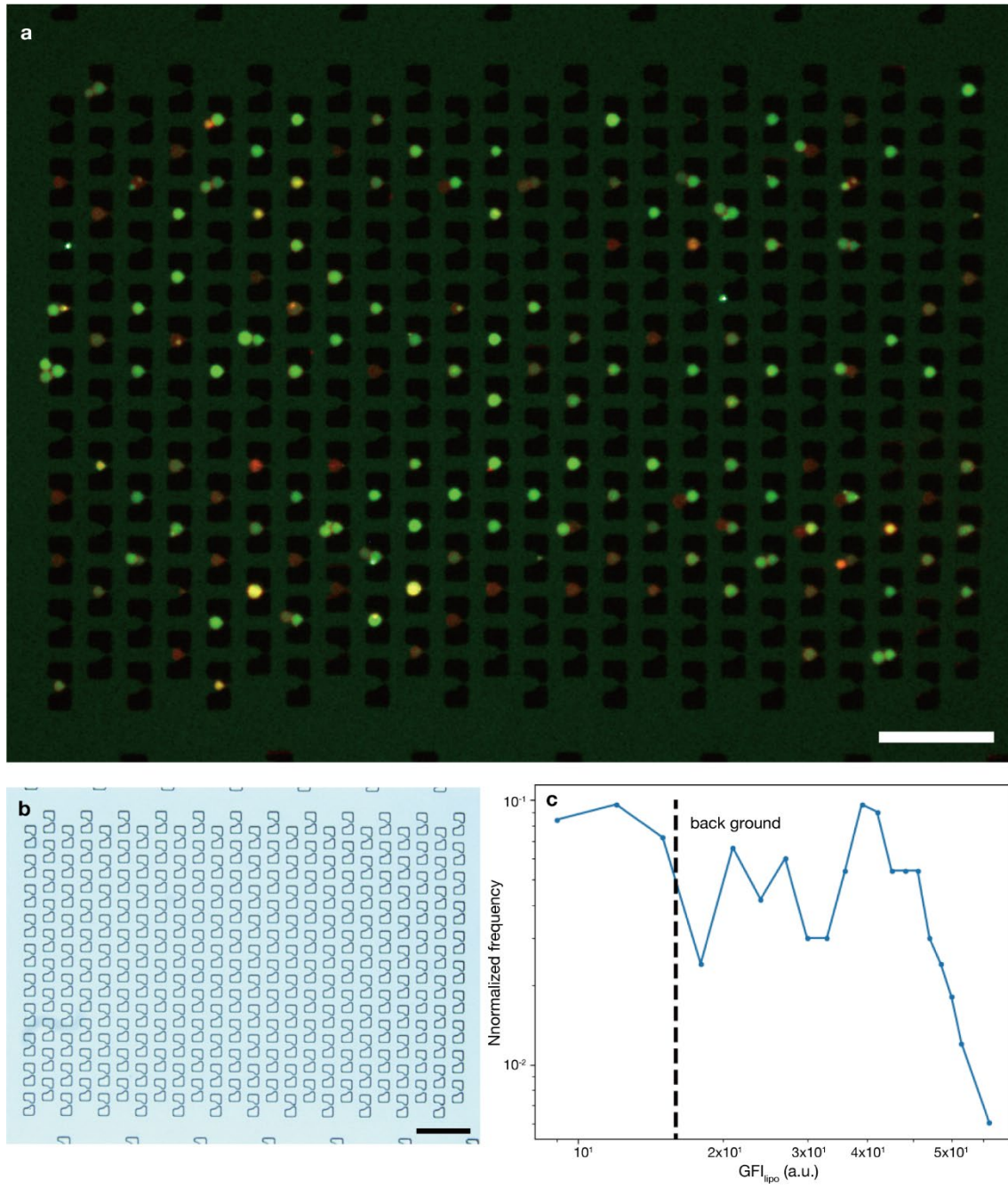


Figure 4. 12 Liposomes trapped and exposed to uranine solution in the arraying device of another trapping structure. (a) EFM image of liposomes in the trapping region. (b) Bright-field microscopy image of trapping region. Scale bars: 100 μm . (c) Double logarithmic plot of the distribution of $GFI_{lipo.in}$ (a). The black dashed line denotes GFI_{BG} .

Besides, we observed the liposomes flowed with the 5 μ M uranine/1 mM fructose solution in the size-sorting module of the arraying device. Interestingly, the large liposomes swimming in bump-mode gradually showed green fluorescence, and the GFI_{lipo} became larger than the GFI_{BG} (Figure 4. 13-a–e). On the contrary, the liposomes of zigzag-mode (small liposomes) did not show stronger fluorescence intensity than the background (Figure 4. 13-f, g). Noteworthy, the small liposomes could be brighter than the background when they were trapped at the dummy traps placed under the trapping region to equalize the flow resistance (Figure 4. 13-h, i). In other words, the size dependency was significant only at the size-sorting region. To justify the obtained result, we focused on the mechanism of the size-sorting. The micro-posts in the size-sorting module separate large particles according to their excluded volume collided to the surface of the microposts¹⁶². Thus, intermittent contact to the micro-posts was imposed only on the large liposomes in the bump-mode. This hypothesis was consistent with the fact that the brighter liposomes were observed at the trapping region since the trapped liposomes were continuously pressed to the device wall by the external flow. Together, we hypothesized that the accumulation was induced by the flow field and physical contact to some surface.

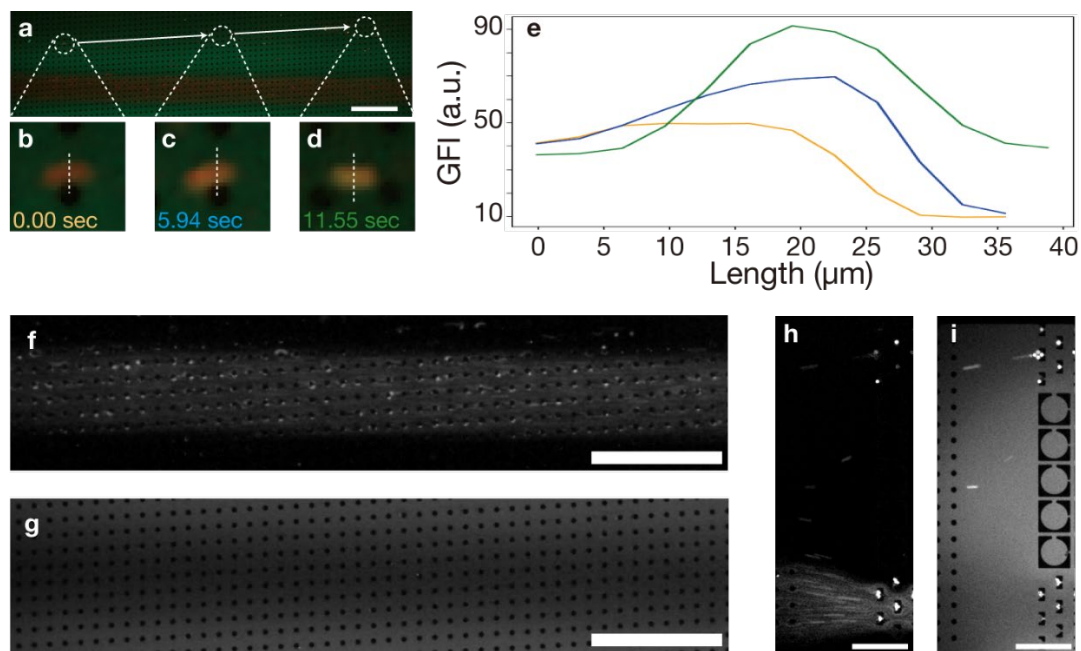


Figure 4. 13 Accumulation of uranine during the size-sorting region. (a–d) EFM images of (a) size-sorting region and (b–d) sequential snapshots tracking a liposome flowing there. (e) Line profiles of the liposome at 0.00 sec (orange), 5.94 sec (blue), and 11.54 sec (green). (f, g) Monochromatic EFM images decomposed from the original image of the size-sorting region focusing on the liposomes move in zig-zag mode. Scale bars: 500 μm . (h, i) Monochromatic EFM images decomposed from the original image of the end of the size-sorting region. Scale bars: 200 μm . (f) and (h) are corresponding to the red channel (liposomes) and (g), (i) are corresponding to the green channel (uranine). Scale bars: 500 μm .

Then, the effect of the flow field on the accumulation was verified. The flow was abruptly stopped after 30 min of the prior exposure to the 5 μ M uranine/1 mM fructose solution (for the abrupt stop, see Figure 2. 7). In this situation, the concentration of the outer solution was able to be kept constant while the flow ceased. Note that to avoid the production of photo-bleached uranine, we did not apply the irradiation light to the liposomes before the abrupt stop, and then the measurement was performed with a long interval (interval: 20 min, optical exposure time: 300 msec). As a result, the ratio of the GFI_{lipo} to GFI_{BG} decreased over time (approximately 90% after 60 min) (Figure 4. 14). Since GFI_{BG} was almost constant, the decrease of the GFI_{lipo} was attributed to passive diffusion. In other words, a flow field was crucial to accumulate uranine against the concentration gradient.

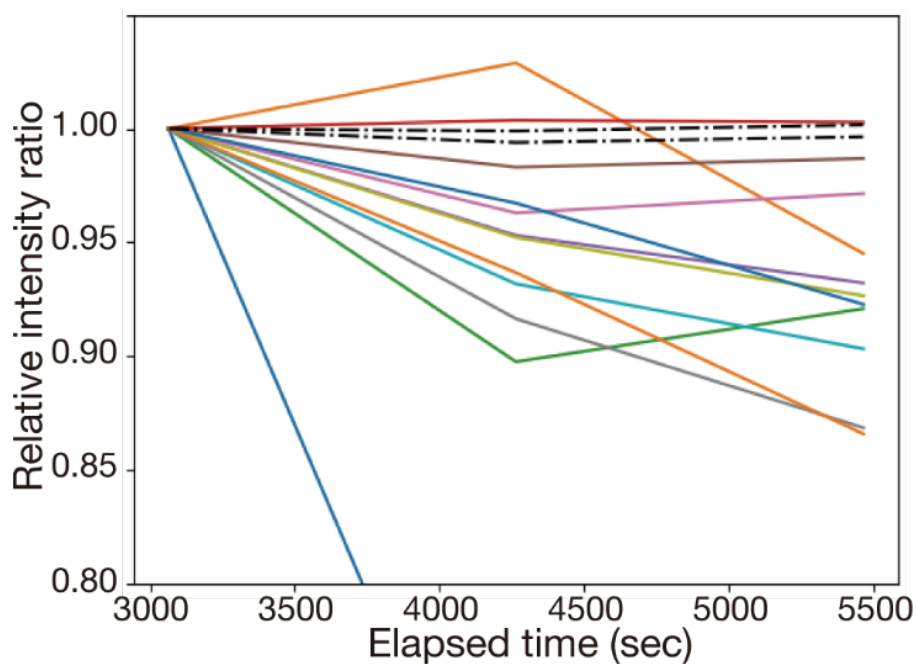


Figure 4. 14 Effect of the flow field on the origin of non-equivalent kinetics of permeation. Time courses of the relative ratio of GFI_{lipo} to GFI_{BG} (colored solid lines) and relative GFI_{BG} (black dashed lines) after the stoppage of the external flow (at 1800 sec). The time courses are normalized by each value at 3000 sec.

The effect of the flow field was then quantitatively examined. We measured the time course of the GFI_{lipo} under flow rates of 0, 6.5, 10, 20, 30, 40, and 60 $\mu\text{L h}^{-1}$. The flow rate of 0 $\mu\text{L h}^{-1}$ denoted the abrupt stop of the flow. In this experiment, liposomes were exposed to the 5 μM uranine/1 mM fructose solution at 40 $\mu\text{L h}^{-1}$ for 30 min in advance so that the outer and inner concentration of uranine were constant and equivalent for all of the flow rates examined. We observed the liposomes over a short interval (interval: 16 sec, optical exposure time: 300 msec) to enhance the effect of photo-bleaching. With a faster intake of intact uranine, the time course of the GFI_{lipo} is more likely to become flat. For example, comparing the results of 0 $\mu\text{L h}^{-1}$ and 60 $\mu\text{L h}^{-1}$ (Figure 4. 15-a, b), the decay rate (the ratio of GFI_{lipo} to that of the same liposome before 16 sec) was maintained near 1.00 for 60 $\mu\text{L h}^{-1}$. In comparison, a sigmoidal transition from approximately 0.98 to 1.00 was obtained for 0 $\mu\text{L h}^{-1}$. Note for calculating the decay ratio, original time courses of GFI_{lipo} were smoothened with four consecutive GFI values for each time point. We plotted the ratio of GFI_{lipo} at the final time point (1200 sec) to that at the initial time point (0 sec) for each flow rate. As a result, this ratio tended to increase with an increase of the flow rate, at least in the range from 0 $\mu\text{L h}^{-1}$ to 20 $\mu\text{L h}^{-1}$ (Figure 4. 15-c). Namely, the high flow rate afforded the large difference of kinetics between the intake and release of uranine, which presumably resulted in the accumulation.

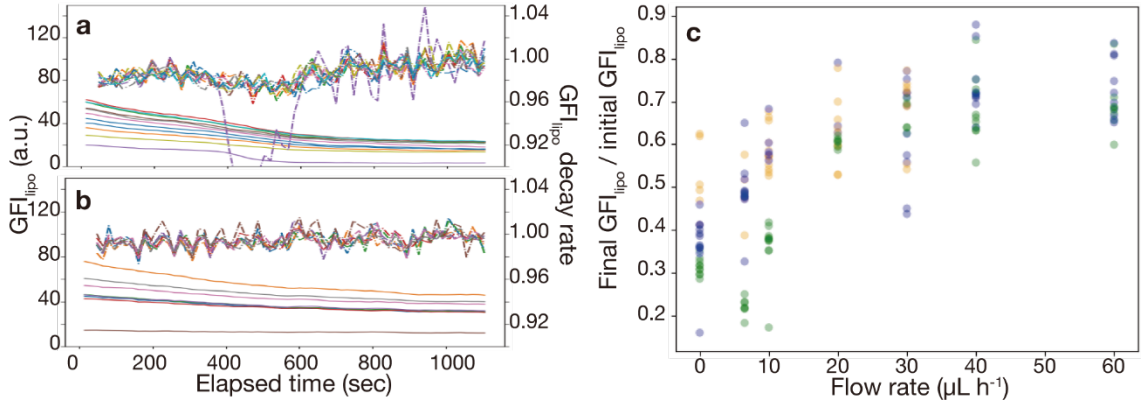


Figure 4.15 Flow rate dependency of accumulation of uranine in trapped liposomes. (a, b) Time courses of GFI_{lipo} (solid line) and the decay rate of GFI_{lipo} (dashed line) after the flow rate was changed from 40 $\mu\text{L h}^{-1}$ to (a) 0 $\mu\text{L h}^{-1}$ and (b) 60 $\mu\text{L h}^{-1}$ at 0 sec, respectively. (c) Dot plot of the ratio of GFI_{lipo} at 1200 sec (final GFI_{lipo}) to that at 0 sec (initial GFI_{lipo}). Colors (orange, green, and blue) correspond to three independent measurements.

We also compared the effect of the flow rate to the equilibrated distribution of GFI_{lipo}. Liposomes were exposed to uranine without irradiating light under different experimental conditions: exposure time t (min), uranine concentration c (μM), and flow rate v ($\mu\text{L/h}$); abbreviated as $[t, c, v]$. The distributions of GFI_{lipo} obtained from three independent experiments for each condition were combined and tested by Mann-Whitney's U-test. Note that to avoid the difference of the irradiation light, we calculated the pseudo-concentration of uranine inside based on the GFI_{BG}. As a result, the datasets [30, 15, 20] and [15, 15, 40] were statistically distinguishable in a two-sided test ($p < 0.05$) (Figure 4.16). Since the two conditions afforded the same amount of uranine molecules to the trapped liposomes, the obtained data suggested that the flow field affected the equilibrated concentration of uranine.

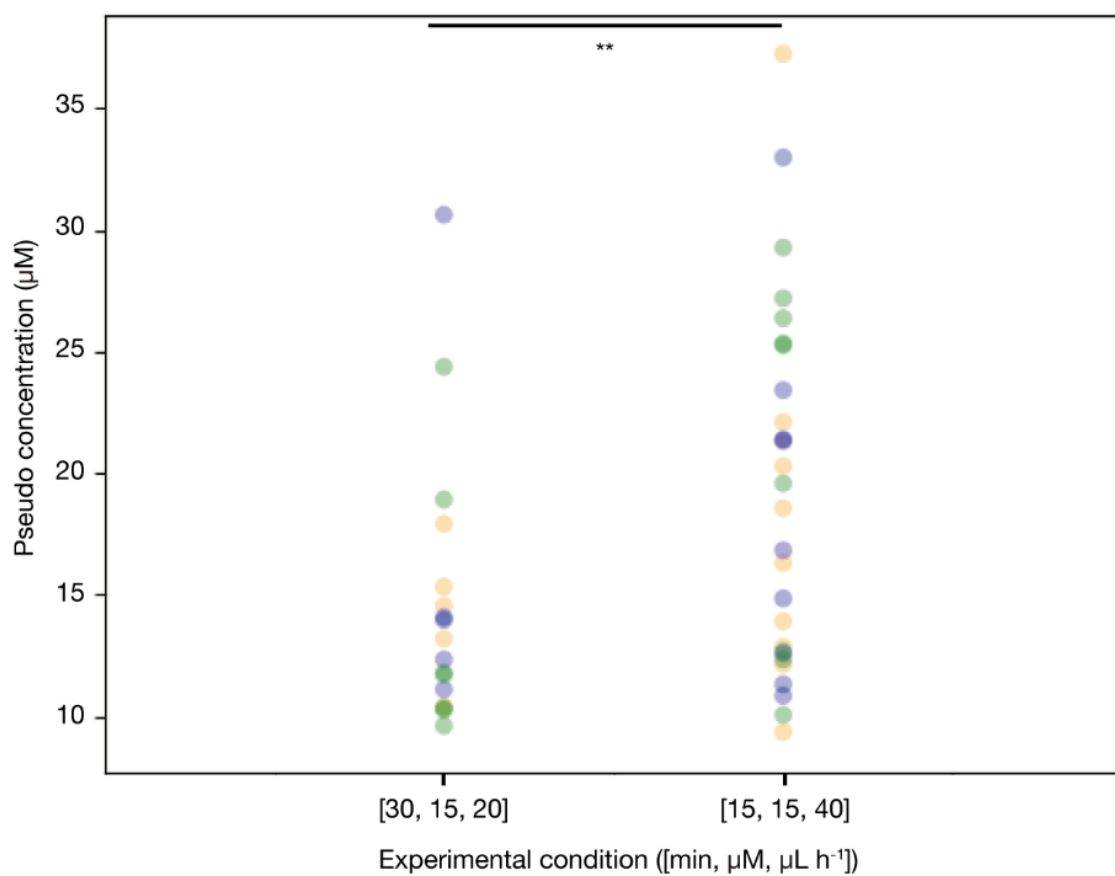


Figure 4. 16 Distributions of the pseudo concentration of uranine: effect of flow rate during exposure to the uranine solution. Distributions of the pseudo concentration of uranine in liposomes calculated from GFI_{lipo} and GFI_{BG} under different flow rates ([minutes, μM , $\mu L h^{-1}$] = [30, 15, 20] and [15, 15, 40]). Data are plotted from three independent measurements for each condition (orange, blue, and green). ** indicates p-value (0.033) < 0.05, evaluated by two-sided Mann-Whitney's U-test.

4.5. Permeation and accumulation of fluorescein-tagged ATP

To examine whether the observed accumulation is extended to other small molecules, especially those that are biologically relevant, we exposed the trapped liposomes to an aqueous solution of an ATP analog, fluorescein-12-adenosine triphosphate (FL-ATP). The concentration and flow rate of the outer solution was fixed at 15 μM FL-ATP/1 mM fructose and 40 $\mu\text{L h}^{-1}$, respectively. EFM images were taken every 5 min throughout the following experiments.

When the liposomes were exposed to the FL-ATP solution, 40% of the measured liposomes showed an increase in the GFI_{lipo} that was approximately 3 times higher than the GFI_{BG} in the first 5 min, and the fluorescence inside was detectable even after the 4 h of washout by 1 mM fructose solution (Figure 4. 17-a–c). With the same experimental procedure but using fluorescein instead of FL-ATP as a reference experiment, GFI_{lipo} also became higher than GFI_{BG} during exposure to the fluorescein solution. However, after 30 min of washout, GFI_{lipo} was almost the same as the initial value before exposure (Figure 4. 17-d). Therefore, the intake and release of FL-ATP were remarkably more imbalanced than fluorescein, probably because of its ATP moiety.

Interestingly, the time course of the GFI_{lipo} showed a non-monotonic tendency during exposure to the FL-ATP solution (15 min) and following washout (Figure 4. 17-c). Namely, GFI_{lipo} decreased rapidly during the first 5–10 min, and then gradually recovered during the washout. Note that this tendency was not observed when fluorescein was used (Figure 4. 17-d). Thus, the trend was also arising from ATP-moiety. This characteristic time course can be explained by the small pKa of ATP (the first pKa is less than 1.0)¹⁶³. Namely, the suppression of the fluorescence of fluorescein under a low pH condition (Figure 4. 18) could bring the self-quenching of the emission of FL-ATP due to its acidity.

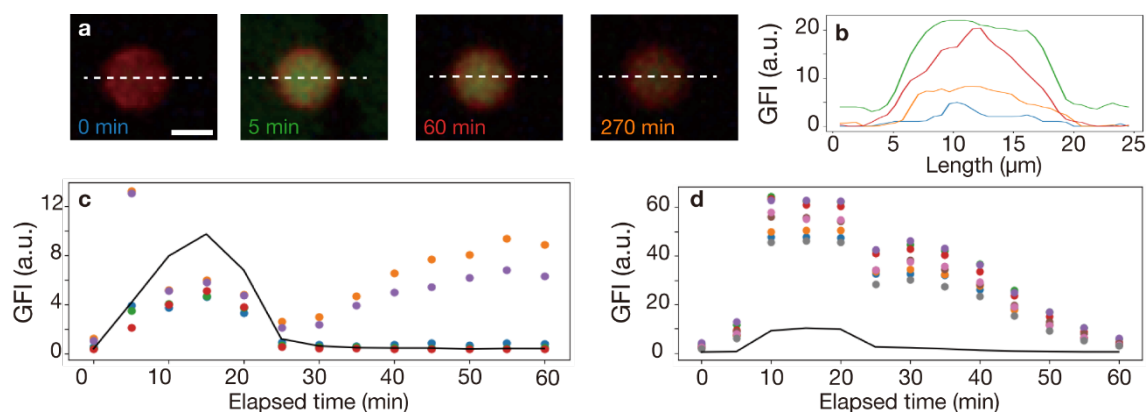


Figure 4. 17 Permeation of FL-ATP into liposomes. (a) Representative EFM images of a liposome exposed to FL-ATP. The contrast was modified for visual readability. Scale bar: 10 μm . (b) Line profiles of the liposome at 0 (blue), 5 (green), 60 (red), and 270 (orange) min (indicated as white dashed lines in (a)). (c) Whole time course of GFI_{lipo} (colored dots) and GFI_{BG} (black line). (d) Time course of GFI_{lipo} (colored dots) and GFI_{BG} (black line) obtained when fluorescein was used instead of FL-ATP.

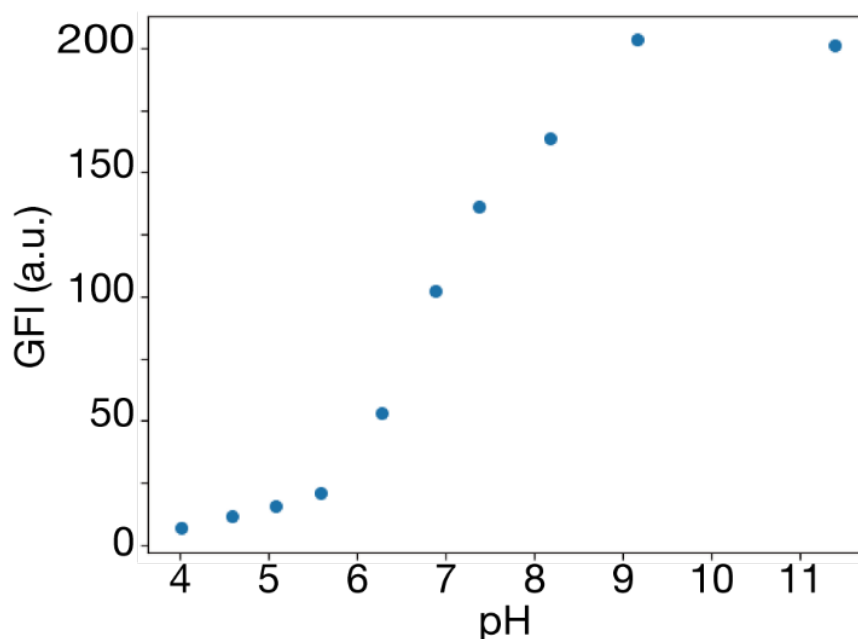


Figure 4. 18 Diagram of the dependency of GFI of the EFM image of FL-ATP solution on pH.

The concentration of FL-ATP was fixed at 5 μM , and the exposure time was 100 msec.

This non-monotonic time course of GFI_{lipo} is also significant as proof of the higher concentration of FL-ATP inside than that of the outer solution. First, the recovery of fluorescence intensity of FL-ATP during the washout (30–60 min) suggested the continuous encapsulation of FL-ATP during 5–20 min. Second, the strength of suppression of fluorescence from FL-ATP was positively related to the amount of FL-ATP. Third, at a couple of liposomes, GFI_{lipo} was higher than GFI_{BG} at 5 min, although at 10 min, the fluorescence intensity of FL-ATP inside the liposome was more strongly suppressed than the outer solution. Therefore, the concentration of FL-ATP inside liposomes upon the FL-ATP exposure was presumably higher than that of the outer FL-ATP solution.

To bolster this claim, we conducted a stoichiometric estimation to show that the amount of FL-ATP supplied to one liposome is enough to suppress the fluorescence from FL-ATP due to its acidity. According to the pH dependence of FL-ATP (Figure 4. 18), the fluorescence intensity became significantly weak under $pH < 4$. ATP ionizes in multi-steps: the first $pK_a < 1$ and secondary $pK_a \sim 1.7$.¹⁶³ Let us assume that at least one proton is always deprotonated, and the fluorescence intensity could be smaller than that of the background under the following condition:

$$[H^+]_{lipo} \geq [ATP]_{lipo} = 10^{-4}(\text{mol})$$

, where $[H^+]_{lipo}$ and $[ATP]_{lipo}$ are the concentration of proton and ATP, respectively.

The volume (V) of a liposome with a diameter of 10 μm is:

$$V = \frac{4}{3}\pi r^3 |_{r=5 \times 10^{-6}(\text{m}^3)} \sim 500 \times 10^{-15}(\text{L}) = 0.5 (\text{pL})$$

Thus, the amount of ATP required (R_{ATP}) is calculated as follows:

$$R_{ATP} = [H^+]_{lipo} \times V \sim 0.5 \times 10^{-16} (\text{mol})$$

Here, as a secondary assumption, the percentage of fluids passing one nest is proportional to the ratio of the width of the nest (100 μm) to the whole width of the arraying device (2100 μm). The concentration of FL-ATP was 15 μM , and the flow rate was 40 $\mu\text{L h}^{-1}$. Therefore, the total amount of FL-ATP introduced into one nest (T_{ATP}) in 5 min is estimated as follows:

$$T_{ATP} = 15 \times 10^{-6} \times \left(40 \times \frac{5}{60}\right) \times \frac{100}{2100} \sim 2.5 \times 10^{-12} (\text{mol})$$

Therefore,

$$\frac{R_{ATP}}{T_{ATP}} \sim 2.0 \times 10^{-5}$$

Thus, if one molecule per 50,000 molecules could be entrapped in the liposome, the considerable suppression of the fluorescence emission of FL-ATP within 5 min could be achieved. The value was consistent with the result.

4.6. Significance and future perspectives of the current findings

For the spontaneous emergence of a functional compartment at the origin of life, how the substrates can be steadily concentrated inside the compartment is one of the most puzzling questions. There were various candidates of plausible environment for the origin of life, such as warm little pond¹⁶⁴, intertidal zone²⁶, hydrothermal vent¹⁶⁵, but the accumulation of substances into the pre-formed compartment was relatively overlooked. The flow field is easy to be expected even in the prebiotic era, and our system does not contain any sophisticated proteins. Therefore, the phenomena we found here could be implemented to a wide range of possible protocells.

It was also worth emphasizing that FL-ATP is an analog of a chemical energy source to drive enzymatic reactions and other biological reaction networks. Thus, the hydrodynamic accumulation even against the concentration gradient, which was

elucidated for the first time by observing liposomes under a steady flow environment, could be a practical methodology to provide an energy source to liposome-based cell models, which would lead to the remarkable progress of constructive biology and the investigation of the origin of life.

4.7. Conclusion

This chapter demonstrated that small molecules and ions were encapsulated and further accumulated into liposomes against a concentration gradient under a microfluidic environment. We quantitatively and statistically clarified that the accumulation against the concentration gradient was caused only by an external flow and physical contact with a substrate. While we have emphasized the importance of the current finding in the view of the origin of life, the hydrodynamic accumulation is also useful for the practical methodology to supply substrates inside liposome-based cell models^{34, 65, 166, 167}. As discussed thus far, the microfluidic environment was critical to the current finding from the view of the experimental condition and the view of methodology. Namely, high-throughput and efficient direct observation of cell-sized liposomes enabled by MANSIONs was indispensable for the quantitative and statistical proof of the hydrodynamic accumulation of molecules. The current finding would not only stimulate various related research and further development of the field but also provide a significance of the concept of MANSIONs based on microfluidics.

5. Flow-induced disparity in disturbance between the inner/outer leaflets of charged liposomes enabled rapid accumulation of molecules against a concentration gradient

5.1.Introduction

Thus far, the permeability of small molecules and ions across the lipid membrane has been extensively studied for liposomes of sub-micrometers in bulk assay^{83, 84, 168-170}. As a result, it was evidenced that the mechanism of passive permeation across the lipid bilayer is close to the partitioning process rather than pore-formation, and the kinetics of transportation was slow even for small molecules and ions. In the view of methodology, the scope of these reports was limited to the relaxation process of electrochemical potential from non-equilibrium to equilibrium state.

Besides, the use of microfluidics on liposome investigations has been sought in the increasing need for the precise measurements under well-regulated condition^{43, 72, 171}. Chapters 2 and 3 in the thesis also presented promising developments of the microfluidic platform to observe cell-sized liposomes. Several successive applications of these microfluidic developments are found in measuring transportation across the liposomal membrane^{71, 131, 172}. The new technology has enabled a punctual evaluation of the diversity of individual liposomes, but the fundamental picture of the transportation was the same as the previous bulk measurements. Notably, in these trials, the external flow, one of the inevitable characteristics in the microfluidic measurement, has been regarded as an artifact to be addressed^{58, 172}. Although several studies focused on the explicit effect of the shear for the liposomal dynamics^{63, 84, 126}, still fewer interests have been paid to the proactive roles of the external flow, which also put liposomes under a non-equilibrium steady environment.

On the contrary, in the thesis, we explicitly focus on the dynamics of liposomes under a steady flow environment. Chapter 4 described one extreme example: we demonstrated that without ad-hoc mechanics, such as membrane proteins, liposomes exposed to the steady flow under microfluidic trapping accumulated small molecules and ions (including adenosine triphosphate) even against a concentration gradient, termed as hydrodynamic accumulation (HDA). In the practical viewpoint, HDA is significant as an efficient methodology to supply substances to pre-formed liposomes against the concentration gradient, which would promote the construction of sustainable liposome-based artificial cells. Since the well-known relaxation of the concentration gradient under the static condition results in the diminution of the gradient by Fick's rule, the phenomenon is interesting as a new class of transportation across the liposomal membrane. Although we pointed out the relationship between HDA and external flow in the previous chapter, little is known about the behaviors of lipid membrane under such a non-equilibrium steady environment.

In this chapter, we focused on how the liposomal membrane is disturbed in the hydrodynamic condition and how the disturbance is linked to HDA. By changing the phospholipid species and the composition of liposomes, and the kind and concentration of solutes to be exposed, we discuss that microfluidic condition induces asymmetric distribution of anionic phospholipids. We also report that the hydrophobic energetic barrier, typically considered as the origin of the hindrance of the passive permeation across the lipid bilayer, is strikingly reduced, yet in the absence of pores. We also describe the improvement of MANSIONS described in chapter 2. Namely, we extended MANSIONS and enabled more comfortable access to the degree of freedom in the research activity (the extended platform was termed as ExMANSIONS).

5.2. Materials and Method (This section is currently omitted because it includes unpublished data).

5.3. This section is currently omitted because it includes unpublished data.

5.4. Scrutiny of candidates of the physicochemical key factors (A part of this section is currently omitted because it includes unpublished data)

First, we investigated the effect of temperature on HDA. The high temperature would enhance the membrane fluidity, hence the permeability across the membrane for both intake and release of uranine. We tested whether the decrease of the relative difference between these two kinetics could cease HDA. However, even when we increased the temperature ($\sim 40^\circ\text{C}$) from the room temperature (25°C) using instant heat pads placed near the device, the accumulation of uranine was observed (Figure 5. 3).

Second, we tested the effect of membrane constituents other than POPC: cholesterol, fructose, and POPG. In using liposomes prepared in the absence of cholesterol (Figure 5. 4) or fructose (Figure 5. 5), the trapped liposomes with low lamellarity having the GFI_{lipo} larger than GFI_{BG} were observed during the uranine exposure.

On the other hand, liposomes prepared without POPG were not trapped in the device even after 12 h of introducing the liposome dispersion because of their smaller diameters of liposomes. To trap the smaller liposomes, we newly designed and fabricated a device (Figure 5. 6-a). Even in this arraying device, for 66% of trapped liposomes prepared with POPG, GFI_{lipo} was larger than GFI_{BG} ($n=45$; Figure 5. 6-b). As a result, the number of liposomes showing a higher value of GFI_{lipo} than that of GFI_{BG} (Figure 5. 7) was negligible (1 in 15) for liposomes prepared without POPG.

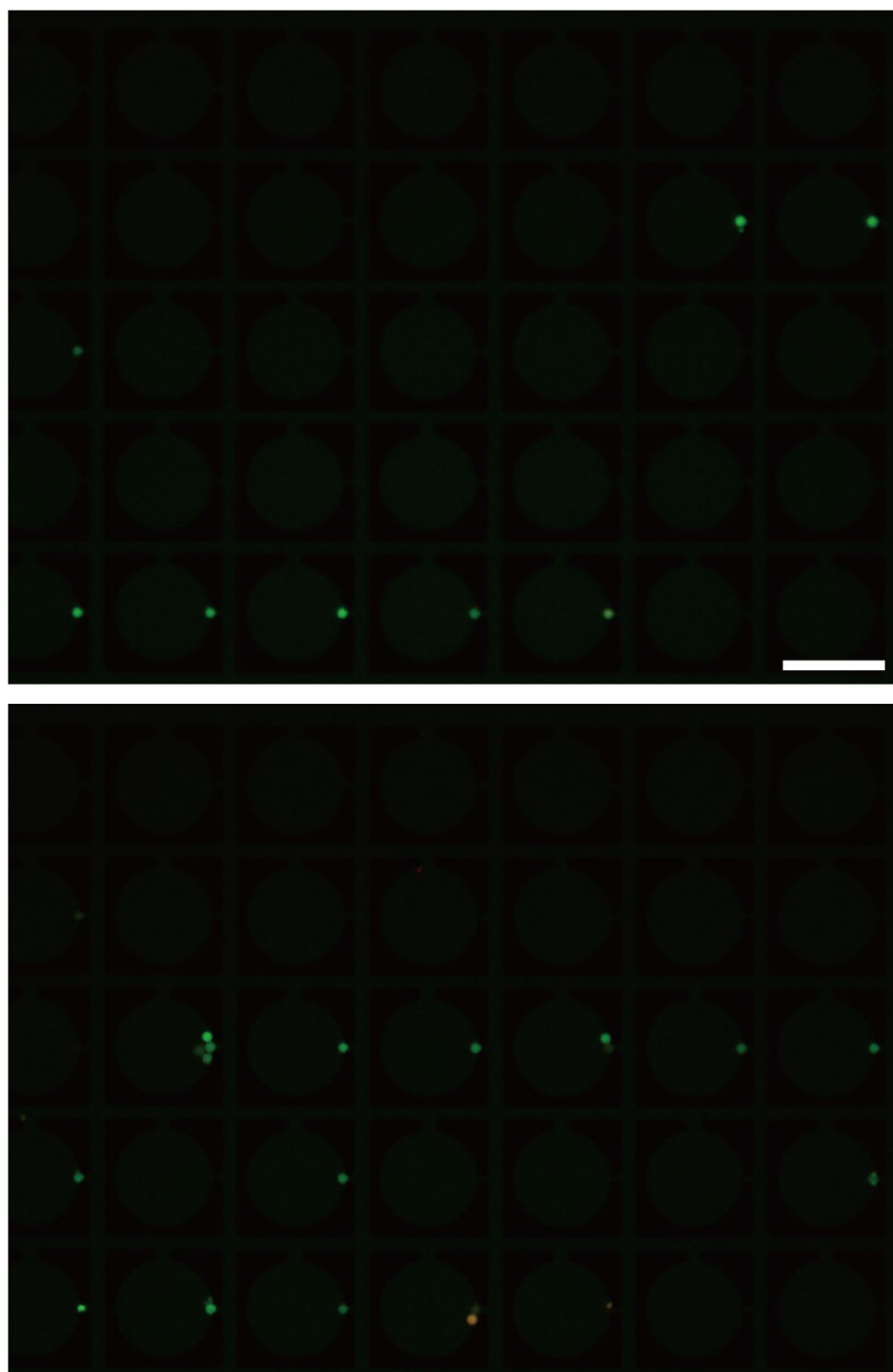


Figure 5. 1 Liposomes exposed to the uranine under high temperature. Two representative EFM images of the trapping region upon 30 min of exposure to the uranine solution (5 μ M uranine/1 mM fructose solution) at about 40 $^{\circ}$ C taken at the individual experimental trials. Scale bars: 100 μ m.

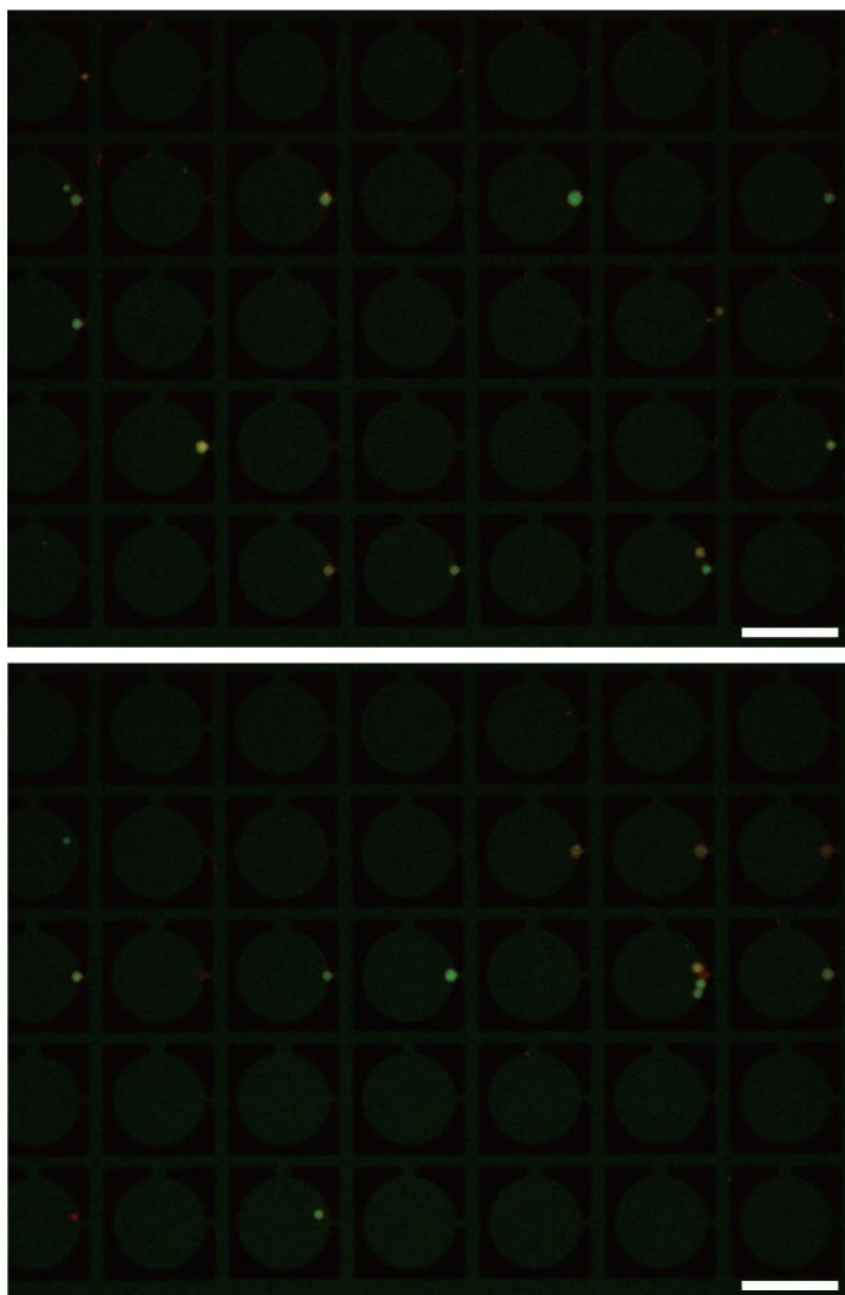


Figure 5. 2 Exposing liposomes prepared without cholesterol to the uranine. Two representative EFM images of the trapping region upon 30 min of exposure to the uranine solution for liposomes prepared without cholesterol taken at the individual experimental trials. Used uranine solutions were 5 μ M uranine/1 mM fructose solution and 5 μ M uranine solution, respectively. Optical exposure time was 300 msec. Scale bars: 100 μ m.

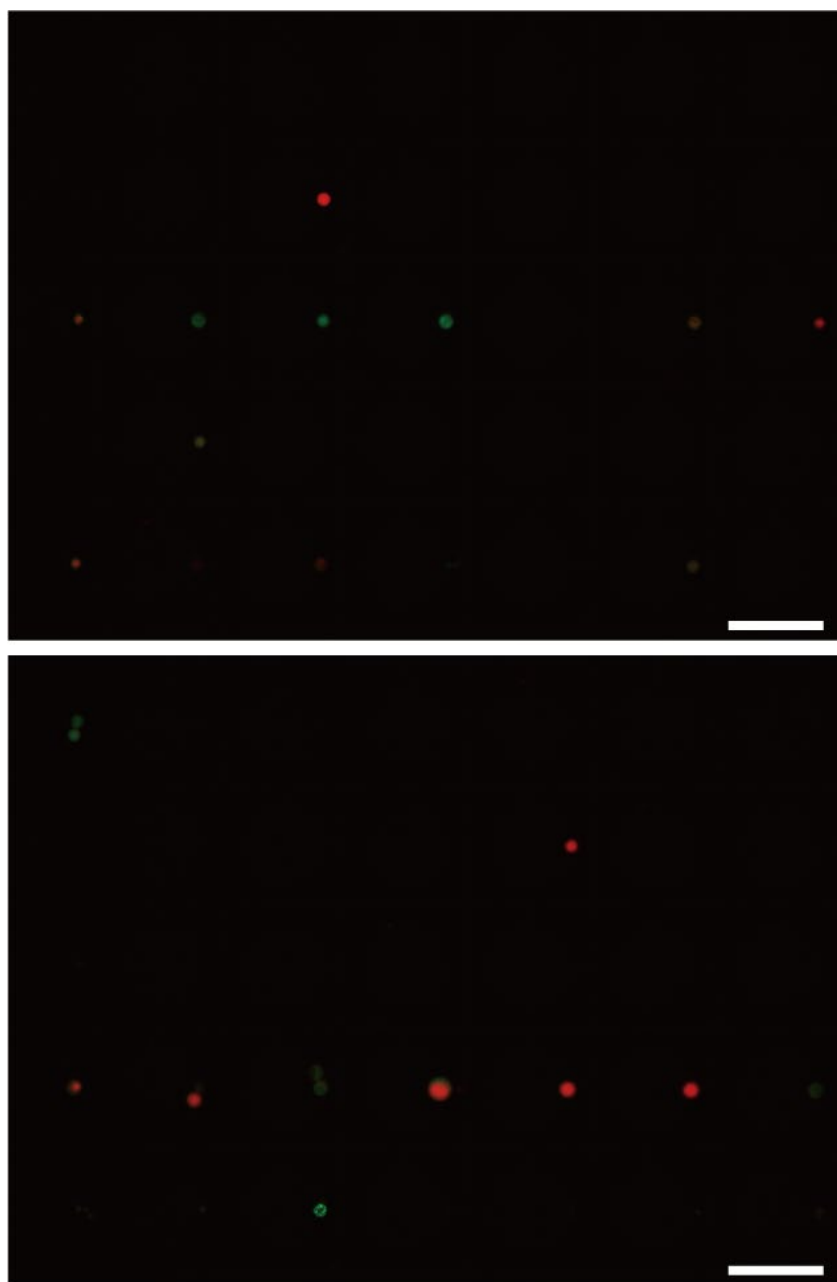


Figure 5. 3 Exposing liposomes prepared without fructose to the uranine. Two representative EFM images of the trapping region upon 30 min of exposure to the uranine solution for liposomes prepared without fructose taken at the individual experimental trials. Used uranine solutions were 5 μ M uranine/1 mM fructose solution and 5 μ M uranine solution, respectively. Optical exposure time was 100 msec. Scale bars: 100 μ m.

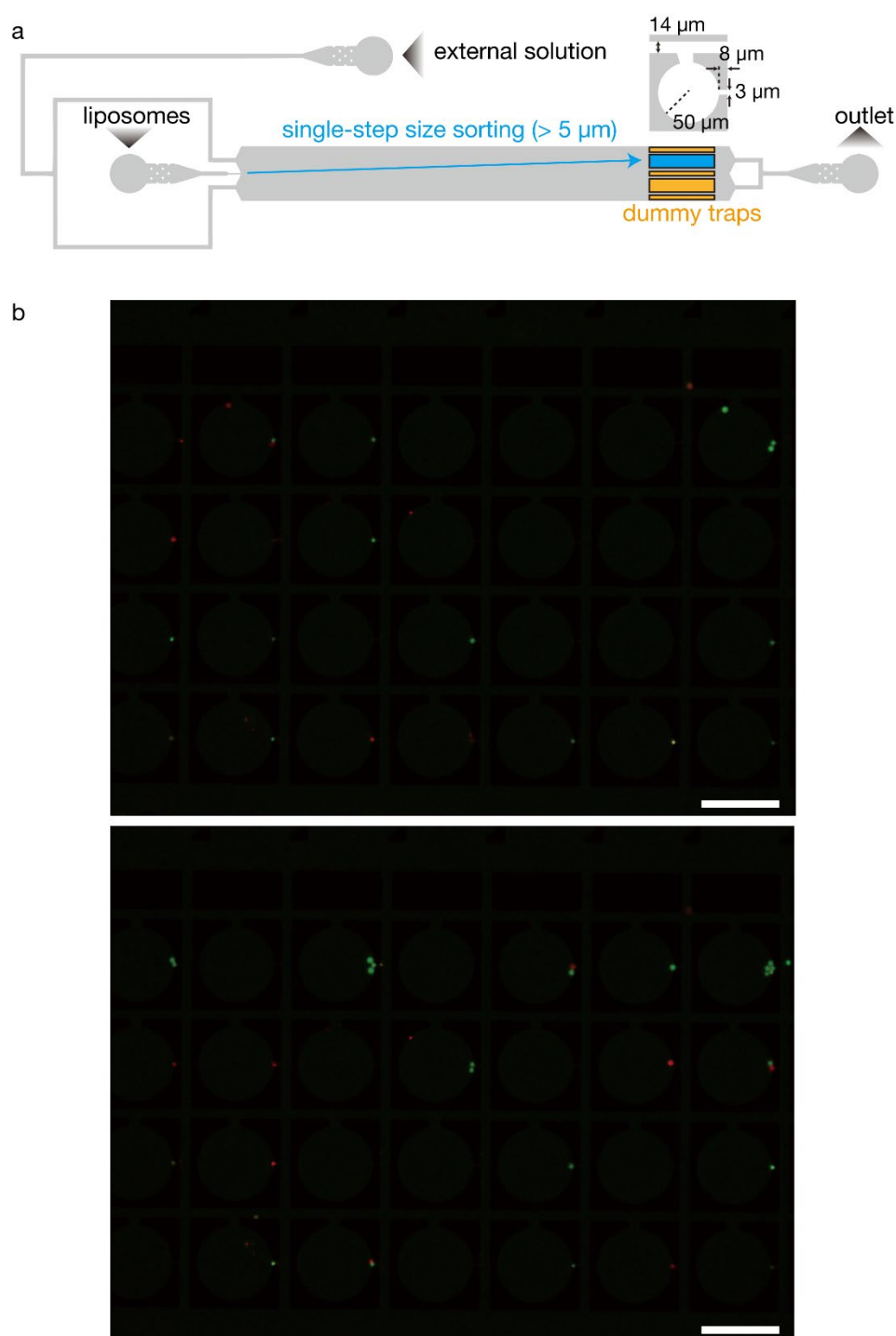


Figure 5. 4 Exposing liposomes under the newly designed device to uranine. (a) Graphical summary of the design of the device. (b) Two representative EFM images of the trapping region upon 30 min of exposure to the uranine solution (5 μM uranine/1 mM fructose solution) for liposomes prepared with POPG taken at the individual experimental trials. Scale bars: 100 μm.

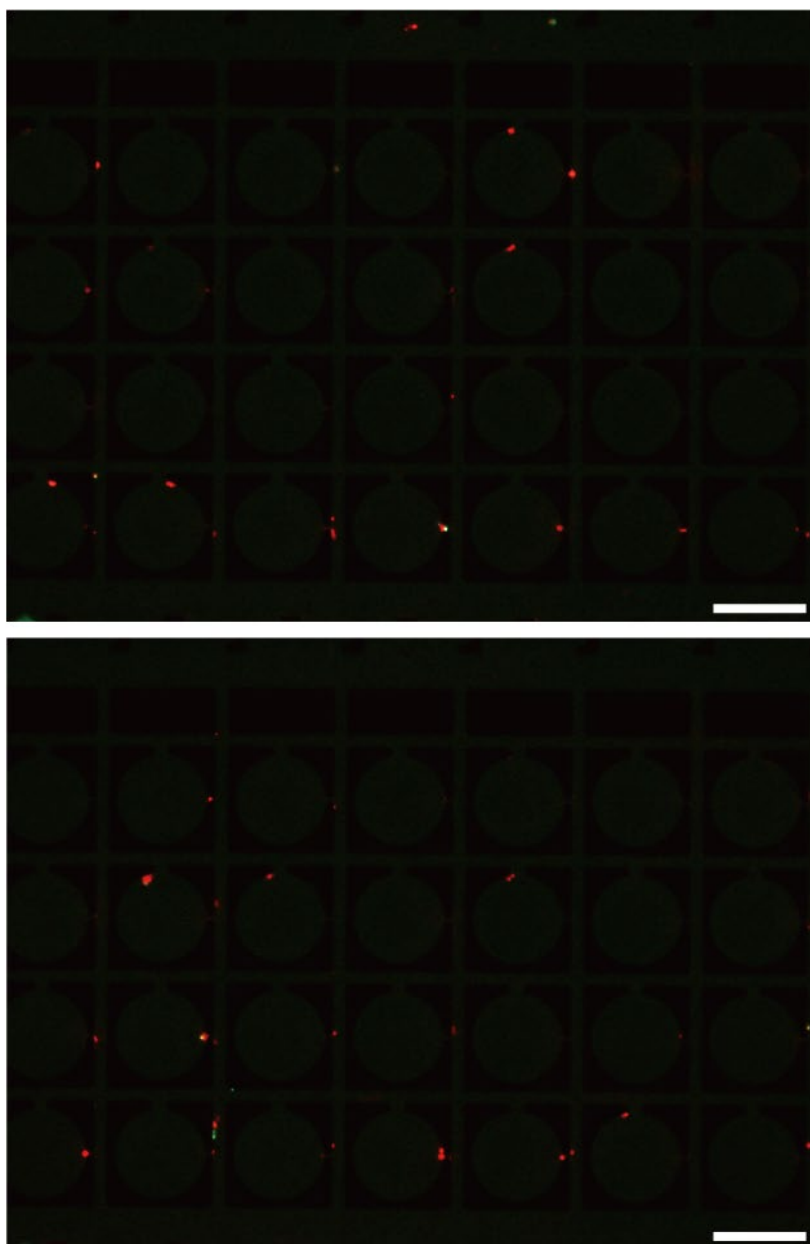


Figure 5. 5 Exposing liposomes without POPG to uranine. Two representative EFM images of the trapping region upon 30 min of exposure to the uranine solution (5 μ M uranine/1 mM fructose solution) for liposomes prepared without POPG taken at the individual experimental trials. Scale bars: 100 μ m.

Temperature and cholesterol are known to affect the membrane fluidity and hence the permeability^{129, 173}, while POPG does not influence at least the water permeability⁵⁹. Thus, we focused on the anionic charge of POPG for the unequal transportation of substances across the phospholipid bilayer membrane. The zeta potentials of the liposome dispersions prepared with and without POPG were -74.9 ± 1.5 mV and -35.7 ± 0.27 mV, respectively (n=3 for each condition) (Figure 5. 8). This result indicates that the surface of the liposomes accumulating the small molecules upon the external flow of their solutions had a strong negative charge.

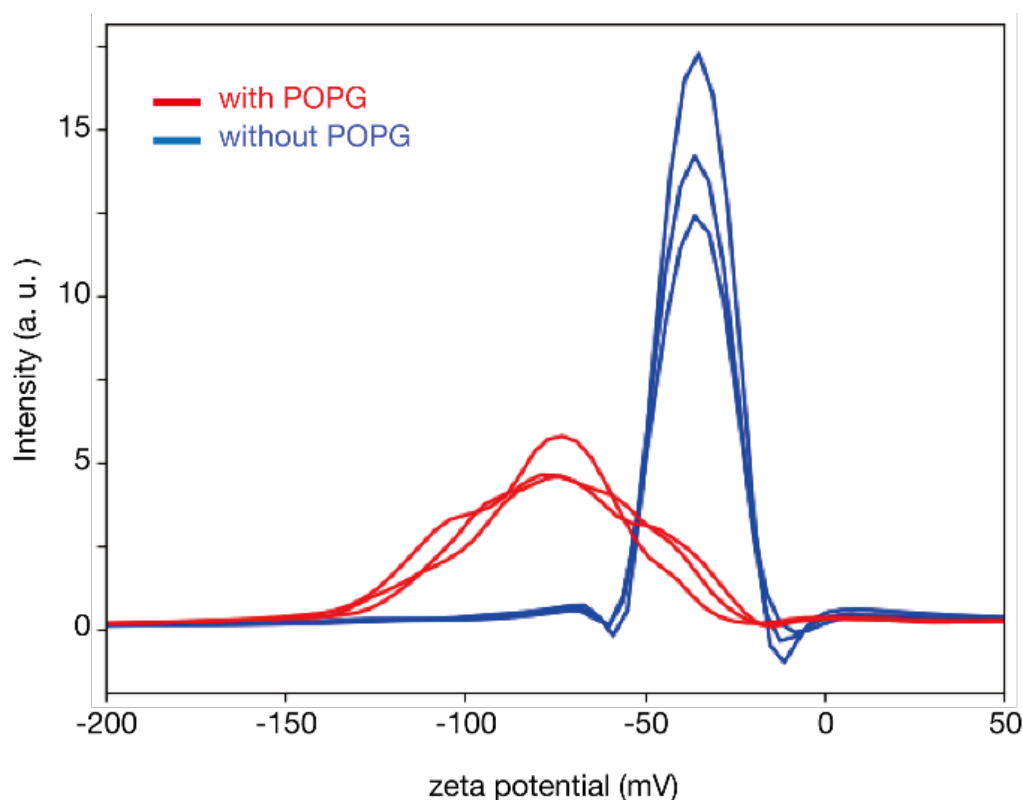


Figure 5. 6 Effect of POPG on the zeta potential of liposomes. Diagrams of zeta potential for liposomes prepared in the presence (red) and absence (blue) of POPG.

The following contents in this section are currently omitted because they include unpublished data.

5.5.This section is currently omitted because it includes unpublished data.

5.6.This section is currently omitted because it includes unpublished data.

5.7.Conclusion (A part of this section is currently omitted because it mentions to unpublished data)

In this chapter, we investigated the unexplored behavior of liposomal membrane under a non-equilibrium steady environment by elucidating the mechanism behind a unique class of transportation across the lipid bilayer, termed hydrodynamic accumulation (HDA).

(Following contents are currently omitted because it mentions to unpublished data)

Besides the expectation on the practical application of HDA as an efficient methodology to supply molecules into the liposome-based artificial cell, the current findings are significant as unexplored dynamics of the liposomal membrane under a non-equilibrium steady environment. We believe that the current findings presented here will open new research interests to the nature of the biological membrane under dynamic conditions.

6. General Conclusion (A part of this section is currently omitted because it mentions to unpublished data)

As the general introduction, in chapter 1, we first summarized the history and the prospect of constructive biology and how the liposome-based cell models can contribute to the progress of the research field. Then we introduced the microfluidic device as a promising tool to meet the requirements on the measurement methodology to further develop constructive biology toward the exploration of sustainability. During the overview of the recent achievements of the microfluidic technology, we discussed that the external flow had been regarded as an undesirable byproduct derived from the method. On the other hand, we pointed out several reports demonstrating the unique effect of external flow on liposomal behaviors. Thus, we set the focus of the thesis to explore the liposome under a steady flow environment.

The recent development of microfluidic technology brought significant progress in terms of the throughput and accuracy of one experimental procedure. However, for the assurance of the statistical and quantitative analysis toward the rigid progress of the research field, repeatability and reproducibility of the procedure should also be addressed.

Thus, in chapter 2, we described a machine-assisted observation platform of the cell-sized liposomes. We termed the system as MANSIONs, which integrated two newly designed microfluidic devices and peripheral of microfluidic experiments via the in-house-developed Python programs. We first verified the design principles of each elemental microfluidic device and then demonstrated the performance of MANSIONs by measuring the behaviors of the liposomes exposed to the osmotic stress. The fundamental concepts to be established (throughput, accuracy, and reproducibility) were reliably

confirmed. Through the detailed analysis of the morphology of the liposomes, we found that the stability of the trapped liposomes was determined not only by their diameters but also by their reduced volume. The result also showed the potential of the device for the deformability assay of the liposomes under a steady flow environment. It was also noteworthy that as the system implemented the sudden stop of the external flow at an arbitrary timing, liposomes can be measured under the condition closely similar to the bulk experiments. The developed machine-assisted observation platform, MANSIONs, was a promising tool to investigate liposomes under a steady flow environment quantitatively and statistically.

Chapter 3 was devoted to the expansion of the scope of MANSIONs to more complicated liposome-based cell models. We introduced the water-in-oil emulsion transfer (WOET) method as a promising preparation protocol by which liposomes can encapsulate even macromolecules and micrometer-sized colloidal particles efficiently. We showed that the innate microfluidic device did not suit the liposomes prepared by the WOET method because of the strong adhesion on the surface possibly due to contaminated oil residues in the membrane. We confirmed that the grafted perfluoroalkyl group on the PDMS wall considerably change the surface property to hydro/lipo-phobic. As a result, the stable capture of the liposomes prepared by the WOET method was established in the microfluidic device whose surface was modified by the perfluoroalkyl group. We found convection inside the liposomes when we observed the liposomes encapsulating fluorescent microbeads with the microfluidic device. As the convection ceased by the stoppage of the external flow, the driving force of the convection was the external flow. Besides, by plotting the histogram of the number of the encapsulated microbeads, we visualized that the long-tailed distribution of the encapsulation yield was

not biased even under the microfluidic investigation. The result was important to ensure the compatibility of the microfluidic exploration to the traditional experimental data as the encapsulation yield was the core of the reconstructed system in the liposomes. On the contrary, we clarified that the water permeability of the liposomes prepared by the WOET method was considerably decreased to almost 10 % of the previously known value. We suspected the oil residue contaminated in the liposomal membrane during the preparation as the cause. It was the first quantitative identification of the decreased water permeability across the membrane of the liposomes prepared by the WOET method to the best of our knowledge. As the permeation across the liposomal membrane was of great interest, the result should be noted as an inevitable feature of the liposomes prepared by the WOET method. As for the perspectives for future research, we emphasized the convection observed in the liposomes. One of the promising directions of the liposomes prepared by the WOET method is to encapsulate bio-functional molecules and reconstruct the cellular functions. Since the convection could enhance the mixing efficiency inside the liposomes, the microfluidic environment could work as an accelerator of the inner reaction.

Based on the developed platform, in the following two chapters, we focused on measuring the unique behavior of liposomes under a steady flow environment. To define and expand the scope of the following two chapters, at the beginning of chapter 4, we first discussed how constructive biology could be linked to the origin of life research. At the origin, the link between simplicity and complexity was more emphasized. In such a case, the efficient transportation across the membrane could be the key to elucidate the contribution of the lipid compartment to the fundamental design principle of the cellular system.

Chapter 4 described the unique transportation by which molecules were accumulated into the liposomes, even against a concentration gradient. The liposomes did not contain any proteins or additional components other than phospholipid. Passive permeation, which was the only mechanism that could be assumed at first sight, never transport molecules against a concentration gradient. The observed dynamics required thorough justification and careful proof. We performed the kinetic investigation and time-resolved measurement with the support of the mathematical toy model. As a result, we reliably deduced that the kinetic imbalance of the permeability from inside to outside and vice versa brought the high concentration in the trapped liposomes. We observed that the accumulation already started during the size-sorting region, and the accumulated molecules leaked when the external flow was stopped. Considering that the newly elucidated transportation across the liposomal membrane was deeply related to the external steady flow, we termed it as hydrodynamic accumulation (HDA). Noteworthy, HDA was first demonstrated by uranine, a fluorescent molecule, but we found that other molecules, fluorescein, and fluorescein-tagged adenosine triphosphate, could also be accumulated. Since adenosine triphosphates are used as the chemical energy source in living systems, the potential of HDA was significant not only in the view of constructive biology but also for the origin of life research.

Chapter 5 ///Following contents are currently omitted because they mention to unpublished contents. ///

Hydrodynamic accumulation would open various new research interests. For example, it would be an efficient methodology to steadily supply the inner substrate to the reconstructed liposome-based cell model. In particular, hydrodynamic accumulation

of ATP, a chemical energy source of the bio-functional system, was expected to directly contribute to the construction of the liposome-based artificial cell of sustainability. As summarized in chapter 1, the reconstruction of protein synthesis is one of the main focus of the relevant research field. Since ATP is an indispensable, but hardly permeate lipid membrane under the bulk condition, the use of hydrodynamic accumulation would help the various related research works. For the reconstruction of such liposomes encapsulating bio-functional molecules inside, the water-in-oil-emulsion transfer method is necessary, while previously it has been difficult to apply in the microfluidic measurement. The surface modification of the microfluidic device, described in chapter 3, we are already ready for further investigations using liposomes encapsulating bio-functional molecules by MANSIONS.

Hydrodynamic accumulation also stimulates the engineering of molecules linked to organic chemistry to explore molecules to be concentrated more efficiently. Consideration of the mechanism at a molecular level would accelerate the physics of lipid molecules under a continuous flow of external energy. The exploration of the molecular structure that fit to the efficient HDA is promising in terms of the investigation of plausible construction of protocell at the origin of life. The emergence of the function requires the substantial concentration of the functional molecules into the compartment while the very compartment hinders the accumulation of the molecules. The elucidation of molecular structure that accelerate the accumulation even against the concentration gradient could restrict the plausible candidates for the constituents of protocell.

As for the extension of the scope of hydrodynamic accumulation, it is important to investigate the minimum condition that emerges hydrodynamic condition. In the thesis, we found and discussed hydrodynamic accumulation only inside the microfluidic device.

Although microfluidic device provides the efficiency and accuracy to the direct observation of the liposomes, close collaborations with the traditional electrochemical measurements are not fully developed, which hindered the closest clarification of the mechanism of hydrodynamic accumulation. Expansion of the microfluidic technology to the traditional electrochemical measurements are the challenge in the future works whose benefits bring the considerable progress of the wide range of science. However, limiting to the exploration of hydrodynamic accumulation, it would be also promising to study hydrodynamic accumulation in a condition that is somewhat close to bulk condition, such as capillary assays. During these trials, if we could extend the scope of hydrodynamic accumulation to the physiological condition, more therapeutic applications of hydrodynamic accumulation would be possible since the shear forced environments are also ordinary in the living organisms, such as inside the vessels.

Thus, using the newly developed microfluidic platform, MANSIONs, the quantitative and statistical analysis of the dynamics of cell-sized liposomes under a steady flow environment was performed. We clarified the unique transportation across the liposomal membrane caused by the membrane disturbance, which was never observed. It was MANSIONs that enabled the efficient acquisition of the data by providing easy access for the high throughput, accurate, and reproducible experimental procedures, which was indispensable for the careful and thorough justification of the observed dynamics of liposomes under a steady flow environment. The overall study described in the thesis was of significance, which will lead to the progress of constructive biology.

References

1. Hooke, R., *Micrographia*. 1665; Vol. 13.
2. Alberts, B.; Johnson, A.; Lewis, J.; Morgan, D.; Raff, M.; Roberts, K.; Walter, P., *Molecular Biology of the CELL*. 6 ed.; 2014.
3. Watson, J. D.; Crick, F. H. C., Molecular structure of nucleoc acids - a structure for deoxyribose nucleic acid. *Nature* **1953**, *171* (4356), 737-738.
4. Crick, F. In *On protein synthesis*, Symp. Soc. Exp. Biol., 1958.
5. Crick, F. In *The genetic code - yesterday, today, and tomorrow*, Cold Spring Harb. Symp. Quant. Biol., 1966.
6. Sander, J. D.; Joung, J. K., CRISPR-Cas systems for editing, regulating and targeting genomes. *Nat. Biotechnol.* **2014**, *32* (4), 347-355.
7. Joung, J. K.; Sander, J. D., Innovation TALENs: a widely applicable technology for targeted genome editing. *Nat. Rev. Mol. Cell Biol* **2013**, *14* (1), 49-55.
8. Hartwell, L. H.; Hopfield, J. J.; Leibler, S.; Murray, A. W., From molecular to modular cell biology. *Nature* **1999**, *402* (6761), C47-C52.
9. Kitano, H., Systems biology: A brief overview. *Science* **2002**, *295* (5560), 1662-1664.
10. Hatakeyama, T. S.; Kaneko, K., Generic temperature compensation of biological clocks by autonomous regulation of catalyst concentration. *Proc. Natl. Acad. Sci. U. S. A.* **2012**, *109* (21), 8109-8114.
11. Sawai, S.; Thomason, P. A.; Cox, E. C., An autoregulatory circuit for long-range self-organization in Dictyostelium cell populations. *Nature* **2005**, *433* (7023), 323-326.
12. Keasling, J. D., Synthetic biology for synthetic chemistry. *ACS Chem. Biol.* **2008**, *3* (1), 64-76.
13. Xie, Z.; Wroblewska, L.; Prochazka, L.; Weiss, R.; Benenson, Y., Multi-Input RNAi-Based Logic Circuit for Identification of Specific Cancer Cells. *Science* **2011**, *333* (6047), 1307-1311.
14. Szostak, J. W.; Bartel, D. P.; Luisi, P. L., Synthesizing life. *Nature* **2001**, *409* (6818), 387-390.
15. Blain, J. C.; Szostak, J. W., Progress Toward Synthetic Cells. *Annu. Rev. Biochem.* **2014**, *83*, 615-640.
16. Stano, P.; Luisi, P. L., Achievements and open questions in the self-reproduction of vesicles and synthetic minimal cells. *Chem. Commun.* **2010**, *46* (21), 3639-3653.
17. Kuruma, Y.; Stano, P.; Ueda, T.; Luisi, P. L., A synthetic biology approach to

the construction of membrane proteins in semi-synthetic minimal cells. *Biochim. Biophys. Acta Biomembr.* **2009**, *1788* (2), 567-574.

18. Forlin, M.; Lentini, R.; Mansy, S. S., Cellular imitations. *Curr. Opin. Chem. Biol.* **2012**, *16* (5-6), 586-592.

19. Kaneko, K., *Life: An Introduction to Complex Systems Biology*. 2006.

20. Bangham, A. D.; Horne, R. W., Negative staining of phospholipids and their structural modification by surface-active agents as observed in the electron microscope. *J. Mol. Biol.* **1964**, *8* (5), 660-668.

21. Sessa, G.; Weissmann, G., Phospholipid spherules (liposomes) as a model for biological membranes. *J. Lipid Res.* **1968**, *9* (3), 310-318.

22. Nagarajan, R., Molecular packing parameter and surfactant self-assembly: The neglected role of the surfactant tail. *Langmuir* **2002**, *18* (1), 31-38.

23. Kunitake, T.; Okahata, Y., Totally synthetic bilayer membrane. *J. Am. Chem. Soc.* **1977**, *99* (11), 3860-3861.

24. Kunitake, T.; Okahata, Y.; Shimomura, M.; Yasunami, S. I.; Takarabe, K., Formation of stable bilayer assemblies in water from single-chain amphiphiles - relationship between the amphiphile structure and the aggregate morphology. *J. Am. Chem. Soc.* **1981**, *103* (18), 5401-5413.

25. Walde, P.; Cosentino, K.; Engel, H.; Stano, P., Giant vesicles: preparations and applications. *ChemBiochem* **2010**, *11* (7), 848-865.

26. Deamer, D. W., The first living systems: a bioenergetic perspective. *Microbiol. Mol. Biol. Rev.* **1997**, *61* (2), 239-261.

27. Horio, T.; Hotani, H., Visualization of the dynamic instability of individual microtubules by dark-field microscopy. *Nature* **1986**, *321* (6070), 605-607.

28. Hotani, H., Transformation pathways of liposomes. *J. Mol. Biol.* **1984**, *178* (1), 113-120.

29. Kaneko, T.; Itoh, T. J.; Hotani, H., Morphological transformation of liposomes caused by assembly of encapsulated tubulin and determination of shape by microtubule-associated proteins (MAPs). *J. Mol. Biol.* **1998**, *284* (5), 1671-1681.

30. Terasawa, H.; Nishimura, K.; Suzuki, H.; Matsuura, T.; Yomo, T., Coupling of the fusion and budding of giant phospholipid vesicles containing macromolecules. *Proc. Natl. Acad. Sci. U. S. A.* **2012**, *109* (16), 5942-5947.

31. Natsume, Y.; Pravaz, O.; Yoshida, H.; Imai, M., Shape deformation of giant vesicles encapsulating charged colloidal particles. *Soft Matter* **2010**, *6* (21), 5359-5366.

32. Noireaux, V.; Libchaber, A., A vesicle bioreactor as a step toward an artificial cell assembly. *Proc. Natl. Acad. Sci. U. S. A.* **2004**, *101* (51), 17669-17674.

33. Hamada, S.; Tabuchi, M.; Toyota, T.; Sakurai, T.; Hosoi, T.; Nomoto, T.; Nakatani, K.; Fujinami, M.; Kanzaki, R., Giant vesicles functionally expressing membrane receptors for an insect pheromone. *Chem. Commun.* **2014**, *50* (22), 2958-2961.
34. Berhanu, S.; Ueda, T.; Kuruma, Y., Artificial photosynthetic cell producing energy for protein synthesis. *Nat. Commun.* **2019**, *10*, 1325.
35. Keber, F. C.; Loiseau, E.; Sanchez, T.; DeCamp, S. J.; Giomi, L.; Bowick, M. J.; Marchetti, M. C.; Dogic, Z.; Bausch, A. R., Topology and dynamics of active nematic vesicles. *Science* **2014**, *345* (6201), 1135-1139.
36. Adamala, K. P.; Martin-Alarcon, D. A.; Guthrie-Honea, K. R.; Boyden, E. S., Engineering genetic circuit interactions within and between synthetic minimal cells. *Nat. Chem.* **2017**, *9* (5), 431-439.
37. Osawa, M.; Erickson, H. P., Liposome division by a simple bacterial division machinery. *Proc. Natl. Acad. Sci. U. S. A.* **2013**, *110* (27), 11000-11004.
38. Kohyama, S.; Yoshinaga, N.; Yanagisawa, M.; Fujiwara, K.; Doi, N., Cell-sized confinement controls generation and stability of a protein wave for spatiotemporal regulation in cells. *Elife* **2019**, *8*, e44591.
39. Godino, E.; Lopez, J. N.; Foschepoth, D.; Cleij, C.; Doerr, A.; Castella, C. F.; Danelon, C., De novo synthesized Min proteins drive oscillatory liposome deformation and regulate FtsA-FtsZ cytoskeletal patterns. *Nat. Commun.* **2019**, *10* (1), 4969.
40. Murtas, G.; Kuruma, Y.; Bianchini, P.; Diaspro, A.; Luisi, P. L., Protein synthesis in liposomes with a minimal set of enzymes. *Biochem. Biophys. Res. Commun.* **2007**, *363* (1), 12-17.
41. Hutchison, C. A., III; Chuang, R.-Y.; Noskov, V. N.; Assad-Garcia, N.; Deerinck, T. J.; Ellisman, M. H.; Gill, J.; Kannan, K.; Karas, B. J.; Ma, L.; Pelletier, J. F.; Qi, Z.-Q.; Richter, R. A.; Strychalski, E. A.; Sun, L.; Suzuki, Y.; Tsvetanova, B.; Wise, K. S.; Smith, H. O.; Glass, J. I.; Merryman, C.; Gibson, D. G.; Venter, J. C., Design and synthesis of a minimal bacterial genome. *Science* **2016**, *351* (6280), aad6253.
42. Stano, P.; Luisi, P. L., Semi-synthetic minimal cells: origin and recent developments. *Curr. Opin. Biotechnol.* **2013**, *24* (4), 633-638.
43. Sugiyama, H.; Toyota, T., Toward Experimental Evolution with Giant Vesicles. *Life* **2018**, *8* (4), 53.
44. Walde, P.; Wick, R.; Fresta, M.; Mangone, A.; Luisi, P. L., Autopoietic self-reproduction of fatty acid vesicles. *J. Am. Chem. Soc.* **1994**, *116* (26), 11649-11654.
45. Wick, R.; Walde, P.; Luisi, P. L., Light-microscopic investigations of the

- autocatalytic self-reproduction of giant vesicles. *J. Am. Chem. Soc.* **1995**, *117* (4), 1435-1436.
46. Budin, I.; Devaraj, N. K., Membrane assembly driven by a biomimetic coupling reaction. *J. Am. Chem. Soc.* **2012**, *134* (2), 751-753.
 47. Hardy, M. D.; Yang, J.; Selimkhanov, J.; Cole, C. M.; Tsimring, L. S.; Devaraj, N. K., Self-reproducing catalyst drives repeated phospholipid synthesis and membrane growth. *Proc. Natl. Acad. Sci. U. S. A.* **2015**, *112* (27), 8187-8192.
 48. Kurihara, K.; Tamura, M.; Shohda, K.; Toyota, T.; Suzuki, K.; Sugawara, T., Self-reproduction of supramolecular giant vesicles combined with the amplification of encapsulated DNA. *Nat. Chem.* **2011**, *3* (10), 775-781.
 49. Kurihara, K.; Okura, Y.; Matsuo, M.; Toyota, T.; Suzuki, K.; Sugawara, T., A recursive vesicle-based model protocell with a primitive model cell cycle. *Nat. Commun.* **2015**, *6*, 8352.
 50. Matsuo, M.; Kan, Y.; Kurihara, K.; Jimbo, T.; Imai, M.; Toyota, T.; Hirata, Y.; Suzuki, K.; Sugawara, T., DNA Length-dependent Division of a Giant Vesicle-based Model Protocell. *Sci. Rep.* **2019**, *9*, 6916.
 51. Elowitz, M. B.; Levine, A. J.; Siggia, E. D.; Swain, P. S., Stochastic gene expression in a single cell. *Science* **2002**, *297* (5584), 1183-1186.
 52. Wakamoto, Y.; Dhar, N.; Chait, R.; Schneider, K.; Signorino-Gelo, F.; Leibler, S.; McKinney, J. D., Dynamic persistence of antibiotic-stressed mycobacteria. *Science* **2013**, *339* (6115), 91-95.
 53. Kodama, A.; Sakuma, Y.; Imai, M.; Kawakatsu, T.; Puff, N.; Angelova, M. I., Migration of Phospholipid Vesicles Can Be Selectively Driven by Concentration Gradients of Metal Chloride Solutions. *Langmuir* **2017**, *33* (40), 10698-10706.
 54. Kurisu, M.; Aoki, H.; Jimbo, T.; Sakuma, Y.; Imai, M.; Serrano-Luginbuhl, S.; Walde, P., Reproduction of vesicles coupled with a vesicle surface-confined enzymatic polymerisation. *Commun. Chem.* **2019**, *2*, 117.
 55. Eyer, K.; Paech, F.; Schuler, F.; Kuhn, P.; Kissner, R.; Belli, S.; Dittrich, P. S.; Kramer, S. D., A liposomal fluorescence assay to study permeation kinetics of drug-like weak bases across the lipid bilayer. *J. Control. Release* **2014**, *173*, 102-109.
 56. Kuhn, P.; Eyer, K.; Allner, S.; Lombardi, D.; Dittrich, P. S., A Microfluidic Vesicle Screening Platform: Monitoring the Lipid Membrane Permeability of Tetracyclines. *Anal. Chem.* **2011**, *83* (23), 8877-8885.
 57. Paterson, D. J.; Reboud, J.; Wilson, R.; Tassieri, M.; Cooper, J. M., Integrating microfluidic generation, handling and analysis of biomimetic giant unilamellar vesicles. *Lab on a Chip* **2014**, *14* (11), 1806-1810.

58. Robinson, T.; Kuhn, P.; Eyer, K.; Dittrich, P. S., Microfluidic trapping of giant unilamellar vesicles to study transport through a membrane pore. *Biomicrofluidics* **2013**, 7 (4), 044105.
59. Kazayama, Y.; Teshima, T.; Osaki, T.; Takeuchi, S.; Toyota, T., Integrated Microfluidic System for Size-Based Selection and Trapping of Giant Vesicles. *Anal. Chem.* **2016**, 88 (2), 1111-1116.
60. Sebastian, B.; Favero, T.; Dittrich, P. S., The Effects of Shear Force Transmission Across Vesicle Membranes. *J. Phys. Chem. Lett.* **2017**, 8 (24), 6128-6134.
61. Abreu, D.; Levant, M.; Steinberg, V.; Seifert, U., Fluid vesicles in flow. *Adv. Colloid Interface Sci.* **2014**, 208, 129-141.
62. Woodhouse, F. G.; Goldstein, R. E., Shear-driven circulation patterns in lipid membrane vesicles. *J. Fluid Mech.* **2012**, 705, 165-175.
63. Sturzenegger, F.; Robinson, T.; Hess, D.; Dittrich, P. S., Membranes under shear stress: visualization of non-equilibrium domain patterns and domain fusion in a microfluidic device. *Soft Matter* **2016**, 12 (23), 5072-5076.
64. Gotanda, M.; Kamiya, K.; Osaki, T.; Fujii, S.; Misawa, N.; Miki, N.; Takeuchi, S., Sequential generation of asymmetric lipid vesicles using a pulsed-jetting method in rotational wells. *Sensor. Actuat. B-Chem.* **2018**, 261, 392-397.
65. Weiss, M.; Frohnmayer, J. P.; Benk, L. T.; Haller, B.; Janiesch, J. W.; Heitkamp, T.; Borsch, M.; Lira, R. B.; Dimova, R.; Lipowsky, R.; Bodenschatz, E.; Baret, J. C.; Vidakovic-Koch, T.; Sundmacher, K.; Platzman, I.; Spatz, J. P., Sequential bottom-up assembly of mechanically stabilized synthetic cells by microfluidics. *Nat. Mater.* **2018**, 17 (1), 89-95.
66. Deshpande, S.; Caspi, Y.; Meijering, A. E. C.; Dekker, C., Octanol-assisted liposome assembly on chip. *Nat. Commun.* **2016**, 7.
67. Matosevic, S.; Paegel, B. M., Layer-by-layer cell membrane assembly. *Nat. Chem.* **2013**, 5 (11), 958-963.
68. Miao, L.; Seifert, U.; Wortis, M.; Dobereiner, H. G., Budding transition of fluid-bilayer vesicles - the effect of area-difference elasticity. *Phys. Rev. E* **1994**, 49 (6), 5389-5407.
69. Nishimura, K.; Hosoi, T.; Sunami, T.; Toyota, T.; Fujinami, M.; Oguma, K.; Matsuura, T.; Suzuki, H.; Yomo, T., Population analysis of structural properties of giant liposomes by flow cytometry. *Langmuir* **2009**, 25 (18), 10439-10443.
70. Kodama, A.; Morandi, M.; Ebihara, R.; Jimbo, T.; Toyoda, M.; Sakuma, Y.; Imai, M.; Puff, N.; Angelova, M. I., Migration of Deformable Vesicles Induced by Ionic Stimuli. *Langmuir* **2018**, 34 (38), 11484-11494.

71. Kuhn, P.; Eyer, K.; Allner, S.; Lombardi, D.; Dittrich, P. S., A microfluidic vesicle screening platform: monitoring the lipid membrane permeability of tetracyclines. *Anal. Chem.* **2011**, *83* (23), 8877-8885.
72. Gopfrich, K.; Platzman, I.; Spatz, J. P., Mastering Complexity: Towards Bottom-up Construction of Multifunctional Eukaryotic Synthetic Cells. *Trends Biotechnol.* **2018**, *36* (9), 938-951.
73. Nilsson, J.; Evander, M.; Hammarstrom, B.; Laurell, T., Review of cell and particle trapping in microfluidic systems. *Anal. Chim. Acta* **2009**, *649* (2), 141-157.
74. Velve-Casquillas, G.; Le Berre, M.; Piel, M.; Tran, P. T., Microfluidic tools for cell biological research. *Nano Today* **2010**, *5* (1), 28-47.
75. Le Gac, S.; van den Berg, A., Single cells as experimentation units in lab-on-a-chip devices. *Trends Biotechnol.* **2010**, *28* (2), 55-62.
76. Skelley, A. M.; Kirak, O.; Suh, H.; Jaenisch, R.; Voldman, J., Microfluidic control of cell pairing and fusion. *Nat. Methods* **2009**, *6* (2), 147-152.
77. Robinson, T.; Verboket, P. E.; Eyer, K.; Dittrich, P. S., Controllable electrofusion of lipid vesicles: initiation and analysis of reactions within biomimetic containers. *Lab on a Chip* **2014**, *14* (15), 2852-2859.
78. Nuss, H.; Chevallard, C.; Guenoun, P.; Malloggi, F., Microfluidic trap-and-release system for lab-on-a-chip-based studies on giant vesicles. *Lab on a Chip* **2012**, *12* (24), 5257-5261.
79. Huang, L. R.; Cox, E. C.; Austin, R. H.; Sturm, J. C., Continuous particle separation through deterministic lateral displacement. *Science* **2004**, *304* (5673), 987-990.
80. Inglis, D. W.; Davis, J. A.; Austin, R. H.; Sturm, J. C., Critical particle size for fractionation by deterministic lateral displacement. *Lab on a Chip* **2006**, *6* (5), 655-658.
81. Kronholm, E.; Puusniekka, R.; Jokela, J.; Villberg, J.; Urrila, A. S.; Paunio, T.; Valimaa, R.; Tynjala, J., Trends in self-reported sleep problems, tiredness and related school performance among Finnish adolescents from 1984 to 2011. *J. Sleep Res.* **2015**, *24* (1), 3-10.
82. Boroske, E.; Elwenspoek, M.; Helfrich, W., Osmotic shrinkage of giant egg-lecithin vesicles. *Biophys. J.* **1981**, *34* (1), 95-109.
83. Chakravarthy, S. R.; Giorgio, T. D., Shear stress-facilitated calcium-ion transport across lipid bilayers. *Biochim. Biophys. Acta* **1992**, *1112* (2), 197-204.
84. Bernard, A. L.; Guedeau-Boudeville, M. A.; Marchi-Artzner, V.; Gulik-Krzywicki, T.; di Meglio, J. M.; Jullien, L., Shear-induced permeation and fusion of lipid vesicles. *J. Colloid Interface Sci.* **2005**, *287* (1), 298-306.

85. Tan, W.-H.; Takeuchi, S., A trap-and-release integrated microfluidic system for dynamic microarray applications. *Proc. Natl. Acad. Sci. U. S. A.* **2007**, *104* (4), 1146-1151.
86. Meijer, H. E. H.; Singh, M. K.; Kang, T. G.; den Toonder, J. M. J.; Anderson, P. D., Passive and Active Mixing in Microfluidic Devices. *Macromolecular Symposia* **2009**, *279*, 201-209.
87. Wen, C. Y.; Yeh, C. P.; Tsai, C. H.; Fu, L. M., Rapid magnetic microfluidic mixer utilizing AC electromagnetic field. *Electrophoresis* **2009**, *30* (24), 4179-4186.
88. Wen, C. Y.; Liang, K. P.; Chen, H.; Fu, L. M., Numerical analysis of a rapid magnetic microfluidic mixer. *Electrophoresis* **2011**, *32* (22), 3268-3276.
89. Lee, C. Y.; Wang, W. T.; Liu, C. C.; Fu, L. M., Passive mixers in microfluidic systems: A review. *Chem. Eng. J.* **2016**, *288*, 146-160.
90. Aref, H., Stirring by chaotic advection. *J. Fluid Mech.* **1984**, *143*, 1-21.
91. Jen, C. P.; Wu, C. Y.; Lin, Y. C., Design and simulation of the micromixer with chaotic advection in twisted microchannels. *Lab on a Chip* **2003**, *3* (2), 77-81.
92. Wang, W. T.; Zhao, S. F.; Shao, T.; Jin, Y.; Cheng, Y., Visualization of micro-scale mixing in miscible liquids using mu-LIF technique and drug nano-particle preparation in T-shaped micro-channels. *Chem. Eng. J.* **2012**, *192*, 252-261.
93. Parsa, M. K.; Hormozi, F.; Jafari, D., Mixing enhancement in a passive micromixer with convergent-divergent sinusoidal microchannels and different ratio of amplitude to wave length. *Computers & Fluids* **2014**, *105*, 82-90.
94. Fang, Y. Q.; Ye, Y. H.; Shen, R. Q.; Zhu, P.; Guo, R.; Hu, Y.; Wu, L. Z., Mixing enhancement by simple periodic geometric features in microchannels. *Chemical Engineering Journal* **2012**, *187*, 306-310.
95. Lee, C. Y.; Lin, C. F.; Hung, M. F.; Ma, R. H.; Tsai, C. H.; Lin, C. H.; Fu, L. M., Experimental and numerical investigation into mixing efficiency of micromixers with different geometric barriers. *Mater. Sci. Forum 2006* **2006**, *505-507*, 391-396.
96. Yandrapalli, N.; Robinson, T., Ultra-high capacity microfluidic trapping of giant vesicles for high-throughput membrane studies. *Lab on a Chip* **2019**, *19* (4), 626-633.
97. Neurohr, G. E.; Terry, R. L.; Lengefeld, J.; Bonney, M.; Brittingham, G. P.; Moretto, F.; Miettinen, T. P.; Vaites, L. P.; Soares, L. M.; Paulo, J. A.; Harper, J. W.; Buratowski, S.; Manalis, S.; van Werven, F. J.; Holt, L. J.; Amon, A., Excessive Cell Growth Causes Cytoplasm Dilution And Contributes to Senescence. *Cell* **2019**, *176* (5), 1083-1097.
98. Meleard, P.; Gerbeaud, C.; Pott, T.; FernandezPuente, L.; Bivas, I.; Mitov, M. D.; Dufourcq, J.; Bothorel, P., Bending elasticities of model membranes:

Influences of temperature and sterol content. *Biophys. J.* **1997**, 72 (6), 2616-2629.

99. Eyer, K.; Kuhn, P.; Hanke, C.; Dittrich, P. S., A microchamber array for single cell isolation and analysis of intracellular biomolecules. *Lab on a Chip* **2012**, 12 (4), 765-772.
100. Krinsky, N.; Kaduri, M.; Zinger, A.; Shainsky-Roitman, J.; Goldfeder, M.; Benhar, I.; HersHKovitz, D.; Schroeder, A., Synthetic Cells Synthesize Therapeutic Proteins inside Tumors. *Adv. Healthc. Mater.* **2018**, 7 (9), 1701163.
101. Fujiwara, K.; Adachi, T.; Doi, N., Artificial Cell Fermentation as a Platform for Highly Efficient Cascade Conversion. *ACS Synth. Biol.* **2018**, 7 (2), 363-370.
102. Luo, C.; Hu, X.; Peng, R.; Huang, H.; Liu, Q.; Tan, W., Biomimetic Carriers Based on Giant Membrane Vesicles for Targeted Drug Delivery and Photodynamic/Photothermal Synergistic Therapy. *ACS Appl. Mater. Interfaces.* **2019**, 11 (47), 43811-43819.
103. Mayer, L. D.; Hope, M. J.; Cullis, P. R., Vesicles of variable sizes produced by a rapid extrusion procedure. *Biochim. Biophys. Acta* **1986**, 858 (1), 161-168.
104. Mayer, L. D.; Hope, M. J.; Cullis, P. R.; Janoff, A. S., Solute distributions and trapping efficiencies observed in freeze-thawed multilamellar vesicles. *Biochim. Biophys. Acta* **1985**, 817 (1), 193-196.
105. Angelova, M. I.; Dimitrov, D. S., Liposome electroformation. *Faraday Discuss. Chem. Soc.* **1986**, 81, 303-311.
106. Tsumoto, K.; Matsuo, H.; Tomita, M.; Yoshimura, T., Efficient formation of giant liposomes through the gentle hydration of phosphatidylcholine films doped with sugar. *Colloids. Surf. B* **2009**, 68 (1), 98-105.
107. Pautot, S.; Frisken, B. J.; Weitz, D. A., Production of unilamellar vesicles using an inverted emulsion. *Langmuir* **2003**, 19 (7), 2870-2879.
108. Pautot, S.; Frisken, B. J.; Weitz, D. A., Engineering asymmetric vesicles. *Proc. Natl. Acad. Sci. U. S. A.* **2003**, 100 (19), 10718-10721.
109. van Swaay, D.; deMello, A., Microfluidic methods for forming liposomes. *Lab on a Chip* **2013**, 13 (5), 752-767.
110. Kamiya, K.; Kawano, R.; Osaki, T.; Akiyoshi, K.; Takeuchi, S., Cell-sized asymmetric lipid vesicles facilitate the investigation of asymmetric membranes. *Nat. Chem.* **2016**, 8 (9), 881-889.
111. Bodas, D.; Khan-Malek, C., Hydrophilization and hydrophobic recovery of PDMS by oxygen plasma and chemical treatment - An SEM investigation. *Sensor. Actuat. B-Chem.* **2007**, 123 (1), 368-373.
112. Ocvirk, G.; Munroe, M.; Tang, T.; Oleschuk, R.; Westra, K.; Harrison, D.

- J., Electrokinetic control of fluid flow in native poly(dimethylsiloxane) capillary electrophoresis devices. *Electrophoresis* **2000**, *21* (1), 107-115.
113. Gokaltun, A.; Yarmush, M. L.; Asatekin, A.; Usta, O. B., Recent advances in nonbiofouling PDMS surface modification strategies applicable to microfluidic technology. *Technology* **2017**, *5* (1), 1-12.
114. Hu, S. W.; Ren, X. Q.; Bachman, M.; Sims, C. E.; Li, G. P.; Allbritton, N., Surface modification of poly(dimethylsiloxane) microfluidic devices by ultraviolet polymer grafting. *Anal. Chem.* **2002**, *74* (16), 4117-4123.
115. Schneider, M. H.; Willaime, H.; Tran, Y.; Rezgui, F.; Tabeling, P., Wettability Patterning by UV-Initiated Graft Polymerization of Poly(acrylic acid) in Closed Microfluidic Systems of Complex Geometry. *Anal. Chem.* **2010**, *82* (21), 8848-8855.
116. Hwang, S.; Choi, C.-H.; Lee, C.-S., Regioselective surface modification of pdms microfluidic device for the generation of monodisperse double emulsions. *Macromol. Res.* **2012**, *20* (4), 422-428.
117. Jass, J.; Tjarnhage, T.; Puu, G., From liposomes to supported, planar bilayer structures on hydrophilic and hydrophobic surfaces: An atomic force microscopy study. *Biophys. J.* **2000**, *79* (6), 3153-3163.
118. Alexandrova, L.; Karakashev, S. I.; Grigorov, L.; Phan, C. M.; Smoukov, S. K., Wetting properties of phospholipid dispersion on tunable hydrophobic SiO₂-glass plates. *Adv. Colloid Interface Sci.* **2015**, *220*, 1-7.
119. Lamour, G.; Hamraoui, A.; Buvailo, A.; Xing, Y.; Keuleyan, S.; Prakash, V.; Eftekhari-Bafrooei, A.; Borguet, E., Contact Angle Measurements Using a Simplified Experimental Setup. *J. Chem. Educ.* **2010**, *87* (12), 1403-1407.
120. Kocisova, E.; Petr, M.; Sipova, H.; Kylian, O.; Prochazka, M., Drop coating deposition of a liposome suspension on surfaces with different wettabilities: "coffee ring" formation and suspension preconcentration. *Phys. Chem. Chem. Phys.* **2017**, *19* (1), 388-393.
121. Mizuno, M.; Toyota, T.; Konishi, M.; Kageyama, Y.; Yamada, M.; Seki, M., Formation of Monodisperse Hierarchical Lipid Particles Utilizing Microfluidic Droplets in a Nonequilibrium State. *Langmuir* **2015**, *31* (8), 2334-2341.
122. Kazayama, Y.; Teshima, T.; Osaki, T.; Takeuchi, S.; Toyota, T., Integrated microfluidic system for size-based selection and trapping of giant vesicles. *Anal. Chem.* **2016**, *88* (2), 1111-1116.
123. Nishimura, K.; Suzuki, H.; Toyota, T.; Yomo, T., Size control of giant unilamellar vesicles prepared from inverted emulsion droplets. *J. Colloid. Interface Sci.*

2012, 376 (1), 119-125.

124. Morita, M.; Onoe, H.; Yanagisawa, M.; Ito, H.; Ichikawa, M.; Fujiwara, K.; Saito, H.; Takinoue, M., Droplet-Shooting and Size-Filtration (DSSF) Method for Synthesis of Cell-Sized Liposomes with Controlled Lipid Compositions. *Chembiochem* **2015**, 16 (14), 2029-2035.

125. Natsume, Y.; Toyota, T., Giant Vesicles Containing Microspheres with High Volume Fraction Prepared by Water-in-oil Emulsion Centrifugation. *Chem. Lett.* **2013**, 42 (3), 295-297.

126. Honerkamp-Smith, A. R.; Woodhouse, F. G.; Kantsler, V.; Goldstein, R. E., Membrane Viscosity Determined from Shear-Driven Flow in Giant Vesicles. *Phys. Rev. Lett.* **2013**, 111 (3), 038103.

127. Chiba, M.; Miyazaki, M.; Ishiwata, S., Quantitative Analysis of the Lamellarity of Giant Liposomes Prepared by the Inverted Emulsion Method. *Biophys. J.* **2014**, 107 (2), 346-354.

128. Bucher, P.; Fischer, A.; Luisi, P. L.; Oberholzer, T.; Walde, P., Giant vesicles as biochemical compartments: The use of microinjection techniques. *Langmuir* **1998**, 14 (10), 2712-2721.

129. Lande, M. B., The relationship between membrane fluidity and permeabilities to water, solutes, ammonia, and protons. *J. Gen. Physiol.* **1995**, 106 (1), 67-84.

130. Gensure, R. H.; Zeidel, M. L.; Hill, W. G., Lipid raft components cholesterol and sphingomyelin increase H⁺/OH⁻ permeability of phosphatidylcholine membranes. *Biochem. J.* **2006**, 398, 485-495.

131. Runas, K. A.; Malmstadt, N., Low levels of lipid oxidation radically increase the passive permeability of lipid bilayers. *Soft Matter* **2015**, 11 (3), 499-505.

132. Barba-Bon, A.; Pan, Y. C.; Biedermann, F.; Guo, D. S.; Nau, W. M.; Hennig, A., Fluorescence Monitoring of Peptide Transport Pathways into Large and Giant Vesicles by Supramolecular Host-Dye Reporter Pairs. *J. Am. Chem. Soc.* **2019**, 141 (51), 20137-20145.

133. Segré, D.; Ben-Eli, D.; Deamer, D. W.; Lancet, D., The lipid world. *Orig. Life Evol. Biosph.* **2001**, 31 (1-2), 119-145.

134. Deamer, D.; Dworkin, J. P.; Sandford, S. A.; Bernstein, M. P.; Allamandola, L. J., The first cell membranes. *Astrobiology* **2002**, 2 (4), 371-381.

135. Szostak, J. W., Origins of life: systems chemistry on early earth. *Nature* **2009**, 459 (7244), 171-172.

136. de Souza, T. P.; Fahr, A.; Luisi, P. L.; Stano, P., Spontaneous Encapsulation and Concentration of Biological Macromolecules in Liposomes: An Intriguing

- Phenomenon and Its Relevance in Origins of Life. *J. Mol. Evol.* **2014**, *79* (5-6), 179-192.
137. Ichihashi, N.; Usui, K.; Kazuta, Y.; Sunami, T.; Matsuura, T.; Yomo, T., Darwinian evolution in a translation-coupled RNA replication system within a cell-like compartment. *Nat. Commun.* **2013**, *4*, 2494.
 138. Matsumura, S.; Kun, A.; Ryckelynck, M.; Coldren, F.; Szilagy, A.; Jossinet, F.; Rick, C.; Nghe, P.; Szathmary, E.; Griffiths, A. D., Transient compartmentalization of RNA replicators prevents extinction due to parasites. *Science* **2016**, *354* (6317), 1293-1296.
 139. Luisi, P. L.; Allegretti, M.; de Souza, T. P.; Steiniger, F.; Fahr, A.; Stano, P., Spontaneous Protein Crowding in Liposomes: A New Vista for the Origin of Cellular Metabolism. *Chembiochem* **2010**, *11* (14), 1989-1992.
 140. Fanti, A.; Gammuto, L.; Mavelli, F.; Stano, P.; Marangoni, R., Do protocells preferentially retain macromolecular solutes upon division/fragmentation? A study based on the extrusion of POPC giant vesicles. *Integr. Biol.* **2018**, *10* (1), 6-17.
 141. Chakrabarti, A. C.; Breaker, R. R.; Joyce, G. F.; Deamer, D. W., Production of RNA by a polymerase protein encapsulated within phospholipid-vesicles. *J. Mol. Evol.* **1994**, *39* (6), 555-559.
 142. Ruiz-Mirazo, K.; Briones, C.; de la Escosura, A., Prebiotic systems chemistry: new perspectives for the origins of life. *Chem. Rev.* **2014**, *114* (1), 285-366.
 143. Hicke, L.; Dunn, R., Regulation of membrane protein transport by ubiquitin and ubiquitin-binding proteins. *Annu. Rev. Cell Dev. Biol.* **2003**, *19*, 141-172.
 144. Tester, M.; Davenport, R., Na⁺ tolerance and Na⁺ transport in higher plants. *Annals of Botany* **2003**, *91* (5), 503-527.
 145. Muchowska, K. B.; Varma, S. J.; Moran, J., Synthesis and breakdown of universal metabolic precursors promoted by iron. *Nature* **2019**, *569* (7754), 104-107.
 146. Ritson, D.; Sutherland, J. D., Prebiotic synthesis of simple sugars by photoredox systems chemistry. *Nat. Chem.* **2012**, *4* (11), 895-899.
 147. Powner, M. W.; Gerland, B.; Sutherland, J. D., Synthesis of activated pyrimidine ribonucleotides in prebiotically plausible conditions. *Nature* **2009**, *459* (7244), 239-242.
 148. Kebukawa, Y.; Chan, Q. H. S.; Tachibana, S.; Kobayashi, K.; Zolensky, M. E., One-pot synthesis of amino acid precursors with insoluble organic matter in planetesimals with aqueous activity. *Sci. Adv.* **2017**, *3* (3), e1602093.
 149. Gibard, C.; Bhowmik, S.; Karki, M.; Kim, E. K.; Krishnamurthy, R., Phosphorylation, oligomerization and self-assembly in water under potential prebiotic conditions. *Nat. Chem.* **2018**, *10* (2), 212-217.

150. Neumann, E.; Kakorin, S.; Toensing, K., Fundamentals of electroporative delivery of drugs and genes. *Bioelectrochem. Bioenerg.* **1999**, *48* (1), 3-16.
151. Langecker, M.; Arnaut, V.; Martin, T. G.; List, J.; Renner, S.; Mayer, M.; Dietz, H.; Simmel, F. C., Synthetic lipid membrane channels formed by designed DNA nanostructures. *Science* **2012**, *338* (6109), 932-936.
152. Fujii, S.; Matsuura, T.; Sunami, T.; Kazuta, Y.; Yomo, T., In vitro evolution of alpha-hemolysin using a liposome display. *Proc. Natl. Acad. Sci. U. S. A.* **2013**, *110* (42), 16796-16801.
153. Melkikh, A. V.; Sutormina, M., Protocells and LUCA: Transport of substances from first physicochemical principles. *Prog. Biophys. Mol. Biol.* **2019**, *145*, 85-104.
154. Schmitt, C.; Lippert, A. H.; Bonakdar, N.; Sandoghdar, V.; Voll, L. M., Compartmentalization and Transport in Synthetic vesicles. *Front. Bioeng. Biotechnol.* **2016**, *4*, 19.
155. Lawless, J. G.; Yuen, G. U., Quantification of monocarboxylic acids in the murchison carbonaceous meteorite. *Nature* **1979**, *282* (5737), 396-398.
156. Herd, C. D. K.; Blinova, A.; Simkus, D. N.; Huang, Y. S.; Taroza, R.; Alexander, C. M. O.; Gyngard, F.; Nittler, L. R.; Cody, G. D.; Fogel, M. L.; Kebukawa, Y.; Kilcoyne, A. L. D.; Hiltz, R. W.; Slater, G. F.; Glavin, D. P.; Dworkin, J. P.; Callahan, M. P.; Elsila, J. E.; De Gregorio, B. T.; Stroud, R. M., Origin and Evolution of Prebiotic Organic Matter As Inferred from the Tagish Lake Meteorite. *Science* **2011**, *332* (6035), 1304-1307.
157. Deamer, D. W.; Georgiou, C. D., Hydrothermal Conditions and the Origin of Cellular Life. *Astrobiology* **2015**, *15* (12), 1091-1095.
158. Sojo, V.; Herschy, B.; Whicher, A.; Camprubi, E.; Lane, N., The Origin of Life in Alkaline Hydrothermal Vents. *Astrobiology* **2016**, *16* (2), 181-197.
159. Merkle, D.; Kahya, N.; Schwille, P., Reconstitution and Anchoring of Cytoskeleton inside Giant Unilamellar Vesicles. *Chembiochem* **2008**, *9* (16), 2673-2681.
160. Kurihara, K.; Tamura, M.; Shohda, K.-i.; Toyota, T.; Suzuki, K.; Sugawara, T., Self-reproduction of supramolecular giant vesicles combined with the amplification of encapsulated DNA. *Nat. Chem.* **2011**, *3* (10), 775-781.
161. Larsen, J.; Hatzakis, N. S.; Stamou, D., Observation of inhomogeneity in the lipid composition of individual nanoscale liposomes. *J. Am. Chem. Soc.* **2011**, *133* (28), 10685-10687.
162. Inglis, D. W.; Davis, J. A.; Austin, R. H.; Sturm, J. C., Critical particle size for fractionation by deterministic lateral displacement. *Lab Chip* **2006**, *6* (5), 655-8.
163. Kaczmarek, P.; Szczepanik, W.; Jezowska-Bojczuk, M., Acid-base,

coordination and oxidative properties of systems containing ATP, L-histidine and Ni(II) ions. *Dalton Trans* **2005**, (22), 3653-3657.

164. Darwin, C., *On the origin of species*. 1859.

165. Martin, W.; Baross, J.; Kelley, D.; Russell, M. J., Hydrothermal vents and the origin of life. *Nat. Rev. Microbiol.* **2008**, 6 (11), 805-814.

166. Kaneda, M.; Nomura, S. M.; Ichinose, S.; Kondo, S.; Nakahama, K.; Akiyoshi, K.; Morita, I., Direct formation of proteo-liposomes by in vitro synthesis and cellular cytosolic delivery with connexin-expressing liposomes. *Biomaterials* **2009**, 30 (23-24), 3971-3977.

167. Castro, J. M.; Sugiyama, H.; Toyota, T., Budding and division of giant vesicles linked to phospholipid production. *Sci. Rep.* **2019**, 9, 165.

168. Lande, M. B.; Donovan, J. M.; Zeidel, M. L., The relationship between membrane fluidity and permeabilities to water, solutes, ammonia, and protons. *J. Gen. Physiol.* **1995**, 106 (1), 67-84.

169. Komatsu, H.; Okada, S., Increased permeability of phase-separated liposomal membranes with mixtures of ethanol-induced interdigitated and noninterdigitated structures. *Biochim. Biophys. Acta Biomembr.* **1995**, 1237 (2), 169-175.

170. Paula, S.; Volkov, A. G.; VanHoek, A. N.; Haines, T. H.; Deamer, D. W., Permeation of protons, potassium ions, and small polar molecules through phospholipid bilayers as a function of membrane thickness. *Biophys. J.* **1996**, 70 (1), 339-348.

171. Kamiya, K.; Takeuchi, S., Giant liposome formation toward the synthesis of well-defined artificial cells. *J. Mater. Chem. B* **2017**, 5 (30), 5911-5923.

172. Li, S.; Hu, P. C.; Malmstadt, N., Confocal imaging to quantify passive transport across biomimetic lipid membranes. *Anal. Chem.* **2010**, 82 (18), 7766-7771.

173. Zocher, F.; van der Spoel, D.; Pohl, P.; Hub, J. S., Local partition coefficients govern solute permeability of cholesterol-containing membranes. *Biophys. J.* **2013**, 105 (12), 2760-2770.

Acknowledgement

The study was performed with countless support from Prof. Taro Toyota. He trusted me and gave me a lot of research autonomy while patiently and continuously discussing the data we obtained. I sincerely appreciate him for his superlative supervision on my thesis.

The research was conducted in collaboration with Prof. Shoji Takeuchi and Dr. Toshihisa Osaki. Without their insightful advice and generous assistance, I would never accomplish the microfluidic devices used in the thesis. I am grateful for their kind aid and uncompromising discussion.

I also thank Mr. Hirofumi Yoshida. He has professional skills and know-how for the fabrication of the microfluidic device. He kept the equipment up to a high standard and tirelessly instructed me. I learned a lot from him.

Mr. Akio Kaneko and Mr. Shingo Kobayashi from Senshu Scientific Corporation contributed to the setup of MANSIONS. Their in-depth knowledge cultivated in their daily work was beneficial.

Prof. Yuichi Wakamoto gave me the first opportunity to be involved in a scientific research activity when I was an undergraduate student. I could not stand here without his guide and energetic encouragement. I would like to express my sincere gratitude to him.

I would like to thank Prof. Kunihiro Kaneko, Prof. Takashi Ikegami, Prof. Satoshi Sawai, Prof. Miho Yanagisawa, Prof. Masayuki Imai, Prof. Shinichiro M. Nomura, Prof. Yutetsu Kuruma, Prof. Tony Z. Jia, Prof. Juan M. Castro, Prof. Pier L. Luisi, Prof. Peter J. Walde, Prof. Norman H. Packard, Prof. Martin M. Hanczyc, and Prof. Jitka Cejkova. The exciting discussions with them brought the indelible motivation to seek the fundamentals of the living system.

Colleagues at Toyota Lab have given me invaluable lessons. It is nearly impossible to list their support thoroughly. I especially acknowledge Dr. Yuki Kazayama, who mentored me in the first year, and Dr. Muneyuki Matsuo, who advised me frequently and kindly.

On top of that, the strong support and warm understanding of my family was the vital and essential driving force to finish the thesis. Words are not enough to describe my gratitude.